IntechOpen

Land Degradation and Desertification

a Global Crisis

Edited by Abiud Kaswamila

LAND DEGRADATION AND DESERTIFICATION - A GLOBAL CRISIS

Edited by **Abiud Kaswamila**

Land Degradation and Desertification - a Global Crisis
http://dx.doi.org/10.5772/61629
Edited by Abiud Kaswamila

Contributors

Martin Enrique Romero-Sanchez, Antonio Gonzalez-Hernandez, Francisco Moreno-Sanchez, Jiangbo Gao, Shaohong Wu, Wenjuan Hou, Kewei Jiao, Phesheya Dlamini, Vincent Chaplot, Ertuğrul Karaş, İrfan Oğuz, Sabit Erşahin, Tekin Susam, Mykola Kharytonov, Sergey Stankevich, Tamara Dudar, Anna Kozlova

Notice

First published in Croatia, 2016 by INTECH d.o.o.
eBook (PDF) Published by IN TECH d.o.o.
Place and year of publication of eBook (PDF): Rijeka, 2019.
IntechOpen is the global imprint of IN TECH d.o.o.
Printed in Croatia

Legal deposit, Croatia: National and University Library in Zagreb

Additional hard and PDF copies can be obtained from orders@intechopen.com

Land Degradation and Desertification - a Global Crisis
Edited by Abiud Kaswamila

p. cm.

Print ISBN 978-953-51-2706-2

Online ISBN 978-953-51-2707-9

eBook (PDF) ISBN 978-953-51-5084-8

Meet the editor

Abiud Kaswamila is a full professor of rural land-use planning in protected area bionetworks. He obtained his undergraduate degree from the University of Dar es Salaam in 1991. He did his MSc at ITC in the Netherlands in 1995 and his PhD at Greenwich University in the United Kingdom in 2006. For more than three decades, Professor Kaswamila has worked as an Agricultural Research Officer at Mlingano Agricultural Research Institute and a Don at Mweka Wildlife College and later at the University of Dodoma. Professor Kaswamila has published widely in areas of land-use planning, land management, agriculture, poverty and livelihood, biodiversity conservation, and community conservation. He is currently a Professot at the College of Humanities and Social Sciences Research and Publications Coordinator at the University of Dodoma, Tanzania.

Contents

Preface

Land degradation is a major concern globally and is accepted as one of the most serious ecological and socioeconomic problems worldwide. The subject has received and will continue to receive a lot of international attention in the twenty-first and twenty-second centuries, respectively. Available data show that in dry areas of the world, for example, degraded lands amount to 3.6 billion ha out of 5.2 billion ha and that the global extent of land degradation by all processes is about 1.9 billion ha. Furthermore, the current rate of agricultural land degradation worldwide by soil erosion and other factors is leading to an irreversible loss of productivity. It is estimated that human-induced soil degradation has affected more than 24% of the inhabited land area and the values of individual continents range from 12% in North America, 19% in Oceania, 26% in Europe, 27% in Africa, to 31% in Asia (Lal, 1993).

Despite the use of different methods and techniques to halt the problem, the world continues to witness loss of vegetation cover, loss of land productivity, increased soil erosion, and increased poverty. The problem is more serious in developing countries where the majorities depend on natural resources for livelihood. Understanding the relationship between land cover and other environmental processes could be an eye-opener to scholars, land-use planners, and land users in addressing the problem and restoring and/or conserving degraded lands.

This book highlights the scope and extent of land degradation and desertification and land-atmosphere interaction in both developing and developed world and how contemporary methods and techniques can play a great role in understanding and mitigating the problem. The methods and techniques used among others include remote sensing, GIS, modelling, and the use of land quality.

The contributors in this book are renowned scholars and researchers with vast experience in the disciplines of land degradation and desertification. I hope that this book will be a very useful reference material to environmentalists worldwide who wish to see the world being a better place to live in now and in the future.

Abiud Kaswamila
Professor of Land-Use Planning
Department of Geography and Environmental Studies
The University of Dodoma
Dodoma,Tanzania

Section 1

Remote Sensing and Modeling

Chapter 1

The Assessment of Land Degradation and Desertification in Mexico: Mapping Regional Trend Indicators with Satellite Data

Martin Enrique Romero-Sanchez,
Antonio Gonzalez-Hernandez and
Francisco Moreno-Sanchez

Additional information is available at the end of the chapter

http://dx.doi.org/10.5772/64241

Abstract

Understanding the patterns of land degradation and desertification to develop mitigation strategies requires identification of methods for accurate and spatially explicit assessment and monitoring. Remote sensing data offer the possibility to develop strategies that outline degradation and desertification. The free access policy on satellite imagery enables a new pathway to measure, assess, and monitor land degradation using indicators derived from multispectral satellite data. This chapter seeks to explore a methodology for land degradation and desertification assessment and monitoring, based on freely available multispectral satellite data. The method identifies net primary productivity (NPP) and canopy cover (CC) as indicators of degradation. The trajectories of these indicators show patterns and trends over time. The methodological development presented here is intended to be a tool for regional landscape monitoring and assessment, enabling the formulation of corrective action plans. This methodology was tested in a semi-deciduous ecosystem in the southeast of Mexico.

Keywords: land degradation, desertification, satellite data, assessment, monitoring

1. Introduction

Land degradation and desertification not only contribute to the effects of climate change but also to the loss of productivity, biodiversity, and functionality of forest landscapes. Land use

change and associated processes are responsible for around 10% of net global carbon emissions[1]. Land degradation and desertification understood as the loss of productive capacity of the land [1] affect ecosystem productivity, socioeconomic problems, and food security. The UnitedNations through the United Nations Convention to Combat Desertification (UNCCD) seeks to identify and define strategies that support sustainable regional development to reverse and prevent desertification and land degradation. The UNCCD works to help countries to improve living conditions of people in drylands and to maintain and restore land and soil productivity.

One of the main issues in the land degradation and desertification programs is the requirement of robust methods to quantify degradation [2]. The fundamental challenge is providing a reliable account of it, and remote sensor techniques should be reliable and continuous to be a source of information [3–5]. To develop a regional and local mechanism to reverse and prevent degradation, it is imperative then to define monitoring and assessing strategies. The constant and exponential increase of remote sensing technologies offers different options to evaluate phenomena such as land degradation. Organizations dedicated to the production of new remote sensing technologies have implemented new satellite sensors with higher spatial resolution (e.g. IKONOS-2, QuickBird-2,SPOT-5) which indicates a new age of terrestrial observation and digital mapping [2, 6–9].

Satellite imagery has been taking information from the Earth's surface for last 40 years in a continuous and reliable way (i.e. Landsat program). Multispectral satellite imagery such as Landsat has opened new avenues for understanding ecological and land cover dynamics [10]. Landsat mission has been collecting imagery since 1972, providing a record of the status and dynamics of the Earth [11, 12]. Changes to policy data in 2008 make free and available the Landsat archive to any user [13]. The free distribution policy increased the supply of imagery dramatically; thus, the use and analysis of the Landsat archive have increased the opportunities to research in a variety of disciplines [10].

Optical remote sensing has been improved by spatial resolution (pixel size), spectral resolution (number of wavebands), radiometric resolution (sensibility to detect radiation changes), and temporal resolution (data acquisition frequency), which means getting capabilities of measurement in quasi-real-time [14–17]. This scenario opens up the possibility to implement powerful monitoring strategies by taking advantage of the free database policies that many entities have today. Mexico is the perfect example; almost all spatial information is freely available through different government websites. Therefore, some indicators related to degradation are available to be estimated by using remote sensing and ground data. The symbols used are capable, through trajectory or time series analysis, of detecting and mapping out changes over time.

The chapter examines the capabilities of freely available remote sensing, combined with field data, in deriving some degradation indicators. The main idea is the construction of a platform for regional land degradation monitoring and assessment. One of the main assumptions of

[1] IPCC (2013) Intergovernmental Panel on Climate Change. The Physical Science Basis. Contribution of Working Group I to the Fifth Assessment Report of the Intergovernmental Panel on Climate Change.

http://dx.doi.org/10.5772/64241

this approach is that it can be replicated in different regions of the developing world. Additionally, the cost of applications is minimal if remote sensing and field data are available.

2. Assessment of land degradation and desertification approaches

Land degradation, as has been pointed out by the UNCDD, is a global development and environment issue that affects mostly developing countries regarding the economic impact and food security [18]. The assessment and monitoring frameworks developed to provide information about land degradation have been very valuable; however, there are some opportunities to improve and test methodologies according to regional and country needs.

Land degradation and desertification are concepts that are strongly related. Land degradation can be defined as the loss or reduction of the biological production of farmlands, grasslands, forests, and wooded areas and is the result of intense land use or a process (or a combination of the process), including those coming from human actions. It is the outcome of the mismatch between land quality and the intensity of activity part of the actual land use.

According to the UNCCD, land degradation is a complex set of processes of the impoverishment of terrestrial ecosystem, either natural or human-induced, that causes the land to be no longer able to sustain its economic functions or the original ecological functions correctly [18]. The consequences of land degradation are land productivity reduction, socio-economic problems, including uncertainty in food security, migration, and damage to ecosystems.

Desertification, on the other hand, is defined as land degradation occurring in arid-semiarid and dry sub-humid areas caused by a combination of climatic factors and human activities. Therefore, only land degradation occurring in drylands is considered as part of a desertification process [19]. As many climatic scenarios have to point out, many areas across the world are vulnerable to climate change because it is going to accelerate the degradation process.

2.1. The global assessment of human-induced soil degradation (GLASOD)

This project was one of the first attempts to assess the state of degradation of soil from a global perspective [20]. The world map produced by GLASOD showed the status of human-induced soil degradation and was based mainly on expert judgment and reported degrees of land degradation that also included the notion of resilience, which was deemed essential for land management decisions. Although the GLASOD project had some criticism about the methods used, it was the only global assessment available to scientists, decision-makers, and land managers to date [18].

2.2. Land degradation assessment in drylands (LADA)

The LADA approach was developed based on the assumption that human activities on the land are the main drivers causing land degradation [21]. Therefore, defining and mapping of different land use systems are very crucial activities for underpinning the assessment and its implementation. The entire LADA approach gives consideration to the relationships between

the causes and effects that lead to degradation. The LADA project operates by using a variety of technologies, from satellite images to digital databases, to soil and vegetation sampling, and the examination of the linkages between both biophysical and socio-economic issues. Global assessment efforts list net primary productivity (NPP), rainfall use efficiency (RUE), aridity index (AI), rainfall variability (RV), and erosion risk (ER) as the leading indicators of land degradation [20].

The global land degradation assessment (GLADA) was the global component of LADA. GLADA aims at providing a baseline for the assessment of global trends in land degradation using a range of scale-appropriate indicators, many of which are collected through satellite sensors and processing satellite data and existing global databases.

2.3. Remote sensing as a tool for land degradation and desertification assessments

Methods for monitoring current state and changes of landscapes use the advantages and potential of satellite-borne or airborne remote sensing imagery. Most work has focused on identifying the change in detection of decreases in land cover rather than identifying the inversed process [22]. Considerable amount of studies explore the capabilities of remote sensing on different monitoring applications and different remote sensing approaches and data [17, 23–26].

Remote sensing applications can be summarized mainly in four categories that include: cover classification, estimation of structures, change detection, and modeling [27]. Remote sensing has the potential to be decidedly instrumental in the assessment of degradation processes at a much lower cost than any other method [28, 29]. Assessment (i.e. measurement) and monitoring through remote sensing offer a series of advantages such as consistency of data, fairly near real-time reporting, and a source for having spatially explicit data [30].

Although there are several approaches to describe land cover changes using remote sensing technology, forest inventory and limited sampling of degradation on the ground are fundamental to its quantification [31–36]. The methods used are unique to each location and strongly dependent on how its components are clearly identified and responsive to accurate measurement, and how country requirements apply to these methods.

Remote sensing is a suitable tool for the estimation of biomass for large areas, usually at regional or national scales, where field data are scarce [34]. There is an abundance of literature that describes the virtues and capabilities of remote sensing-based methods for forest monitoring assessments [17, 22, 23, 37]. The continuing advances in remote sensing science and technology and the enormous amount of data these platforms and sensors produce daily provide a promising foundation to underpin any degradation monitoring program.

The possibility of integration of optical and multispectral remote sensing data to active sensors such as LiDAR (light detection and ranging) and RADAR (radio detection and ranging), combined with ground data, has gained a significant relevance and a high potential for contributing to the design of degradation assessment and monitoring methodologies.

http://dx.doi.org/10.5772/64241

Direct detection of degradation processes, for example in forest landscapes, relates area changes to, and focuses on, forest canopy damage. These changes in forest attributes occurring during a period of time can be detected using information from natural forest resources inventories (FRI) and some from remote sensing [23, 30, 38]. Medium spatial resolution satellite remote sensing data such as Landsat Thematic Mapper (TM) and SPOT have proven capable of obtaining regional-scale forest variables [39]. Indirect approaches focus on the spatial distribution and the effects that the evolution of human infrastructure has had on the degradation of nearby areas. Often, these "indirect" factors are used as "proxies" for newly degraded areas.

3. Methodology

3.1. Mapping regional trend indicators with satellite data

Any operational monitoring assessment needs to establish as starting a clear understanding of what are the relevant and regionally significant indicators that are used as components of the analysis. This is followed by what will be the practical impact of the utilization of these parameters in the actual implementation of measuring and monitoring methods. Part of the methodological approach presented here was developed by the first author during his doctoral program and was focused on forest degradation. However, the main components were translated to the land degradation and desertification monitoring requirements as both phenomena are intimately linked.

Within the UNCCD, it is necessary to understand what are the drivers and activities causing degradation [30]. According to project needs and based on the literature reviewed, canopy cover and net primary productivity are considered as the leading indicators within this methodological framework. These variables are thus proposed as indicators of degradation (mainly forest landscapes) in practice. Although it is acknowledged that other indicators (biodiversity, disturbances, and fragmentation) are also variables that may merit to be considered, together with those above, as indicators of degradation, are not regarded as part of this chapter. However, the limitations of time and the scope of a rapid assessment do not stretch to encompass them in this study.

3.1.1. Proposed indicators

3.1.1.1. Canopy cover

Canopy cover is recognized as a significant biophysical and structural attribute of the forest [40]. It affects terrestrial energy and water exchanges, photosynthesis and transpiration, net primary production, and carbon and nutrient fluxes, and is the key element for defining forests in international and national accords [41]. Canopy cover provides an attribute that is measurable and can be used to monitor and retrieve site-specific histories of different stages within the forest landscape dynamics [41].

Canopy cover has already been used as an indicator to monitor and map forest degradation in various contexts [32, 35]. Some studies [42] evaluated forest degradation based on canopy closure classes, namely non-degraded (>70%), moderately degraded (40–70%), degraded (10–40%), and severely degraded (<10%). Another study [43] assessed forest degradation using canopy disturbance as a result of gaps produced by logging, road construction, and skid trails as an indication of forest degradation. Another approach suggested for mapping forest degradation and deforestation was the use of canopy cover combined with spectral mixture analysis, normalized difference fraction index, and a decision tree classification [44].

3.1.1.2. Net primary productivity

NPP determines the rate of atmospheric carbon sequestration and storage by vegetation [45, 46]. NPP has been used previously as an indicator of ecosystems' decline [47–49]. These approaches open the door to the possibility of using NPP as both a baseline and indicator of forest degradation [50], based on the assumptions that losses of canopy cover will affect the capacity of the forest to fix carbon and reduce NPP rates.

NPP estimations are regularly based on the light use efficiency (LUE) theory [51]. The LUE theory is estimated on two broad assumptions. First, NPP is related to the absorbed photosynthetically active radiation, APAR, where LUE determines the amount of dry matter produced per unit of APAR. Second, environmental stresses such as low temperature or water shortage have an adverse impact over LUE [52, 53]. Production efficiency models (PEM) are developed from the LUE theory. They require inputs of meteorological data and take advantage of available satellite data to derive the fraction of absorbed photosynthetically active radiation, fPAR [53]. Examples of production efficiency models include the CASA model (Carnegie-Ames-Stanford approach) [54], C-Fix [55–57], and MOD17 [48] used for monitoring NPP at regional and global scale from satellite remote sensing data.

Net primary productivity is employed by the global land degradation assessment in Drylands (LADA) project [21], where NPP is highly relevant to the assessment of degradation. NPP can be readily used as a direct indicator of the condition and trend of changes in the state of ecosystems over time, whereby the decrease in NPP over time would signal the degradation of ecosystems. Through the LADA project conducted by the FAO [18] and within the UNCCD framework [58], mapped out land degradation at national, regional, and local scales in Ethiopia using NPP as one of the major indicators in their studies.

3.1.2. Trajectory analysis and change detection

One of the most frequent uses of remote sensing is change detection [59]. The stock pile of optical satellite imagery freely available (e.g. Landsat program) [13] offers opportunities for the reconstruction and understanding of landscape dynamics. Direct comparison of pairs of images (bi-temporal analysis) is perhaps the most common approach to change detection [60].

Although many change detection methods have been developed [61–63], the question of how to reliably map land-use change remains a central challenge. Land-use change (LUC) can result

http://dx.doi.org/10.5772/64241

in both land cover conversions and land cover modifications, but remote sensing mainly focuses on mapping the former. However, land cover changes may be more prevalent, meaningful, and significant to forest degradation than conversions. Forest degradation is more likely to be the reflection of a land cover change with its particular degree of intensity and duration.

Temporal trajectory analysis is understood in this context as the analysis of the sequence of changes in detection in every pixel of the image part of a stock pile of imagery over a continuous timescale. This type of analysis has been shown particularly useful in characterizing land ecosystem dynamics since it exploits the multi-temporal sequence of images to reveal temporal patterns over several temporal scales [62, 64, 65].

Trajectory analysis from multispectral and optical remote sensing is commonly employed for detecting changes of a set of forest degradation indicator variables over time that can be readily computed from satellite images and that are associated with the state and condition of forests [66, 67].

Examples from the literature have proved the value of the trajectory analysis in forest assessments, especially those that take advantage of the stock pile of Landsat imagery [61, 68, 69]. This methodology incorporates this type of analysis as a part of the degradation assessment.

3.1.2.1. Bi-temporal analysis

The bi-temporal analysis is perhaps the most used method to perform change detection on remote sensing satellite imagery [70]. The bi-temporal change detection methods range from simple image differencing methods to statistically based methods [71]. Change detection methods have been widely used to identify changes in classes (e.g. land cover classification) or the difference between a pair of images (image differencing) [70].

3.2. Land degradation and desertification in Mexico

Mexico has the compromise to present a national report about land degradation and desertification before the UNCDD. According to official reports, 90.7% of land in the country suffers some degree of degradation [72]. On the other hand, desertification affects almost 60% of the land in the country. Degradation and desertification processes in Mexico are complex issues related to poverty and sustainability, and they are affecting all the ecosystems within the country.

3.2.1. Study area: Yucatan Peninsula, Mexico

Mexico, within its ecological and climatic conditions, offers an excellent site for experimentation and application of this methodology. Although the method can be implemented in any part of the country, it has been decided to use a region from the southeast of Mexico, in the Yucatan Peninsula as the experimental site.

The methodological framework for land degradation assessment in drylands [21] is used to support methods to evaluate degradation within a tropical dry forest area located in the

Yucatan peninsula, Mexico. Landsat imagery was used as the main source to estimate indicators such as canopy cover (CC) and net primary productivity (NPP). Use of Landsat imagery enables to see changes over time [68] within a pixel 30 m resolution over 28 years (1986–2014). The methods enabled selection of priority areas and spatial patterns. The MENDA-1 watershed [73] in the Yucatan Peninsula, Mexico, was selected as experimental area (**Figure 1**).

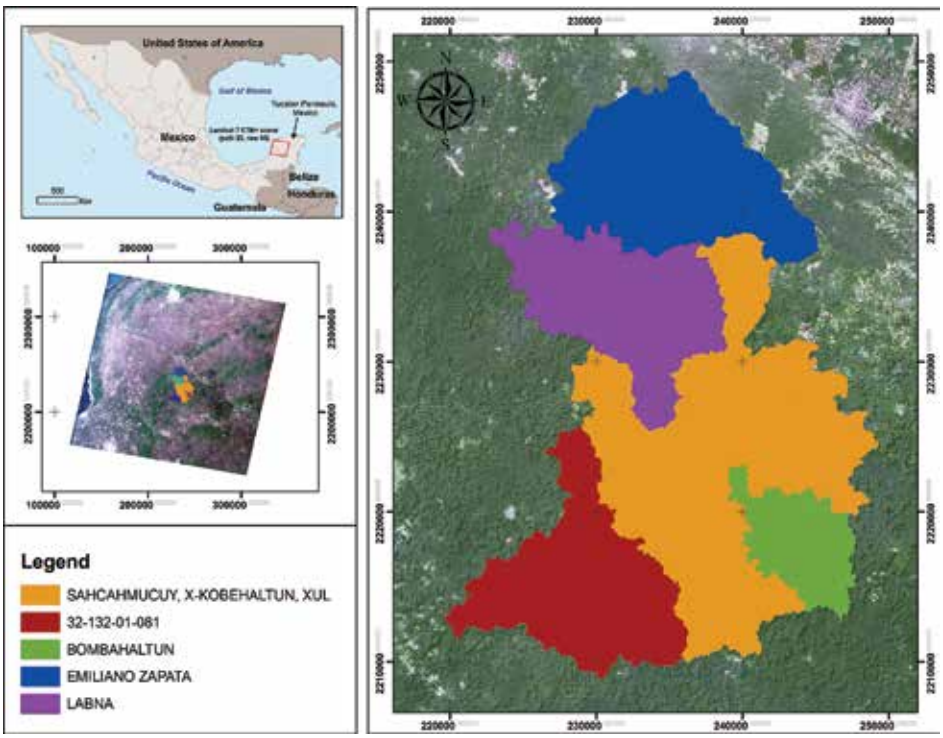

Figure 1. Study area.

The integration of the methodology is described as follows:

Selection of the indicators to monitor and assess degradation was the first step. Each one of the indicators selected was estimated using remote sensing as the primary source of data input. Because of the characteristics and free availability of Landsat archive [13], Landsat imagery is suggested as the major contribution. The indicators were estimated for the period of time required according to particular needs. Although in many tropical regions cloud cover is a significant issue, the probability of acquiring at least one cloud-free or reasonably cloud-free Landsat image per season is relatively high [74]. At least one Landsat image per season ensures continuity in historical estimations of the forest landscape dynamics based on Landsat archive.

Very high-resolution satellite imagery or LiDAR data is recommended as auxiliary data to validate calculations. Another data set crucial for the implementation of this framework was forest inventory databases. Many developing countries (e.g. Mexico) carried out periodical

http://dx.doi.org/10.5772/64241

forest inventories on a regional scale. Forest inventory data were the base for knowing the actual state of the forest and natural resources.

Once each one of the indicators has been calculated, the selection of a strategy for monitoring changes has to be made. As described before, the methods for change detection can be a time series approach (in the case of high frequency of data) or a bi-temporal change detection approach (in the case of low frequency of data). The implementation of this step allows identifying spatial and temporal patterns of the indicators used.

The establishment of a baseline and the definition of the threshold for comparisons was the next step toward the final integration. This was done using field data or high-resolution auxiliary imagery available (e.g. Google Earth™). The comparison of the spatial and temporal trends in the baseline scenario allowed identification of degraded areas regarding the indicators used.

3.2.2. Data preparation

3.2.2.1. Landsat ecosystem disturbance adaptive processing system

Landsat enhanced thematic mapper and thematic sensors imagery was used as the primary source of information. The images were obtained from the USGS website (http://glovis.usgs.gov). In the study area, like other tropical regions, cloud cover limited the choice of imagery available per year. In total, 155 Landsat scenes were downloaded. The images were in L1T geometrically corrected format and atmospherically corrected using the 6S radiative transfer approach [75].

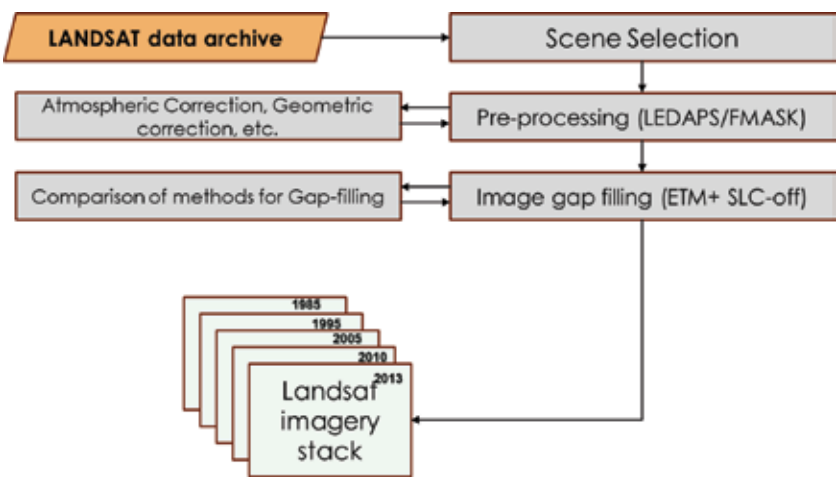

Figure 2. Satellite data preparation flow.

Landsat 7 ETM+ images acquired with the SLC-off (i.e., SLC failure in 2003) were adjusted using the algorithm Geostatistical Neighbor Spatial Pixel Interpolator, GNSPI [76]. The GNSPI

can recover efficiently the pixels missing due to SLC failure, and its outputs are suitable for forest monitoring applications [77]. Landsat imagery was separated according to the date taken (i.e. wet or dry season), and an initial cloud filter was applied. Imagery with more than 10% of cloud cover was avoided for the analysis to focus on high-quality imagery (cloud free). **Figure 2** shows in a very generic way the pre-processing process.

3.2.3. Forest degradation indicators estimation

3.2.3.1. Canopy cover

The CLASlite™ image processing system [78] was used to develop the fractional cover and forest cover maps for the Landsat dates. CLASlite™ produces photosynthetic vegetation, non-photosynthetic vegetation and, bare soil layers from the core process within CLASLite™ called Automated Monte Carlo Unmixed Process (AutoMCU). These outputs provide a quantitative analysis of the fractional or percentage cover (0–100%) of live and dead vegetation, and bare substrate within each Landsat pixel [78]. The Auto MCU submodel is based on a probabilistic algorithm designed for savanna, woodland, and shrubland ecosystems, and later modified for the tropical forest [79, 80].

Photosynthetic vegetation layers (0–100%) were used as an equivalent of field forest cover (0–100%) for subsequent analysis. To validate this assumption, the direct relationship between the PV and CC was measured. Canopy cover derived from LiDAR data was used to support the PV layers. CC LiDAR was estimated using the ratio of the pulse returned from the upper layer of tree crown (sum of all pulses > pre-defined threshold) to total returns. Hence

$$CC = \frac{nh}{n} \tag{1}$$

where

CC: canopy cover

nh: ∑all returns > predefined height

n: total returns.

The predefined height was set to 1.5 m. Range between 1.0 and 2.0 m is appropriate and has no substantial variation in the correlation between canopy cover measured in the field and the one estimated from Lidar data [81, 82].

Validation of the estimated Landsat CC was achieved by computing a residual mean of squares (RMS) of differences between Landsat CC and the Lidar CC product. This comparison was made possible by aggregating Lidar CC to 30 m to correspond to Landsat products spatially.

NPP in this study was calculated according to the theory of light use efficiency (LUE) as follows [46, 83]:

http://dx.doi.org/10.5772/64241

$$NPP = \varepsilon \cdot fPAR \cdot PAR \tag{2}$$

where

PAR is photosynthetically active radiation (MJ/(m^2 month))

fPAR is the fraction of PAR absorbed by vegetation canopy,

ε is the light use efficiency coefficient (g of C/MJ) and includes the plant respiration costs [84].

The light use efficient coefficient ε was derived following the MODIS-GPP approach [85] where ε is calculated using two factors: the biome-specific maximum conversion efficiency ε_{max}, and the effect of temperature *f(T)* and water on plant photosynthesis *f(W)* [83]. The ε_{max} used in this study was 1.044 g of C/MJ according to the lookup tables [84].

f(T) was estimated on a monthly basis using the equation developed for the terrestrial ecosystem model (TEM) [86], as:

$$f(T) = \frac{(T - Tmin)(T - Tmax)}{(T - Tmin)(T - Tmax) - (T - Topt)^2} \tag{3}$$

where *T* is the atmospheric temperature (°C); and *Tmin*, *Tmax*, and *Topt* are the minimum, maximum, and optimal temperatures for photosynthetic activities, respectively. Values of 2°C, 39°C, and 26°C were used for *Tmin*, *Tmax*, and *Topt*, respectively [47, 87].

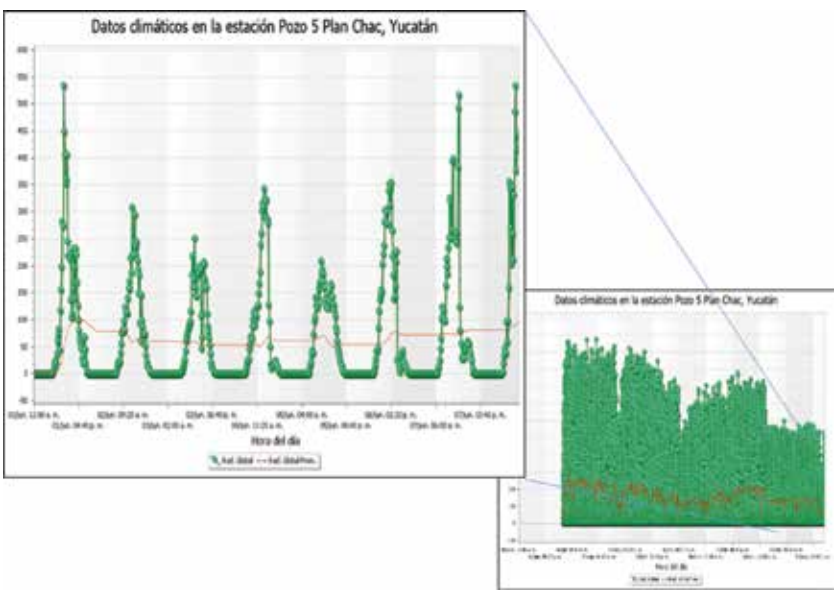

Figure 3. Daily solar radiation from the meteorological network (www.inifap.gob.mx).

The effect of water on plant photosynthesis *f(W)* was derived according to the algorithm suggested by Xiao et al. [88].

$$f(W) = \frac{1 + LSWI}{1 + LSWI_{\max}} \tag{4}$$

$$LSWI = \frac{\rho_{nir} - \rho_{swir}}{\rho_{nir} + \rho_{swir}} \tag{5}$$

where *LSWI* is the land surface water index, and $LSWI_{max}$ is the maximum *LSWI* within the plant growing season. ρ_{nir} and ρ_{swir} are the surface reflectance of the NIR and MIR bands in Landsat ETM+ images.

Meteorological data from the national meteorological network from the National Institute of Forestry, Agriculture, and Livestock Research (INIFAP) were used as inputs for the NPP calculations (**Figure 3**).

3.2.4. Trajectory analysis

Trajectory analysis and change detection on degradation indicators were performed using two different approaches: a time series and a bi-temporal approach. The BFAST [63] model was selected as the time series analysis approach. Canopy cover was the only indicator that went into the BFAST time series analysis because of the high frequency of data available. Change detection on above-ground biomass and NPP were performed using a bi-temporal approach as a result of the low frequency in data available. Next, the implementation of both methods is described.

3.2.4.1. BFAST

The BFAST and BFAST monitor algorithms were applied as a trajectory analysis strategy. Canopy cover derived from Landsat from the period 1988 to 2014 was used to implement the time series analysis. The algorithms were implemented using the BfastSpatial package for R software available at http://github.com/dutri001/bfastSpatial [64, 89]. The steps followed to implement BfastSpatial were (a) pre-processing of surface reflectance data, (b) inventorying and preparing data for analysis, and (c) analysis and formatting of change detection results.

3.2.4.2. Bi-temporal change detection

Change detection on a bi-temporal basis was implemented in NPP layers. The imaging differencing method allowed direct comparison between images and was used for two reasons: it is straightforward and allows an easy interpretation of the results [70]. The image differencing method consisted of precisely co-registered multi-temporal images used to produce a residual image to represent changes. Although the USGS service provides Landsat imagery as

http://dx.doi.org/10.5772/64241

LT1 (geometrically corrected), an automatic image registration was performed for every change detection process.

The difference between layers was measured directly from values of the pixel image. The expression of image differencing is as follows:

$$I_d(x,y) = I_1(x,y) - I_2(x,y) \tag{6}$$

where I_1 and I_2 are images from time t_1 and t_2, (x, y) are coordinates, and I_d is the difference image. Pixels with no change were distributed around the mean while pixels with change were circulated in the tails of the distribution curve. Since change can occur in both directions, it is therefore up to the analyst to decide which image to subtract from which [90].

The image differencing method was carried out by the ENVI™ 5.2 interface. Possible inconstancies between indicators used in this process due to errors associated with estimations were minimized using a normalization process between Time 1 and Time 2 layers. This normalization process applies a gain and an offset to the Time 2 layer so that it has same mean and standard deviation as the time layer.

The next step was to select a threshold value that allows the method to identify areas that have a significant change. Otsu's auto-thresholding method [91] was used to set the threshold for identifying important changes. Otsu's is a histogram shape-based method. It is based on discriminate analysis and uses the zeroth- and the cumulative first-order moments of the histogram for calculating the value of the thresholding level.

A clean-up process was carried out where a kernel size of 3 × 3 pixels was applied to remove speckling noise, and a minimum aggregate size set to 25 was configured to remove minuscule regions.

The outputs produced by the changed detection method were (a) an image change and (b) an image difference. The latest was kept to identify "degraded" areas by applying a classification tree based on field observations and very high-resolution imagery as training sites. This approach followed the same logic described earlier to detect break points in the time series. The image change was used to determine deforestation in the study area.

3.3. Results and discussion

The procedures in this integrated methodology allowed for the identification of areas that have been degraded. The results allowed to highlight areas that have been degraded due to loss of net primary productivity and forest cover. Integration of the different elements in this methodology enabled the identification of areas that maintain a "stable" condition and areas that change over the period evaluated.

According to the results obtained here, Landsat-derived indicators (forest canopy cover and net primary productivity) showed effectiveness in the identification and mapping of degraded forest landscapes. The results of this study also suggest that it is possible to produce explicit and high-resolution canopy cover maps over relatively large areas.

The net primary productivity also showed its value in identifying and mapping forest degradation. NPP is a forest parameter that is difficult to estimate and can be subject to high levels of uncertainty [92–94]. NPP was estimated for the period 2007–2013 showing mean values in the range of 480–512 and maximum values of 742–936 gC/m^2/year. Although NPP estimations are difficult to perform and validate due to lack of field data, programs such the INIFAP meteorological network that register climatic variables every 15 minutes, and Eddy covariance tower networks along with remote sensing data, are promissory elements to support NPP modeling.

Finally, the results of the trajectory analysis of degradation indicators (NPP and CC) showed (overall timescale 28 years) a slight tendency toward forest degradation and decline, punctuated by cyclic oscillations of decline and recovery that indicate the cyclic nature of disturbances of the study area. These trends are shown in **Figure 4**.

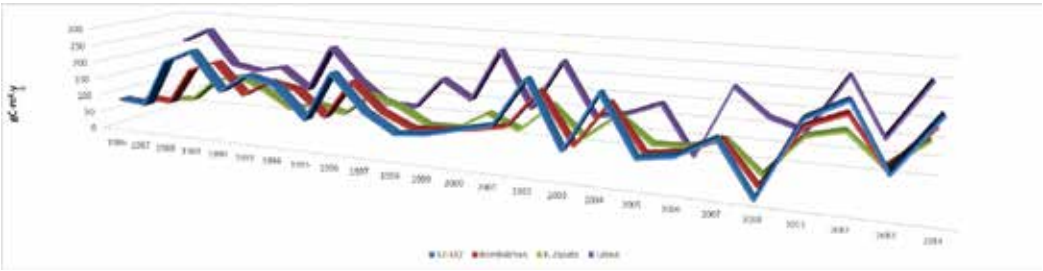

Figure 4. Trajectories of means of net primary productivity, central Yucatan, Mexico.

4. Conclusions

This chapter has shown how free remote sensing data (i.e. Landsat archive) can outline degradation by computing some indicators such as net primary productivity (NPP) and canopy cover (CC).

The key features and benefits of this methodology are (a) it is easy to implement, (b) it can be adaptable to specific site conditions, and (c) it allows an opportunity to identify regional trends by analyzing the indicators of degradation over time.

The main feature of this methodology is its suitability for use in many regions of the developing world where more sophisticated and, therefore, data-rich and demanding procedures are not possible. The trajectories of these degradation indicators can be used as a tool for regional monitoring of ecosystem condition and trends, enabling the formulation of remedial action plans.

The methodology described here also allows for the identification of the temporal and spatial distributions of forest degradation based on the indicators used.

The next steps for this methodology are:

a. To test and validate the method across the country and other regions. Partnership with the National Forestry Commission and the National Institute of Forestry, Agriculture and Livestock Research has been established.

b. To add the Eddy covariance tower network along with remote sensing data that are promissory elements to support NPP modeling in a reliable way in the country.

Acknowledgements

Acknowledgment is extended to the Mexican Council for Science and Technology (CONACyT) and the National Institute of Forestry, Agriculture and Livestock Research (INIFAP) of Mexico for funding this study.

Author details

Martin Enrique Romero-Sanchez*, Antonio Gonzalez-Hernandez and Francisco Moreno-Sanchez

*Address all correspondence to: romero.martin@inifap.gob.mx

National Institute of Forestry, Agriculture and Livestock Research, Mexico City, Mexico

References

[1] UNEP. Global Environment Outlook 3: Past, present and future perspectives. [Internet]. London, UK.: Earthscan; 2002. 34 p. Available from: http://www.unep.org/geo/geo3/english/pdfs/prelims.pdf

[2] Gonzalez P, Asner GP, Battles JJ, Lefsky MA, Waring KM, Palace M. Forest carbon densities and uncertainties from Lidar, QuickBird, and field measurements in California. Remote Sens Environ [Internet]. Elsevier Inc.; 2010 Jul [cited 2014 Jan 21];114(7): 1561–75. Available from: http://linkinghub.elsevier.com/retrieve/pii/S0034425710000702

[3] Baccini A, Laporte N, Goetz SJ, Sun M, Dong H. A first map of tropical Africa's above-ground biomass derived from satellite imagery. Environ Res Lett [Internet]. 2008 Oct 10 [cited 2014 Jan 23];3(4):045011. Available from: http://stacks.iop.org/1748-9326/3/i=4/a=045011?key=crossref.24eaa14be3435d90432b8de989ed79c3

[4] Popescu SC. Estimating biomass of individual pine trees using airborne lidar. Biomass and Bioenergy [Internet]. 2007 Sep [cited 2014 Feb 20];31(9):646–55. Available from: http://linkinghub.elsevier.com/retrieve/pii/S0961953407001316

[5] Wang G, Oyana T, Zhang M, Adu-Prah S, Zeng S, Lin H, et al. Mapping and spatial uncertainty analysis of forest vegetation carbon by combining national forest inventory data and satellite images. For Ecol Manage [Internet]. 2009 Sep [cited 2014 Feb 12]; 258(7):1275–83. Available from: http://linkinghub.elsevier.com/retrieve/pii/S0378112709004253

[6] Martinuzzi S, Gould WA, Ramos Gonzalez OM, Robles AM, Maldonado PC, Pérez-Buitrago N, et al. Mapping tropical dry forest habitats integrating Landsat NDVI, Ikonos imagery, and topographic information in the Caribbean Island of Mona. Rev Biol Trop. 2008;56(2):625–39.

[7] Castillo-Santiago MÁ, Ghilardi A, Oyama K, Hernández-Stefanoni JL, Torres I, Flamenco-Sandoval A, et al. Estimating the spatial distribution of woody biomass suitable for charcoal making from remote sensing and geostatistics in central Mexico. Energy Sustain Dev [Internet]. International Energy Initiative; 2013 Apr [cited 2014 Nov 29];17(2):177–88. Available from: http://linkinghub.elsevier.com/retrieve/pii/S0973082612000762

[8] Karl JW, Maurer BA. Multivariate correlations between imagery and field measurements across scales: comparing pixel aggregation and image segmentation. Landsc Ecol [Internet]. 2009 Dec 11 [cited 2014 Mar 23];25(4):591–605. Available from: http://link.springer.com/10.1007/s10980-009-9439-4

[9] Hu Q, Wu W, Xia T, Yu Q, Yang P, Li Z, et al. Exploring the use of google earth imagery and object-based methods in land use/cover mapping. remote sens [Internet]. 2013 Nov 15 [cited 2014 Mar 27];5(11):6026–42. Available from: http://www.mdpi.com/2072-4292/5/11/6026/

[10] Wulder MA, Masek JG, Cohen WB, Loveland TR, Woodcock CE. Opening the archive: how free data has enabled the science and monitoring promise of Landsat. Remote Sens Environ [Internet]. Elsevier B.V.; 2012 Jul [cited 2014 Apr 29];122:2–10. Available from: http://linkinghub.elsevier.com/retrieve/pii/S003442571200034X

[11] Cohen WB, Goward SN. Landsat's role in ecological applications of remote sensing. Bioscience [Internet]. 2004 [cited 2014 Apr 1];54(6):535. Available from: http://bioscience.oxfordjournals.org/content/54/6/535.full.pdf+html

[12] USGS. SLC-off gap-filled products. Gap-Fill Algorithm Methodology [Internet]. 2004. pp. 1–12. Available from: www.ga.gov.au/servlet/BigObjFileManager?bigobjid=GA4861

[13] Woodcock CE, Allen R, Anderson M, Belward A, Bindschadler R, Cohen W, et al. Free access to landsat imagery. Science [Internet]. 2008 May 23 [cited 2014 Apr 20];320(5879): 1011. Available from: http://www.ncbi.nlm.nih.gov/pubmed/18497274

[14] Roy DP, Wulder MA, Loveland TR, C.E. W, Allen RG, Anderson MC, et al. Landsat-8: science and product vision for terrestrial global change research. Remote Sens Environ [Internet]. Elsevier B.V.; 2014 Apr [cited 2014 Apr 28];145:154–72. Available from: http://linkinghub.elsevier.com/retrieve/pii/S003442571400042X

[15] Zolkos SG, Goetz SJ, Dubayah R. A meta-analysis of terrestrial aboveground biomass estimation using lidar remote sensing. Remote Sens Environ [Internet]. Elsevier Inc.; 2013 Jan [cited 2014 Mar 2];128:289–98. Available from: http://linkinghub.elsevier.com/retrieve/pii/S0034425712004051

[16] Hansen MC, Potapov P V, Moore R, Hancher M, Turubanova S a, Tyukavina a, et al. High-resolution global maps of 21st-century forest cover change. Science [Internet]. 2013 Nov 15 [cited 2014 Mar 20];342(6160):850–3. Available from: http://www.ncbi.nlm.nih.gov/pubmed/24233722

[17] Goetz SJ, Baccini A, Laporte NT, Johns T, Walker W, Kellndorfer J, et al. Mapping and monitoring carbon stocks with satellite observations: a comparison of methods. Carbon Balance Manag [Internet]. 2009 Jan [cited 2014 Feb 21];4:2. Available from: http://www.pubmedcentral.nih.gov/articlerender.fcgi?artid=2667409&tool=pmcentrez&rendertype=abstract

[18] Ahmed OS. Methodology for the assessment of the impacts of climate change on land degradation at multiple scales: use of high resolution satellite imagery, modelling, and ground measurements for the assessment in Ethiopia. Trent University: Ontario, Canada; 2012.

[19] UNCCD. Desertification: the invisible frontline. [Internet]. 2014. Available from: http://www.unccd.int/Lists/SiteDocumentLibrary/Publications/NEW_Invisible_Front_Line_ EN.pdf

[20] LADA Land Degradation Assessment in Drylands. Guidelines for the identification, selection and description of nationally based indicators of land degradation and improvement [Internet]. UNEP: Rome, Italy; 2009. p. 57. Available from: http://www.fao.org/nr/lada/index.php?option=com_content&view=article&id=152&Itemid=168&lang=en

[21] Ponce-Hernandez R, Koohafkan P. A methodology for land degradation assessment at multiple scales based on the DPSIR approach: experiences from applications to drylands. In: Zdruli P, Pagliai M, Kapur S, Faz Cano A, editors. Land Degradation and Desertification: Assessment, Mitigation and Remediation [Internet]. Dordrecht: Springer Netherlands; 2010 [cited 2014 Aug 19]. pp. 49–65. Available from: http://link.springer.com/10.1007/978-90-481-8657-0

[22] GOFC-GOLD. A sourcebook of methods and procedures for monitoring and reporting anthropogenic greenhouse gas emissions and removals caused by deforestation, gain and losses of carbon stocks in forests remaining forests, and forestation. Report Version

COP17-1. [Internet]. Alberta, Canada; 2011. Available from: http://www.gofc-gold.uni-jena.de/redd/

[23] Gibbs HK, Brown S, Niles JO, Foley Ja. Monitoring and estimating tropical forest carbon stocks: making REDD a reality. Environ Res Lett [Internet]. 2007 Oct 5 [cited 2014 Mar 22];2(4):045023. Available from: http://stacks.iop.org/1748-9326/2/i=4/a=045023?key=crossref.4118e8af5a9a3ac02c1bb32f8a92c50f

[24] Olander LP, Gibbs HK, Steininger M, Swenson JJ, Murray BC. Reference scenarios for deforestation and forest degradation in support of REDD: a review of data and methods. Environ Res Lett [Internet]. 2008 Apr 11 [cited 2014 Jan 28];3(2):025011. Available from: http://stacks.iop.org/1748-9326/3/i=2/a=025011?key=crossref.7b824939f979eb52873acc0988b80a16

[25] Asner GP, Powell GVN, Mascaro J, Knapp DE, Clark JK, Jacobson J, et al. High-resolution forest carbon stocks and emissions in the Amazon. Proc Natl Acad Sci U S A [Internet]. 2010 Sep 21 [cited 2014 Feb 21];107(38):16738–42. Available from: http://www.pubmedcentral.nih.gov/articlerender.fcgi?artid=2944749&tool=pmcentrez&rendertype=abstract

[26] Joseph S, Murthy MSR, Thomas AP. The progress on remote sensing technology in identifying tropical forest degradation: a synthesis of the present knowledge and future perspectives. Environ Earth Sci [Internet]. 2010 Dec 30 [cited 2014 Jul 23];64(3):731–41. Available from: http://link.springer.com/10.1007/s12665-010-0893-8

[27] Franklin SE. Remote sensing for sustainable forest management [Internet]. New York: Lewis; 2001. 407 p. Available from: http://www.amazon.ca/exec/obidos/redirect?tag=citeulike09-20&path=ASIN/1566703948

[28] Mascaro J, Detto M, Asner GP, Muller-Landau HC. Evaluating uncertainty in mapping forest carbon with airborne LiDAR. Remote Sens Environ [Internet]. Elsevier Inc.; 2011 Dec [cited 2014 Jan 20];115(12):3770–4. Available from: http://linkinghub.elsevier.com/retrieve/pii/S0034425711002720

[29] Olander LP, Galik CS, Kissinger GA. Operationalizing REDD+: scope of reduced emissions from deforestation and forest degradation. Curr Opin Environ Sustain [Internet]. Elsevier B.V.; 2012 Dec [cited 2014 Feb 18];4(6):661–9. Available from: http://linkinghub.elsevier.com/retrieve/pii/S1877343512000942

[30] Herold M, Román-Cuesta RM, Mollicone D, Hirata Y, Van Laake P, Asner GP, et al. Options for monitoring and estimating historical carbon emissions from forest degradation in the context of REDD+. Carbon Balance Manag [Internet]. BioMed Central Ltd; 2011 Jan [cited 2014 Mar 2];6(1):13. Available from: http://www.pubmedcentral.nih.gov/articlerender.fcgi?artid=3233497&tool=pmcentrez&rendertype=abstract

[31] Souza, Jr C, Firestone L, Moreira Silva L, Roberts D. Mapping forest degradation in the Eastern Amazon from SPOT 4 through spectral mixture models. Remote Sens Environ

[Internet]. 2003 Nov 15 [cited 2014 Nov 22];87(4):494–506. Available from: http://linkinghub.elsevier.com/retrieve/pii/S0034425703002086

[32] Panta M, Kim K, Joshi C. Temporal mapping of deforestation and forest degradation in Nepal: Applications to forest conservation. For Ecol Manage [Internet]. 2008 Oct [cited 2014 Jan 27];256(9):1587–95. Available from: http://linkinghub.elsevier.com/retrieve/pii/S0378112708005616

[33] Tang L, Shao G, Piao Z, Dai L, Jenkins MA, Wang S, et al. Forest degradation deepens around and within protected areas in East Asia. Biol Conserv [Internet]. Elsevier Ltd; 2010 May [cited 2014 Feb 6];143(5):1295–8. Available from: http://linkinghub.elsevier.com/retrieve/pii/S000632071000025X

[34] Eckert S, Ratsimba HR, Rakotondrasoa LO, Rajoelison LG, Ehrensperger A. Deforestation and forest degradation monitoring and assessment of biomass and carbon stock of lowland rainforest in the Analanjirofo region, Madagascar. For Ecol Manage [Internet]. Elsevier B.V.; 2011 Dec [cited 2014 Mar 2];262(11):1996–2007. Available from: http://linkinghub.elsevier.com/retrieve/pii/S0378112711005330

[35] Mon MS, Mizoue N, Htun NZ, Kajisa T, Yoshida S. Factors affecting deforestation and forest degradation in selectively logged production forest: a case study in Myanmar. For Ecol Manage [Internet]. Elsevier B.V.; 2012 Mar [cited 2014 Feb 21];267:190–8. Available from: http://linkinghub.elsevier.com/retrieve/pii/S0378112711007213

[36] Kronseder K, Ballhorn U, Böhm V, Siegert F. Above ground biomass estimation across forest types at different degradation levels in Central Kalimantan using LiDAR data. Int J Appl Earth Obs Geoinf [Internet]. Elsevier B.V.; 2012 Aug [cited 2014 Mar 5];18:37–48. Available from: http://linkinghub.elsevier.com/retrieve/pii/S0303243412000128

[37] Asner GP, Mascaro J. Mapping tropical forest carbon: Calibrating plot estimates to a simple LiDAR metric. Remote Sens Environ [Internet]. Elsevier Inc.; 2014 Jan [cited 2014 Jan 20];140:614–24. Available from: http://linkinghub.elsevier.com/retrieve/pii/S003442571300360X

[38] GFOI. Integrating remote-sensing and ground-based observations for estimation of emissions and removals of greenhouse gases in forests: methods and guidance from global forest observations initiative. 2014th ed. Geneva, Switzerland: Group on Earth Observations; 2013. 164 p.

[39] Wulder MA, Kurz WA, Gillis M. National level forest monitoring and modeling in Canada. Prog Plann [Internet]. 2004 May [cited 2014 Mar 12];61(4):365–81. Available from: http://linkinghub.elsevier.com/retrieve/pii/S0305900603000692

[40] Nadkarni NM, Parker GG, Rinker HB, Jarzen DM. The nature of forest canopies. In: Lowman M, Rinker B, editors. Forest Canopies. second edition. Sarasota, Florida: Elsevier Inc.; 2004. p. 517.

[41] Sexton JO, Song X-P, Feng M, Noojipady P, Anand A, Huang C, et al. Global, 30-m resolution continuous fields of tree cover: landsat-based rescaling of MODIS vegetation

continuous fields with lidar-based estimates of error. Int J Digit Earth [Internet]. Taylor & Francis; 2013 Sep [cited 2014 Feb 13];6(5):427–48. Available from: http://www.tandfonline.com/doi/abs/10.1080/17538947.2013.786146

[42] Nandy S, Kushwaha SPS, Dadhwal VK. Forest degradation assessment in the upper catchment of the river Tons using remote sensing and GIS. Ecol Indic [Internet]. Elsevier Ltd; 2011 Mar [cited 2014 Feb 20];11(2):509–13. Available from: http://linkinghub.elsevier.com/retrieve/pii/S1470160X10001299

[43] Deutscher J, Perko R, Gutjahr K, Hirschmugl M, Schardt M. Mapping tropical rainforest canopy disturbances in 3D by COSMO-SkyMed spotlight InSAR-Stereo data to detect areas of forest degradation. Remote Sens [Internet]. 2013 Feb 4 [cited 2014 Mar 1];5(2): 648–63. Available from: http://www.mdpi.com/2072-4292/5/2/648/

[44] Souza, Jr C, Siqueira J, Sales M, Fonseca A, Ribeiro J, Numata I, et al. Ten-year landsat classification of deforestation and forest degradation in the Brazilian Amazon. Remote Sens [Internet]. 2013 Oct 28 [cited 2014 Feb 25];5(11):5493–513. Available from: http://www.mdpi.com/2072-4292/5/11/5493/

[45] Lu L, Li X, Veroustraete F, Kang E, Wang J. Analysing the forcing mechanisms for net primary productivity changes in the Heihe River Basin, north-west China. Int J Remote Sens [Internet]. 2009 [cited 2014 Mar 12];30(3):793–816. Available from: http://www.tandfonline.com/doi/abs/10.1080/01431160802438530

[46] Huang N, Niu Z, Wu C, Tappert MC. Modeling net primary production of a fast-growing forest using a light use efficiency model. Ecol Modell [Internet]. Elsevier B.V.; 2010 Dec [cited 2014 Mar 12];221(24):2938–48. Available from: http://linkinghub.elsevier.com/retrieve/pii/S0304380010004552

[47] Seaquist JW, Olsson L, Ardö J. A remote sensing-based primary production model for grassland biomes. Ecol Modell. 2003;169:131–55.

[48] Running SW, Nemani RR, Heinsch FA, Zhao M, Reeves M, Hashimoto H. A continuous satellite-derived measure of global terrestrial primary production [Internet]. BioScience. 2004. p. 547. Available from: http://www.jstor.org/stable/3333948

[49] Bai Z, Dent D, Olsson L, Schaepman M. Global assessment of land degradation and improvement. 1. Identification by remote sensing [Internet]. … Soil Reference and Information …. 2008. Available from: http://www.isric.nl/ISRIC/webdocs/docs/report 2008_01_glada international_rev_aug 2008.pdf

[50] Romero-Sanchez ME, Ponce-Hernandez R. The assessment of forest degradation in dry forested lands: mapping regional trend indicators of degradation in the Yucatan Peninsula, Mexico with satellite data. In: Hubert B, Broin M, editors. 3rd UNCCD Scienitific Conference: "Combating desertification/land degradation and drought for poverty reduction and sustainable development: the contribution of science, technology, traditional knowledge and practices". Montpelier, France: Agropolis International; 2015. pp. 284–5.

[51] Monteith JL. Solar radiation and productivity in tropical ecosystems. J Appl Ecol. 1972; 9:747-766.

[52] Verstraeten WW, Veroustraete F, Feyen J. On temperature and water limitation of net ecosystem productivity: implementation in the C-Fix model. Ecol Modell [Internet]. 2006 Nov [cited 2014 Mar 12];199(1):4–22. Available from: http://linkinghub.elsevier.com/retrieve/pii/S0304380006002778

[53] McCallum I, Wagner W, Schmullius C, Shvidenko A, Obersteiner M, Fritz S, et al. Satellite-based terrestrial production efficiency modeling. Carbon Balance Manag [Internet]. 2009 Jan [cited 2014 Jan 23];4:8. Available from: http://www.pubmedcentral.nih.gov/articlerender.fcgi?artid=2754440&tool=pmcentrez&rendertype=abstract

[54] Li S. Monitoring of Net Primary Production in California rangelands using landsat and MODIS satellite remote sensing. Nat Resour [Internet]. 2012 [cited 2014 Mar 5];03(02): 56–65. Available from: http://www.scirp.org/journal/PaperDownload.aspx?DOI=10.4236/nr.2012.32009

[55] Veroustraete F. On the use of a simple deciduous forest model for the interpretation of climate change effects at the level of carbon dynamics. Ecol Modell [Internet]. 1994 Sep [cited 2015 Jan 7];75–76:221–37. Available from: http://linkinghub.elsevier.com/retrieve/pii/0304380094900213

[56] Sabbe H, Veroustraete F. Estimation of net primary and net ecosystem productivity of European terrestrial ecosystems by means of the C-Fix model and NOAA / AVHRR data. 1996;1990(April 1992).

[57] Veroustraete F, Sabbe H, Eerens H. Estimation of carbon mass fluxes over Europe using the C-Fix model and Euroflux data. Remote Sens Environ [Internet]. 2002 Dec;83(3): 376–99. Available from: http://linkinghub.elsevier.com/retrieve/pii/S0034425702000433

[58] Ponce-Hernandez R, Ahmed OS. An approach to the assessment of historic trends of land degradation indicators at national scales: use of MODIS and AVHRR coarse resolution vegetation products for mapping in Ethiopia. In: Hubert B, Broin M, editors. 3rd UNCCD Scienitific Conference: "Combating desertification/land degradation and drought for poverty reduction and sustainable development: the contribution of science, technology, traditional knowledge and practices". Montpelier, France: Agropolis International; 2015. p. 277–8.

[59] Wulder MA, White JC, Goward SN, Masek JG, Irons JR, Herold M, et al. Landsat continuity: issues and opportunities for land cover monitoring. Remote Sens Environ [Internet]. 2008 Mar [cited 2014 Feb 21];112(3):955–69. Available from: http://linkinghub.elsevier.com/retrieve/pii/S0034425707003331

[60] Hansen M, Loveland T. A review of large area monitoring of land cover change using Landsat data. Remote Sens Environ [Internet]. Elsevier Inc.; 2012 Jul [cited 2014 Jan 20]; 122:1–9. Available from: http://linkinghub.elsevier.com/retrieve/pii/

S0034425712000314\nhttp://www.sciencedirect.com/science/article/pii/S0034425712000314

[61] Kennedy RE, Yang Z, Cohen WB. Detecting trends in forest disturbance and recovery using yearly Landsat time series: 1. LandTrendr — Temporal segmentation algorithms. Remote Sens Environ [Internet]. Elsevier Inc.; 2010 Dec 15 [cited 2014 Jan 20];114(12): 2897–910. Available from: http://linkinghub.elsevier.com/retrieve/pii/S0034425710002245

[62] Pflugmacher D, Cohen WB, Kennedy RE. Using Landsat-derived disturbance history (1972–2010) to predict current forest structure. Remote Sens Environ [Internet]. 2012 Jul [cited 2014 Feb 21];122:146–65. Available from: http://linkinghub.elsevier.com/retrieve/pii/S0034425712000533

[63] DeVries B, Verbesselt J, Kooistra L, Herold M. Robust monitoring of small-scale forest disturbances in a tropical montane forest using Landsat time series. Remote Sens Environ [Internet]. Elsevier Inc.; 2015; Available from: http://linkinghub.elsevier.com/retrieve/pii/S0034425715000656

[64] Lhermitte S, Verbesselt J, Verstraeten WW, Coppin P. A comparison of time series similarity measures for classification and change detection of ecosystem dynamics. Remote Sens Environ [Internet]. 2011 Dec [cited 2014 May 24];115(12):3129–52. Available from: http://linkinghub.elsevier.com/retrieve/pii/S0034425711002446

[65] Hilker T, Wulder MA, Coops NC, Seitz N, White JC, Gao F, et al. Generation of dense time series synthetic Landsat data through data blending with MODIS using a spatial and temporal adaptive reflectance fusion model. Remote Sens Environ [Internet]. 2009 Sep [cited 2014 Feb 26];113(9):1988–99. Available from: http://linkinghub.elsevier.com/retrieve/pii/S0034425709001709

[66] Upadhyay TP, Sankhayan PL, Solberg B. A review of carbon sequestration dynamics in the Himalayan region as a function of land-use change and forest/soil degradation with special reference to Nepal. Agric Ecosyst Environ [Internet]. 2005 Feb [cited 2014 Feb 20];105(3):449–65. Available from: http://linkinghub.elsevier.com/retrieve/pii/S0167880904002865

[67] Zhu Z, Woodcock CE, Olofsson P. Continuous monitoring of forest disturbance using all available Landsat imagery. Remote Sens Environ [Internet]. Elsevier Inc.; 2012 Jul [cited 2014 Jan 20];122:75–91. Available from: http://linkinghub.elsevier.com/retrieve/pii/S0034425712000387

[68] Kennedy RE, Cohen WB, Schroeder TA. Trajectory-based change detection for automated characterization of forest disturbance dynamics. Remote Sens Environ [Internet]. 2007 Oct [cited 2014 Mar 24];110(3):370–86. Available from: http://linkinghub.elsevier.com/retrieve/pii/S0034425707001216

[69] Cohen WB, Yang Z, Kennedy R. Detecting trends in forest disturbance and recovery using yearly Landsat time series: 2. TimeSync — Tools for calibration and validation.

Remote Sens Environ [Internet]. Elsevier B.V.; 2010 Dec 15 [cited 2014 Feb 25];114(12): 2911–24. Available from: http://linkinghub.elsevier.com/retrieve/pii/S0034425710002269

[70] Hussain M, Chen D, Cheng A, Wei H, Stanley D. Change detection from remotely sensed images: from pixel-based to object-based approaches. ISPRS J Photogramm Remote Sens [Internet]. International Society for Photogrammetry and Remote Sensing, Inc. (ISPRS); 2013;80:91–106. Available from: http://dx.doi.org/10.1016/j.isprsjprs.2013.03.006

[71] Lu D, Mausel P, Brondízio E, Moran E. Change detection techniques. Int J Remote Sens [Internet]. 2004 Jun [cited 2014 Jul 21];25(12):2365–401. Available from: http://www.tandfonline.com/doi/abs/10.1080/0143116031000139863

[72] CONAFOR, Chapingo UA. Land Degradation and Desertification baseline: Final report. Jalisco, Mexico. 2014.

[73] CONAFOR. National system of forest information: national forest and soils inventory. [Internet]. 2012. Available from: http://www.cnf.gob.mx:8080/snif/portal/infys

[74] Ju J, Roy DP. The availability of cloud-free Landsat ETM+ data over the conterminous United States and globally. Remote Sens Environ [Internet]. 2008 Mar [cited 2014 Apr 17];112(3):1196–211. Available from: http://linkinghub.elsevier.com/retrieve/pii/S0034425707004002

[75] Masek JG, Vermote EF, Saleous NE, Wolfe R, Hall FG, Huemmrich KF, et al. A Landsat surface reflectance dataset for North America, 1990–2000. IEEE Geosci Remote Sens Lett [Internet]. 2006 Jan [cited 2014 Apr 29];3(1):68–72. Available from: http://ieeexplore.ieee.org/lpdocs/epic03/wrapper.htm?arnumber=1576692

[76] Zhu X, Liu D, Chen J. A new geostatistical approach for filling gaps in Landsat ETM+ SLC-off images. Remote Sens Environ [Internet]. 2012 Sep [cited 2014 Jan 28];124:49–60. Available from: http://linkinghub.elsevier.com/retrieve/pii/S0034425712001952

[77] Romero-Sanchez ME, Ponce-Hernandez R, Franklin SE, Aguirre-Salado CA. Comparison of data gap-filling methods for Landsat ETM+ SLC-off imagery for monitoring forest degradation in a semi-deciduous tropical forest in Mexico. Int J Remote Sens [Internet]. 2015;36(11):2786–99. Available from: http://www.tandfonline.com/doi/full/10.1080/01431161.2015.1047991

[78] Asner GP. Automated mapping of tropical deforestation and forest degradation: CLASlite. J Appl Remote Sens [Internet]. 2009 Aug 1 [cited 2014 Jan 20];3(1):033543. Available from: http://remotesensing.spiedigitallibrary.org/article.aspx?doi=10.1117/1.3223675

[79] Asner GP, Heidebrecht KB. Spectral unmixing of vegetation, soil and dry carbon in arid regions: comparing multispectral and hyperspectral observations. Int J Remote Sens. 2002;23(19):3939–58.

[80] Asner GP, Keller M, Pereira R, Zweede JC, Jose N, Silva M. Canopy damage and recovery after selective logging in Amazonia: field and satellite studies. Ecol Appl. 2004;14(4):280–98.

[81] Smith AMS, Falkowski MJ, Hudak AT, Evans JS, Robinson AP, Steele CM. A cross-comparison of field, spectral, and lidar estimates of forest canopy cover. Can J Remote Sens. 2009;35(5):447–59.

[82] Ahmed OS, Franklin SE, Wulder MA. Integration of Lidar and Landsat data to estimate forest canopy cover in Coastal British Columbia. Photogramm Eng Remote Sens [Internet]. 2014 Oct 1 [cited 2015 Jan 15];80(10):953–61. Available from: http://essential.metapress.com/openurl.asp?genre=article&id=doi:10.14358/PERS.80.10.953

[83] Yuan W, Liu S, Zhou G, Zhou G, Tieszen LL, Baldocchi D, et al. Deriving a light use efficiency model from eddy covariance flux data for predicting daily gross primary production across biomes. Agric For Meteorol. 2007;143(3–4):189–207.

[84] Running SW, Thornton PE, Nemani RR, Glassy JM. Global terrestrial gross and net primary productivity from the earth observating system. In: Sala OE, Jackson RB, Mooney HA, Howart RW, editors. Methods in ecosystem science. Springer New York; 2000. p. 44–57.

[85] Running SW, Nemani R, Glassy JM, Thornton PE. Modis Daily Photosynthesis (Psn) and Annual Net Primary Production (Npp) Product. Report. Oak Ridge, Tennessee, USA.; 1999. 1-59.

[86] Raich JW, Rastetter EB, Melillo JM, Kicklighter DW, Steudler PA, Peterson BJ, et al. Potential net primary productivity in South America: application of a global model. Ecol Appl [Internet]. 1991;1(4):399–429. Available from: http://www.jstor.org/stable/1941899

[87] Medina E, Klinge H. Productivity of tropical forests and tropical woodlands. In: Lange O., Nobel PS, Osmond CB, Ziegler H, editors. Physiological Plant Ecology IV [Internet]. New York, NY: Springer Berlin Heidelberg; 1983. pp. 281–303. Available from: http://link.springer.com/chapter/10.1007/978-3-642-68156-1_10

[88] Xiao X, Hollinger D, Aber J, Goltz M, Davidson E a., Zhang Q, et al. Satellite-based modeling of gross primary production in an evergreen needleleaf forest. Remote Sens Environ. 2004;89(4):519–34.

[89] Verbesselt J, Zeileis A, Herold M. Near real-time disturbance detection using satellite image time series. Remote Sens Environ [Internet]. Elsevier Inc.; 2012 Aug [cited 2014 Mar 3];123:98–108. Available from: http://linkinghub.elsevier.com/retrieve/pii/S0034425712001150

[90] Gao J. Digital Analysis of Remotely Sensed Imagery. New York, NY: McGraw-Hill; 2009.

[91] Otsu N. A Threshold selection method from gray-level histograms. IEEE Trans Syst Man Cybern [Internet]. 1979;9(1):62–6. Available from: http://ieeexplore.ieee.org/stamp/stamp.jsp?arnumber=4310076

[92] Prieto-Blanco A, North PRJ, Barnsley MJ, Fox N. Satellite-driven modelling of Net Primary Productivity (NPP): theoretical analysis. Remote Sens Environ [Internet]. Elsevier Inc.; 2009 Jan [cited 2014 Feb 7];113(1):137–47. Available from: http://linkinghub.elsevier.com/retrieve/pii/S0034425708002708

[93] Wang L, Gong W, Ma Y, Zhang M. Modeling regional vegetation NPP variations and their relationships with climatic parameters in Wuhan, China. Earth Interact. 2013;17(4):1-20.

[94] Ruimy A, Kergoat L, Bondeau A, Intercomparison TP of the PNPPM. Comparing global models of terrestrial net primary productivity (NPP): analysis of differences in light absorption and light use efficiency. Glob Chang Biol. 1999;5:56–65.

Chapter 2

Land-Atmosphere Interaction in the Southwestern Karst Region of China

Jiangbo Gao, Wenjuan Hou, Kewei Jiao and Shaohong Wu

Additional information is available at the end of the chapter

http://dx.doi.org/10.5772/64740

Abstract

Land-atmosphere interaction in the southwestern Karst region of China was investigated from two aspects: response of land cover to climate change and climatic effects of Karst rocky desertification. The first part focused on the temporal-spatial variation of growing-season normalized difference vegetation index (NDVI) and its relationship with climate variables. The relationships between growing-season NDVI with temperature and precipitation were both positive, indicating its limiting role on the distribution and dynamic of vegetation cover in the study area. The second part was designed to investigate whether the changed vegetation cover and land surface processes in the Karst regions was capable of modifying the summer climate simulation over East Asia. It was shown that land desertification resulted in the reduced net radiation and evaporation in the degraded areas. The East Asian summer monsoon was weakened after land degradation. Such circulation differences favored the increase in moisture flux and clouds, and thereby causing more precipitation in southeast coastal areas. Based on the above findings, it can be concluded that vegetation cover in Karst region was sensitive to climate change at larger scale, and on the other hand, there was significant feedback of vegetation cover change to regional climate by altering water and energy balance.

Keywords: Karst rocky desertification, climate change, land cover, southwest China, land-atmosphere interaction

1. Introduction

During the past decades, the vegetation-climate interaction has been a research focus of meteorology, climatology, geography, and ecology. The contents mainly include the impact of climate change on ecosystem and the feedback of vegetation cover change to atmosphere. Investigation on the correlation between vegetation variation and climate change and its influencing mechanisms are the basis for the studies on climate change adaptation and mitigation.

The response of terrestrial ecosystem to climate change, a complex issue in the field of global change, has been focused on in the last 30 years [1]. Vegetation cover has been proven to be governed by climatic factors, such as precipitation, temperature, solar radiation, and CO_2 concentration. Therefore, variation in vegetation and its relationship with climatic factors reflected the sensitivity and vulnerability of the ecosystem to climate change (i.e., the responding processes) [2]. In many studies, the normalized difference vegetation index (NDVI) was selected to detect the impact of climate change on vegetation activity in Eurasia, [3–5]. Although the temperature increase was detected to dominate the vegetation cover and its dynamic in the northwestern China, western China, and the Tibetan Plateau, the impact of precipitation in the arid and semiarid regions may be more significant. The complicated and spatial heterogeneous effects of climate change on NDVI indicate the need to conduct further investigation at regional scales. Recently, in order to make clear the role of vegetation cover in the regional climate change, several studies on the feedback of land cover to atmosphere were conducted, especially after 1990s [6]. Land cover change (LCC) was documented as important as atmospheric circulation and solar orbit perturbations in climate change [7]. On the other hand, the feedback is regional-dependent due to the complicated climate and LCC in different regions.

The Karst region in the southwest China presents the transformation from vegetation covered landscape to exposed basement rocks, which was defined as the Karst rock desertification (KRD). In this region, the natural ecosystem is vulnerable while the human disturbance is severe. Earlier studies mainly emphasized the impact of land use change on vegetation cover [8–10], lacking consideration of climate change impacts at large scales. Furthermore, it is unknown the climatic effects of land cover change in the Karst region, especially land degradation. Therefore, in this chapter, the southwestern Karst region of China was selected to conduct land-atmosphere interactions research.

2. Study area

The southwestern Karst region of China, at 101°73'–112°44'E and 21°26'–29°25'N, and the Guizhou Karst Plateau, in the center of the southwestern Karst region (**Figure 1**), were selected to conduct research of climatic impacts on vegetation cover and climatic effects of vegetation degradation, respectively. They are located in the subtropical/tropical monsoon climate zone with annual precipitation of above 900 mm. The temperature and precipitation present great

http://dx.doi.org/10.5772/64740

difference in spatial patterns, because of the typical topographical features with widely distributed mountains. Besides the Guizhou Karst Plateau, the southwestern Karst region, approximately 5.5×10^6 km^2, includes Guangxi Zhuang Autonomous Region (GX) and eastern part of Yunnan Province (YN).

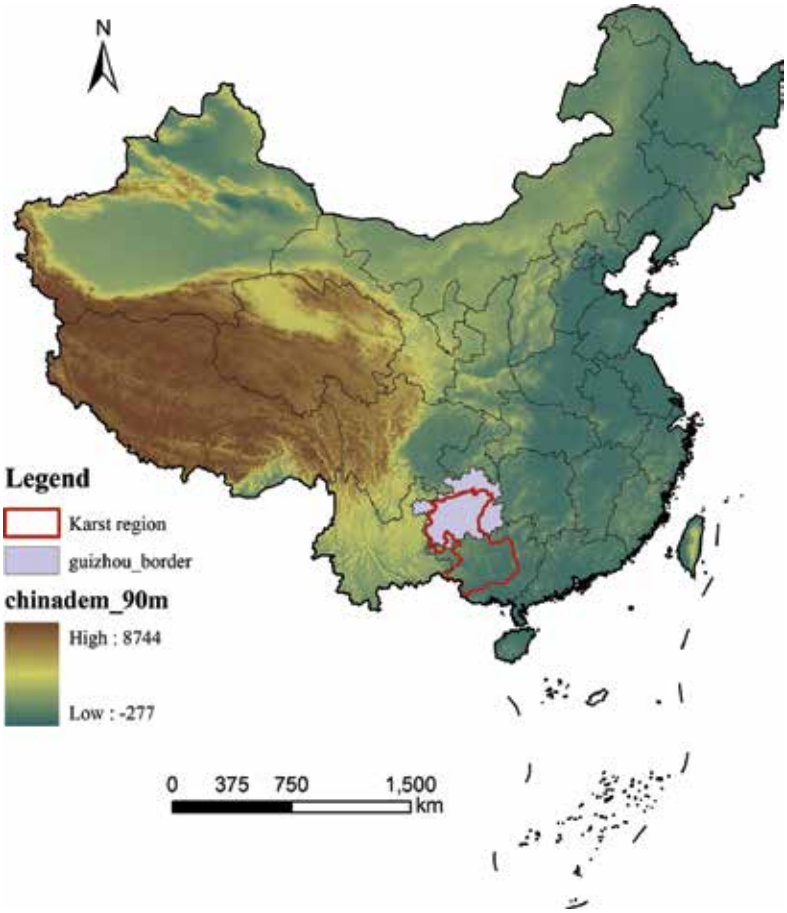

Figure 1. Location of the southwestern Karst region of China and the Guizhou Province of China.

There are six vegetation types in the study area, including broadleaf forest, coniferous forest, shrub, grass, meadow, and cultural vegetation, with shrub covering the largest area. Because of the widely distributing bare limestone and the unsuitable land use since 1950s, KRD covers over 20% of the total area with the desertification rate of 2.5×10^4 km^2 per year, and thus has become the most serious environmental problem in the study area. Rocky desertification in GKP exhibits three characteristics of severe degree, large area and high risk. However, litter research was carried out to assess the long-term vegetation dynamics and its influence on regional climate change.

3. Materials and methods

3.1. Statistical methods

3.1.1. Trend analysis

The NDVI trend from 1982 to 2013 at pixel scale was estimated using the ordinary least squares (OLS) based on the ArcGIS 10.1 platform:

$$\theta_{slope} = \frac{n \times \sum_{i=1}^{n} i \times NDVI - \sum_{i=1}^{n} i \sum_{i=1}^{n} NDVI_i}{n \times \sum_{i=1}^{n} i^2 - \left(\sum_{i=1}^{n} i \right)^2} \quad (1)$$

where θ is the regression slope and n represents the study year during the research period. The positive value of θ means increasing NDVI.

*3.1.2. Mann-Kendall **(MK) test***

Mann-Kendall analysis, applied as a nonparametric, rank-based method for evaluating trends in time-series data [11], was used to detect the changing trend because it is known as more resilient to outliers. A rank sequence (S_k) for time series was built:

$$S_K = \sum_{i=1}^{k} r_{i(k=2,3,\ldots,n)} \quad (2)$$

where k is the dataset record length over years, and r_i is the altered data series for original dataset:

$$r_i = \begin{pmatrix} 1 & x_i > x_j \\ 0 & x_i < x_j \end{pmatrix}_{(j=1,2,\ldots,i)} \quad (3)$$

Under the assumption of random and independent time series, the statistic Z is defined:

$$Z_k = \frac{[S_k - E(S_k)]}{\sqrt{Var(S_k)}} (k = 1, 2, \ldots, n) \quad (4)$$

Moreover, $Z_1 = 0$, $E(S_k)$ and Var (S_k) is the mathematical expectation and variance, respectively:

$$E(S_k) = \frac{n(n-1)}{4} \tag{5}$$

$$Var(S_k) = \frac{n(n-1)(2n+5)}{72} \tag{6}$$

The positive Z_k value means the trend is increasing. Compared Z_k with Z_α, the result of $|Z_k| > Z_\alpha$ ($Z0.05 = 1.96$) means the trend is statistically significant.

3.1.3. Ordinary linear square

In order to compare the relative importance of temperature and precipitation for NDVI, the multivariate regression and the standardized coefficients were applied together. The higher standardized values mean important roles. The MATLAB 8.1 was used to establish multivariate linear model:

$$NDVI = b_0 + b_1 \times Temperature + b_2 \times \mathrm{Pr}ecipitation + \varepsilon \tag{7}$$

where b_0, b_1, and b_2 are the regression parameters, while ε is the regression residual. Because of the different range for values of temperature and precipitation, it required normalization to compare the relative importance of climatic factors in the NDVI variations:

$$b_i^{'} = b_i \times \sqrt{\frac{\sum_{t=1}^{n}\left(x_t - \bar{x}\right)}{\sum_{t=1}^{n}\left(y_t - \bar{y}\right)}} \tag{8}$$

3.1.4. Geographically weighted regression (GWR)

The GWR analysis, coupled in ArcGIS 10.1, was conducted to reveal the spatial variations in relationships between NDVI and climatic variables. Both the spatial distribution and the dynamics of NDVI were considered by the GWR model. GWR extends the traditional OLS to consider the spatial heterogeneity in climate-vegetation correlations by assigning weight values [12]:

$$y_i = \beta_0(\mu_i, \nu_i) + \sum_{k=1}^{p}\beta_k(\mu_i, \nu_i)x_{ik} + \varepsilon_i \tag{9}$$

where y_i, x_{ik}, and ε_i, represent the dependent variable, the independent variables, and the random error term at location i, respectively. Note that (μ_i, ν_i) expresses the coordinate location of the ith point, k denotes the independent variable number. β_0 and β_k are the regression parameters at location i.

The regression coefficients were estimated by:

$$\beta(\mu_i,\nu_i) = (X^T W(\mu_i,\nu_i) X)^{-1} X^T W(\mu_i,\nu_i) Y \tag{10}$$

β is the unbiased estimate of the regression coefficient. W is the weighting matrix, and X and Y are matrices for independent and dependent variables, respectively. The kernel function, used to determine the weight, was performed as the exponential distance decay:

$$\omega_{ij} = \exp = \left(\frac{d_{ij}^2}{b^2} \right) \tag{11}$$

ω_{ij} expresses the weight of observation j for location i, d_{ij} represents the Euclidean distance between points i and j, and b is the kernel bandwidth.

3.2. WRF climate model and experimental design

The WRF-ARW was developed as the next generation for regional climate model. It includes different parameterization schemes for longwave and shortwave radiation, cloud microphysics, cumulus, and land surface processes. The simplified simple biosphere model (SSiB), coupled with WRF model, was selected to simulate land surface energy balance. According to the SSiB model description, there are 12 types of vegetation cover, while the vegetation and soil parameters were set for every types. Defining different vegetation cover types in this study enabled investigation of the impact of land degradation and Karst rocky desertification using the WRF-SSiB model. The domain for WRF model was set as follows: dimensions of 196 × 154 horizontal grid points with center at 35°N and 110°E. In this domain, the influencing factors for East Asian summer monsoon can be included, for example, the upper level westerly jet (ULJ) and low-level jet (LLJ), the Bay of Bengal and the southeast trade wind, and so on [13]. The WRF downscaling ability was assessed by comparing the simulations with different physical schemes (**Table 1**), and the optimal combination was concluded from the assessment. For the execution of the WRF, we used the NCEP DOE Reanalysis-2 [14], hereafter NCEP R-2, at 6-h intervals to provide initial conditions and lateral boundary conditions.

Two experiments were done. One was the Case C, using the original SSiB vegetation map (as shown in **Figure 2a**), the other was Case D with the degraded land cover types (**Figure 2b**). The degraded types were decided based on the spatial pattern of different rocky desertification degrees [15]. For example, if the deserted areas accounted more than 30% of the corresponding counties, the SSiB vegetation was modified to bare soil (type 11 in SSiB model). The type 9

(broadleaf shrubs with bare soil) was used to replace original vegetation types in areas described as desert and potential desert areas larger than 45% of the counties and smaller than 30% of the counties, respectively. Based on the reset of vegetation cover types, two vegetation maps were used in WRF model, and was further used to conduct Case C and Case D.

Cases	Microphysics	Long-wave radiation	Short-wave radiation	Factors	R	Bias	RMSE
1	WSM 3	RRTM	MM5(Dudhia)	Precipitation	0.70	1.68	4.07
				Temperature	0.89	3.48	4.65
2	Kessler	RRTM	MM5(Dudhia)	Precipitation	0.37	1.02	5.50
3	Purdue Lin	RRTM	MM5(Dudhia)	Precipitation	0.65	2.64	6.28
4	WSM5	RRTM	MM5(Dudhia)	Precipitation	0.67	2.84	6.58
5	Ferrier	RRTM	MM5(Dudhia)	Precipitation	0.66	2.81	6.30
6	WSM 3	CAM	CAM	Precipitation	0.65	1.91	4.33
				Temperature	0.88	2.97	4.08
7	WSM 3	RRTMG	RRTMG	Precipitation	0.67	3.04	5.41
				Temperature	0.89	2.24	3.65

R, correlation coefficient; RMSE: root mean square error.

Table 1. Descriptive statistics of precipitation and temperature from WRF/SSiB with different microphysics and radiation schemes for June 2000 over 18°-52°N, 86°-136°E.

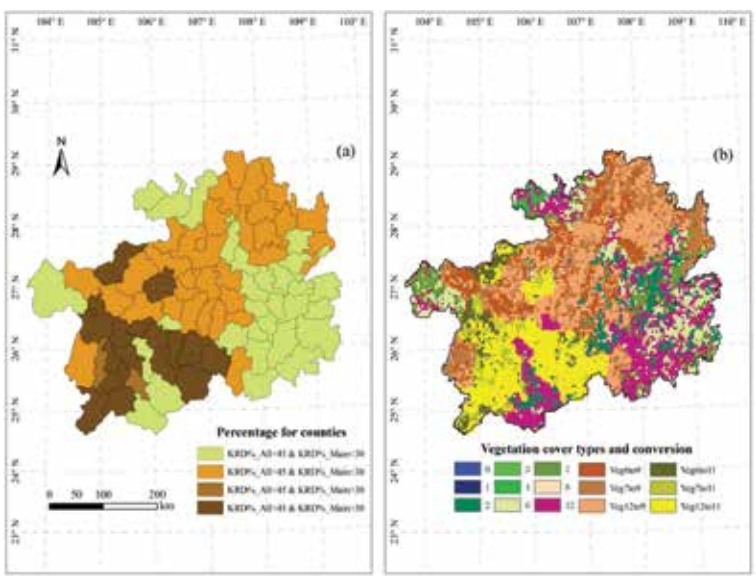

Figure 2. Potential LCC based on the spatial pattern of KRD in GKP. (a) The percentage of areas with KRD for counties. (b) SSiB vegetation map for GKP and vegetation cover conversion.

4. Results and discussion

4.1. Variations in growing-season NDVI

As shown in **Figure 3**, the rate of 0.0015/year during 1982–2013 was estimated for the growing-season NDVI trend in the Karst region of southwest China. The maximum value can be found in 2009 with significant variations between different years. It is indicated in **Figure 3(b)** that the year of 1994 was a tipping point, which means that there were two states before and after this year for the NDVI anomaly. We observed decreasing trend for some years, although the overall trend was increasing. Furthermore, the M-K trend test showed significant increasing trend, especially after the year 2004. As for the variation in NDVI of different vegetation types, the increasing rate was highest for coniferous forest, and the smallest value for meadow (**Table 2**).

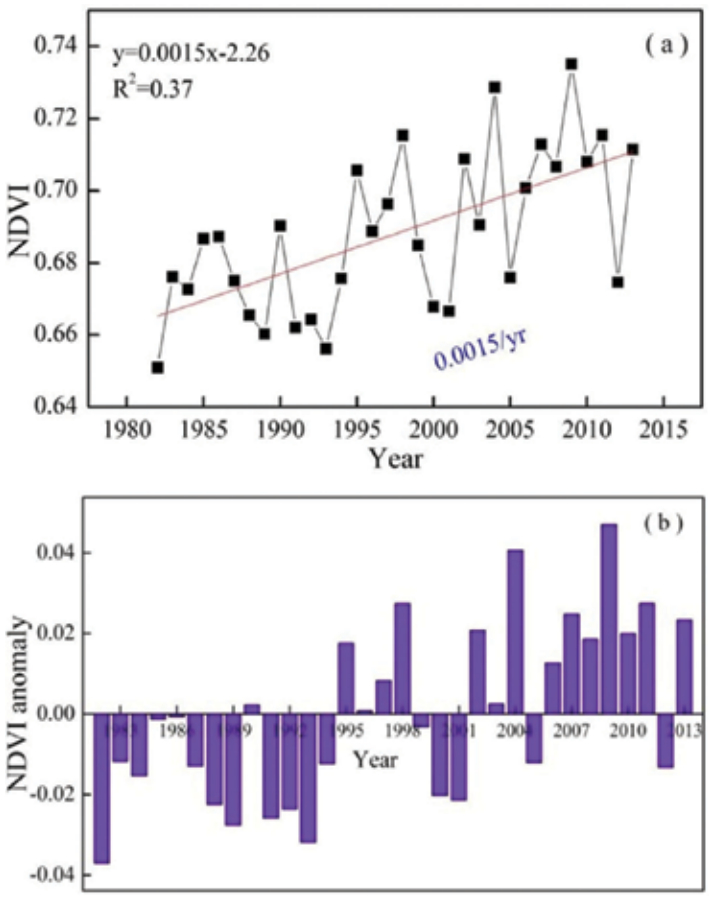

Figure 3. Interannual variations in growing-season NDVI (a) and NDVI anomaly (b) during 1982-2013 in the entire region, using the annual average growing-season NDVI.

http://dx.doi.org/10.5772/64740

Vegetation type	Growing-season NDVI value			NDVI rate	Correlation coefficients	
	Average	Maximum	Minimum		Temperature	Precipitation
Broadleaf forest	0.7412	0.8501	0.5056	0.0013	0.315**	0.173**
Shrub	0.6952	0.8369	0.4866	0.0015	0.149**	0.130**
Grassland	0.6946	0.8405	0.4126	0.0013	0.493**	0.289**
Coniferous forest	0.6871	0.8270	0.3932	0.0016	0.252**	0.063
Cultural vegetation	0.6706	0.8398	0.3576	0.0015	0.374**	0.182**
Meadow	0.5910	0.7319	0.4741	0.0008	0.412**	−0.109

**means a 0.01 significance level.

Table 2. Statistical characteristics of growing-season NDVI for different vegetation types during 1982–2013.

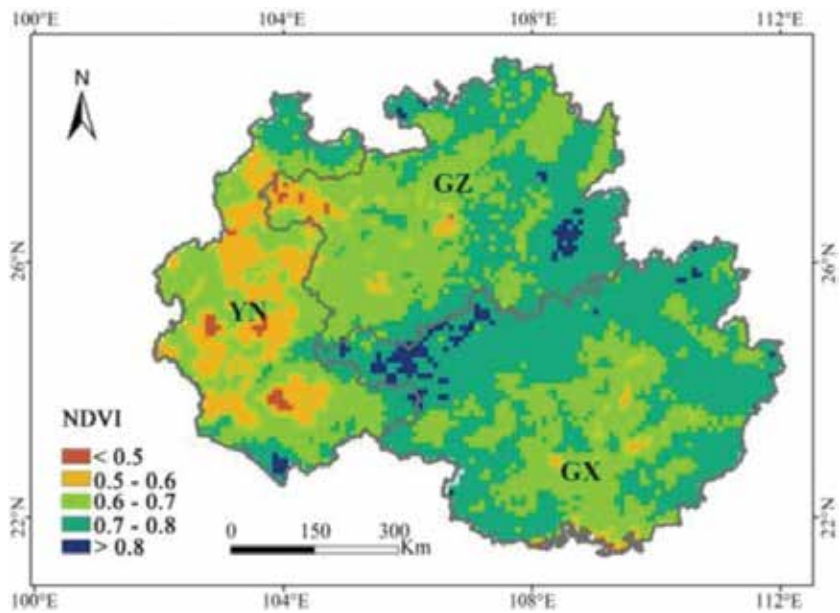

Figure 4. Spatial patterns of average values in growing-season NDVI during 1982–2013.

Figure 4 shows the spatial distribution of NDVI values in the study area, ranging from 0.32 to 0.85. Due to higher temperature and more precipitation in Guangxi Zhuang Autonomous Region, there were high values of NDVI in the east part of the study area. Under the background of complex climate change, there was also spatial heterogeneity for the dynamical variation of NDVI. The higher increasing rate was observed in the northwest and the smaller values in the southeast (**Figure 5**).

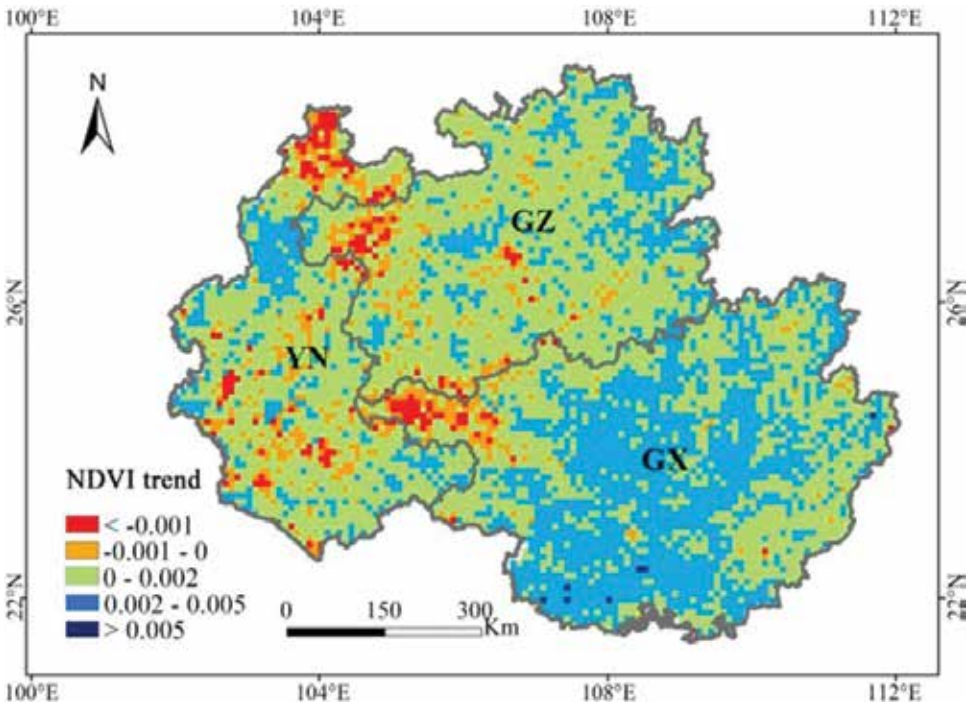

Figure 5. Spatial patterns of temporal trend in growing-season NDVI during 1982–2013.

4.2. Correlations between NDVI and climate factors

We observed warming rate of 0.018°C/year in the study area (**Figure 6a**). It fluctuated from −0.6 ~ 0.8°C for average growing-season temperature. The year of 1995 was a tipping point for temperature and NDVI changes. Specifically, the average temperature for different months presented obvious variations with a maximum temperature (25.2°C) in July. For the changes in precipitation, **Figure 6(c)** shows a decrease of −1.21mm/year during 1982–2013. The dynamic processes for precipitation can be classified as falling under three stages: 1982–1992, 1993–2002, and 2003–2013 (**Figure 6d**). Additionally, the significant uptrend for temperature can be concluded from the Mann-Kendall test.

http://dx.doi.org/10.5772/64740

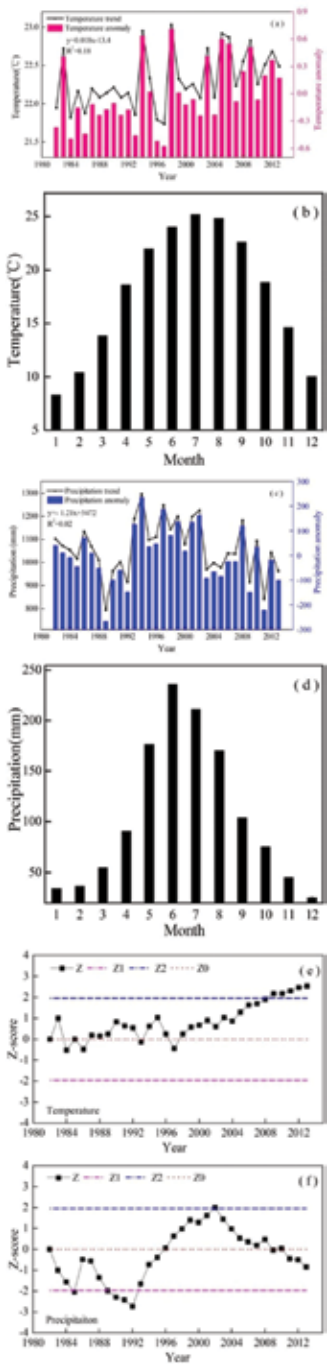

Figure 6. Interannual variations in average growing-season temperature trend and anomaly (**a**); monthly temperature (**b**); precipitation trend and anomaly (**c**); monthly precipitation (**d**); and the results (**e**, **f**) of Mann-Kendall test during 1982–2013 in the entire region.

4.2.1. Traditional linear regression for NDVI and climate variables

As shown in **Figure 7(a)**, there was obvious synergy for NDVI and temperature, but the synergy for NDVI and precipitation was relatively weak (**Figure 7b**). The lower regression coefficients of precipitation indicated the weaker impact of precipitation on vegetation cover change. The reason may be that there was rich rainfall in the study area, and the annual variation cannot play significant roles. Moreover, the correlations between NDVI and climatic variables were different for different vegetation types (shown in **Table 2**). The largest regression coefficient was in grassland.

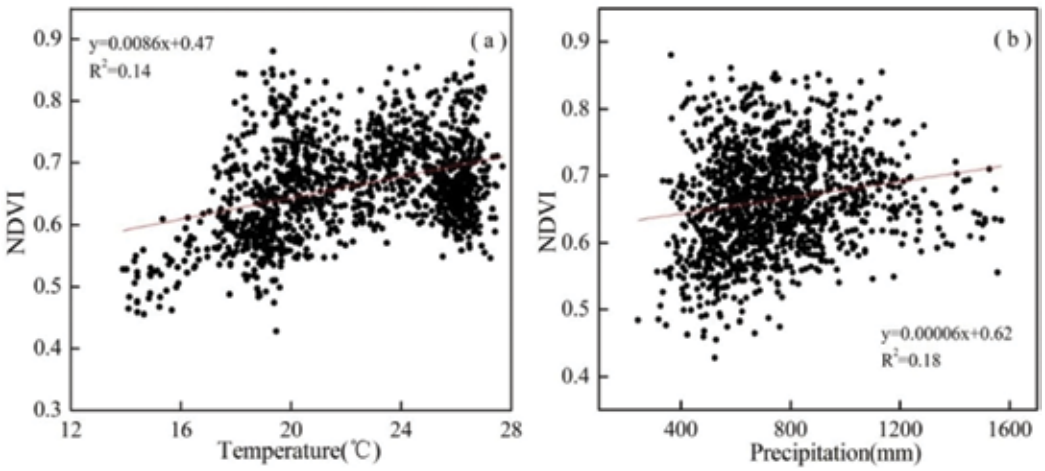

Figure 7. The overall relationship between annual growing-season NDVI and temperature (**a**); precipitation (**b**) during 1982–2013.

In most areas, the relationship between NDVI and temperature (**Figure 8a**) was positive due to the strengthened photosynthesis and vegetation activity by the increase in temperature. It should be pointed out that only within an appropriate range, the temperature rise can result in beneficial effects, and if the temperature is too high, it will cause negative impact on vegetation growth. **Figure 8(b)** shows the regression coefficient for NDVI and precipitation. Although the correlation was positive in most of the areas, there were some negative values in the northern part of the study area.

4.2.2. Local regression for the spatial relationships

The later one means applying the changing rate of NDVI (**Figure 5**) as the dependent variable of GWR while the changing rate of climatic factors as independent variables. **Figure 9** lists the GWR regression coefficients, where colors ranging from blue to red represented values from low to high. Additionally, the standard errors were analyzed by the points with different sizes.

There was positive relationships between multiyear average NDVI and temperature (**Figure 9a**), however, the regression coefficients for NDVI and precipitation contained both

http://dx.doi.org/10.5772/64740

positive and negative values (**Figure 9b**). It was found that the positive values for NDVI and precipitation were mainly located in Yunnan Province, where the climate is more arid than other areas of the study area. The GWR regression coefficients for dynamic relationships were listed in **Figure 9(c)** and **(d)**. The NDVI was lower with increasing surface temperature, which may be explained as more serious aridity due to the warming. On the other hand, the correlation between the changing rate of NDVI with precipitation were positive, meaning that the increase in NDVI during 1982–2013 could have been caused mainly by the precipitation variations.

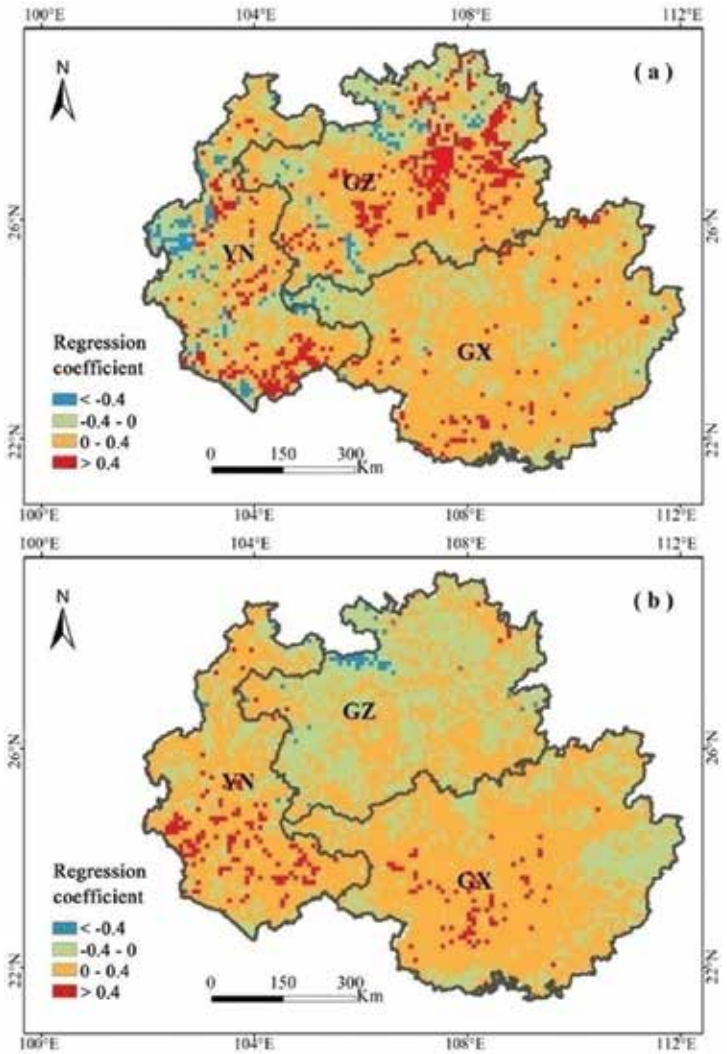

Figure 8. Multivariate regression coefficients of temperature (**a**); and precipitation (**b**) to NDVI based on pixel during 1982–2013.

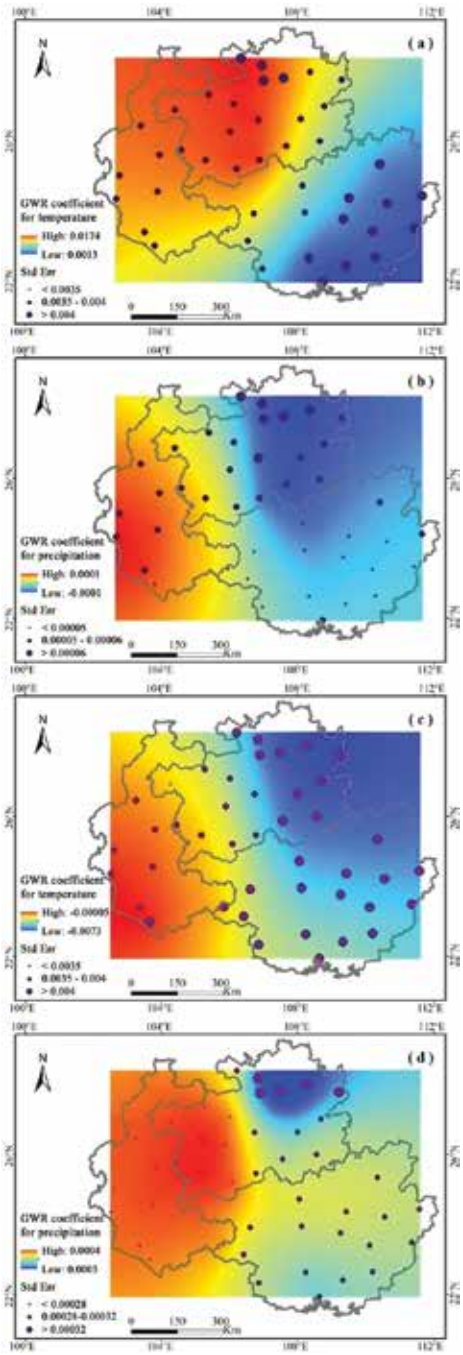

Figure 9. Geographically weighted regression analysis between NDVI and temperature and precipitation during 1982–2013. (**a**) Coefficients image for temperature; (**b**) coefficients image for precipitation; (**c**) coefficients image for temperature trend; (**d**) coefficients image for precipitation trend.

http://dx.doi.org/10.5772/64740

4.3. The decrease in NDVI during 2009–2012 and its climatic explanation

Additional to the uptrend of NDVI from 1982 to 2013, there were some years when the NDVI decreased, that is, from 2009 to 2012. The decreasing rate during this time was −0.017/year. The significant decline was mostly in Guizhou Province where a decreased rate less than −0.02/year was observed (**Figure 10**). Correlation analysis between NDVI and climate change, revealed that the impact of temperature on the decreased NDVI was more profound than that from precipitation (**Figure 11**). Furthermore, the negative relationships between NDVI and precipitation also indicated the indirect impact of precipitation on temperature change. The increase in precipitation with more cloud could have led to the decrease in solar radiation and temperature, thus inhibiting photosynthesis.

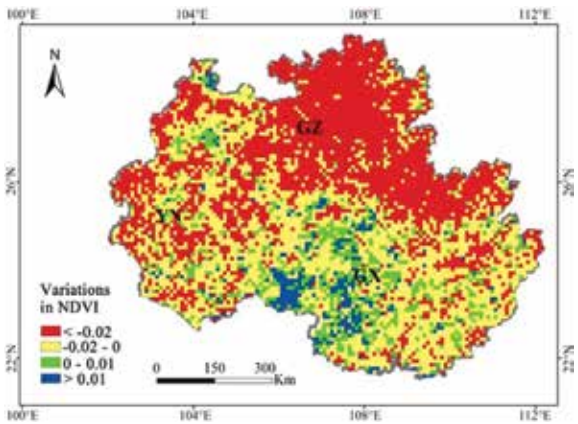

Figure 10. Spatial patterns of variations in growing-season NDVI during 2009–2012.

4.4. Assessing the dynamic downscaling of WRF

Uncertainty on the downscaling capability of regional climate model (RCM) has in most cases led to skepticism for its use. Despite the weakness, the RCM dynamic downscaling is better than the simulations from General Circulation Model (GCM) or reanalysis datasets [13]. Furthermore, the uncertainty increases when the RCM is used to simulate the impact of land cover change on regional climate. In this section, the state-of-the-art RCM's downscaling ability was evaluated first, and was followed by analysis of the climatic effects of land degradation.

To reveal the improvement of WRF simulations over reanalysis dataset, daily rainfall, temperature, and other circulation factors from WRF and reanalysis were compared with the APHROD (Asian Precipitation-Highly-Resolved Observational Data) precipitation dataset, the GTS (Global Telecommunication System) temperature dataset, and the JRA-25 (Japanese 25-year Reanalysis) atmospheric variables dataset. The assessment was conducted from the viewpoint of correlation coefficient (R), bias and root mean square error (RMSE) over the years of 1998, 2000, and 2004 and over 18°–52°N, 86°–136°E (**Table 3**). The lower Bias and RMSE and the higher R values indicate better performance.

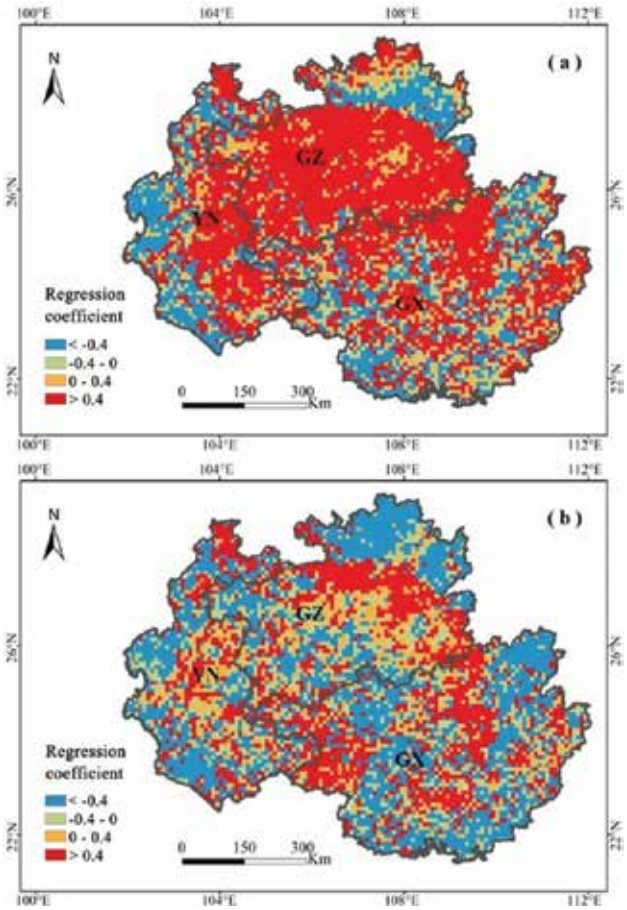

Figure 11. Multivariate regression coefficients of temperature (**a**) and precipitation (**b**) to NDVI based on pixel during 2009–2012.

Variables		Bias	RMSE	R
Precipitation	NCEP R-2	1.95	4.22	0.60
	WRF/SSiB	1.57	3.16	0.78
Temperature	NCEP R-2	−1.93	3.62	0.86
	WRF/SSiB	−2.29	4.21	0.85
VQ700	NCEP R-2	2.89	11.38	0.65
	WRF/SSiB	−1.37	7.49	0.70

VQ700, water vapor flux at 700 hpa (g/kg/ms).

Table 3. Descriptive statistics of ensemble mean JJA daily precipitation, temperature and water vapor flux at 700 hpa from WRF/SSiB and NCEP R-2 over 18°-52°N, 86°-136°E.

http://dx.doi.org/10.5772/64740

We further observed that the phenomenon of most rainfall occurring in the south of China, especially in the south of Yangtze River, can be detected from both WRF simulation and APHROD dataset. From the WRF simulation, there was also an obvious increasing trend from the northwest to southeast in the south of about 38°N with the minimum temperature in Qinghai-Tibetan Plateau. The WRF simulation of precipitation out-performed NCEP R-2, and was probably caused by the improved simulations of low level water vapor flux (**Table 3**), a key factor influencing the atmospheric convection in East Asian summer monsoon. Although the simulated surface temperature from WRF was not improved over NCEP R-2, the clearer spatial information for temperature was presented from WRF output, which suggests that, it is also an applicable tool in downscaling temperature.

4.5. Influence on precipitation and temperature due to KRD

The area over 20°–34°N, 104°–124°E was chosen to investigate the impact of Karst rocky desertification on precipitation and temperature, because the significant and consistent effects were located in this region. There was spatial variation in the precipitation changes among the regions (**Figure 12a**). The reduced rainfall was mainly observed in the middle of Guizhou Karst Plateau. The areas with increased precipitation, mainly the middle and lower parts of Yangtze River and the surrounding areas, were of much larger magnitude and extent than that with decreased rainfall. It can be inferred that the consistent but nonsignificant reduction in rainfall with Guizhou Karst Plateau was due to high moisture influence from the Bay of Bengal. The land surface warming mainly occurred in the areas where the original vegetation types were replaced with bare soil type (**Figure 12b**), while the rainfall changes not only occurred within the desertification area but also beyond the area.

4.6. Influence of KRD on land surface energy balance

As shown in **Figure 13**, the substantial changes of surface energy components occurred in Guizhou Karst Plateau. In the degraded areas, the higher albedo (**Figure 13a**) led to more reflected shortwave radiation from the land surface (**Figure 13b**). Due to the higher surface skin temperature (**Figure 12b**), the outgoing longwave radiation increased significantly, which further caused the reduced net longwave radiation at the surface (**Figure 13c**). Both the reduction of the net shortwave radiation and the net longwave radiation certainly resulted in the decrease in land surface net radiation (**Figure 13d**). More sensible heat flux was also induced by the warmer surface (**Figure 13e**), however, the reduction in surface latent heat flux (**Figure 13f**) was much more than the sensible heat flux increase. The decrease in evaporation was probably contributed by changes in vegetation and soil properties, such as the lower LAI and roughness length, and the higher surface albedo. It can be concluded that evaporation decrease produced the most profound influence on the hydrological balance at land surface. Additionally, the above-mentioned higher temperature in the degraded areas was caused by the reduced evaporative cooling.

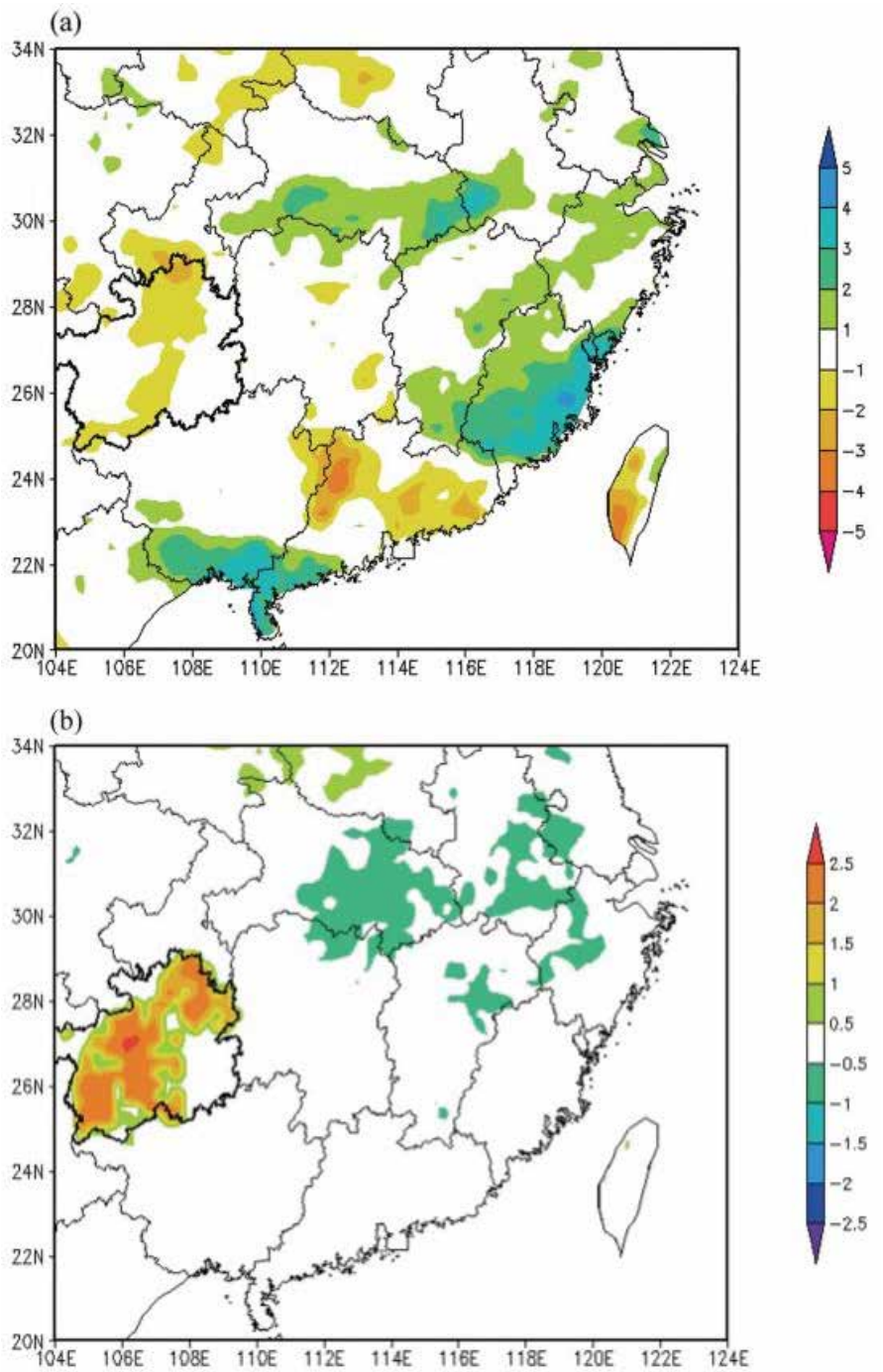

Figure 12. Ensemble mean differences in JJA **(a)** daily precipitation (mm/day) and **(b)** temperature (°C) between Case D and Case C. GKP is bounded by a heavy border.

http://dx.doi.org/10.5772/64740

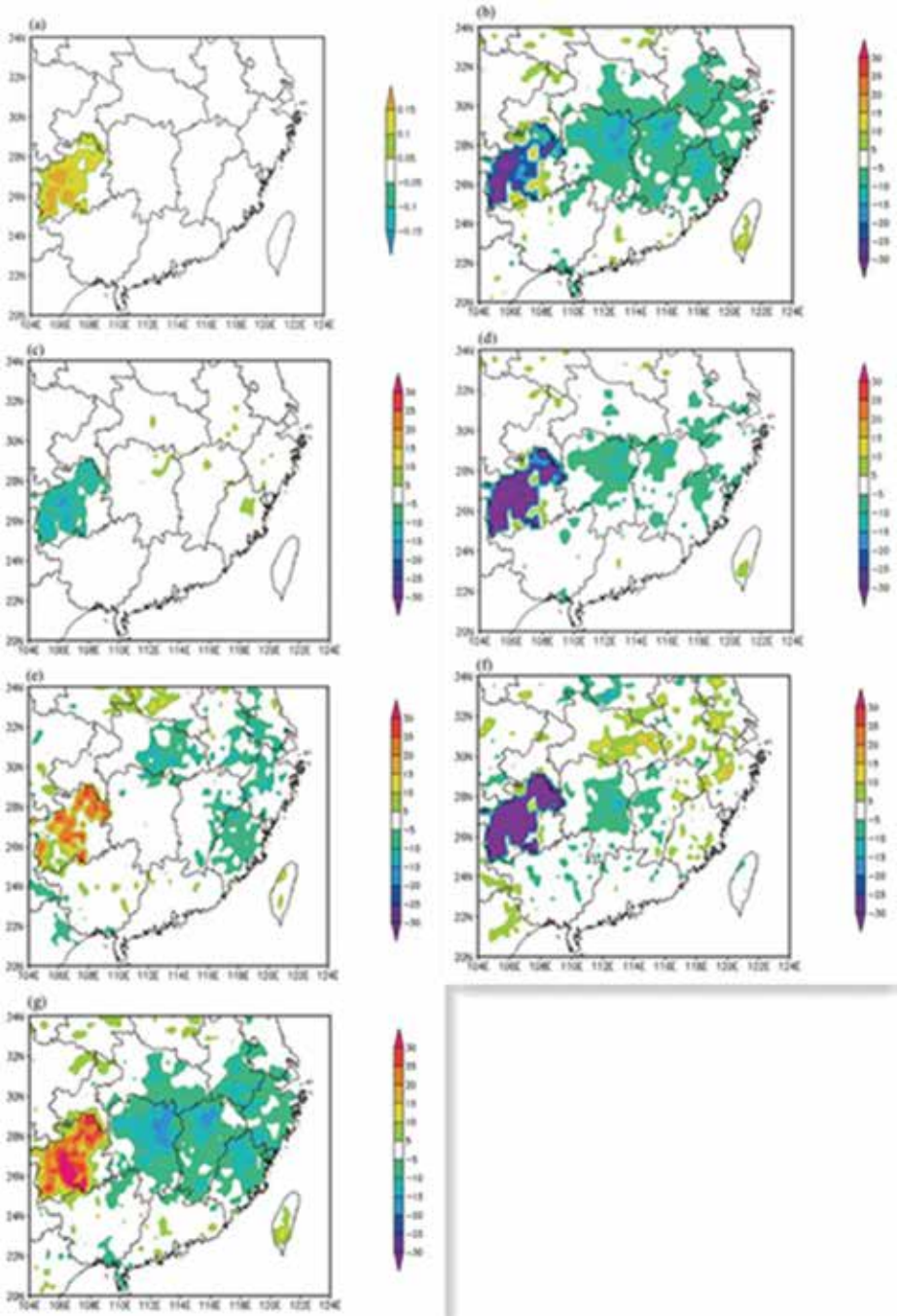

Figure 13. Ensemble mean differences in JJA **(a)** surface albedo, **(b)** net shortwave radiation, **(c)** net longwave radiation, **(d)** net radiation, **(e)** sensible heat flux, **(f)** latent heat flux, and **(g)** incoming shortwave radiation (W/m^2) between Case D and Case C.

Consistent with the spatial changes in precipitation, there were areas with significantly changed energy budget extending beyond the degraded area. Outside the Guizhou Karst Plateau, the variations in sensible heat flux and latent heat flux were controlled by the precipitation differences. For example, in the areas between 30°–34°N, 112°– 120°E (i.e., the southeastern coastal area of China), the increased evaporation (**Figure 13f**) was caused by the increase in precipitation (**Figure 12a**), which further led to the lower temperature (**Figure 12b**), and the lower sensible heat flux (**Figure 13e**). The issue on the impact of atmospheric circulations on precipitation will be discussed in the next section.

Figure 13(g) shows the impacts of cloud albedo and land surface albedo on shortwave radiation. In the degraded areas within Guizhou Karst Plateau, the cloud fraction was reduced due to the less evaporation and moisture flux convergence after land degradation, and the reduced cloud fraction further led to more incoming shortwave radiation. However, the increase in upward shortwave radiation (**Figure 13a**) due to the higher land surface albedo was much more than the downward shortwave radiation, which resulted in the reduced net shortwave radiation (**Figure 13b**). Moreover, in the southeastern coastal areas of China, the increased cloud fractions, consistent with more rainfall, led to the decrease in incoming shortwave radiation, dominating the alteration in net shortwave radiation.

4.7. Effects of KRD on atmospheric circulation

The modified water and energy budget due to Karst rocky desertification was the first-order effects. Because of the different input of heat and moisture into atmospheric circulation, the large-scale circulation features were altered, resulting in climatic effects beyond the desertification area. As shown in **Figure 14**, the weakened 3-month mean wind vector at 700 hPa

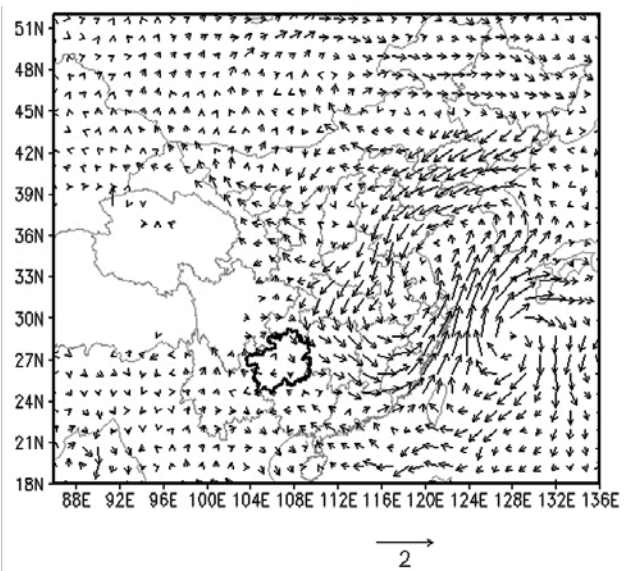

Figure 14. Ensemble mean differences in JJA wind vector (m/s) at 700 hPa between Case D and Case C.

http://dx.doi.org/10.5772/64740

between Case D and Case C was caused by the lower surface heating in GKP (**Figure 13d**). The monsoon airflow from the Bay of Bengal, an important moisture source for the East Asia, was weakened from the degraded areas to the northeast. Furthermore, the weakened southwest airflow had significant impacts on the East Asian monsoon, especially, the anomaly cyclone (**Figure 14**) and the stronger horizontal convergence in the southeastern coastal area that led to the strengthened vertical ascending motion and the increase in precipitation.

On the other hand, the longitude-height section of the composite difference of zonal circulation along 24°–30°N between Case D and Case C was plotted to conduct further analysis (**Figure 15**). After the land degradation in GKP, an anomalous descending motion appeared in both the upper and middle level of troposphere over GKP and the middle and lower troposphere of the adjacent regions to the east. Such circulation modification caused the strengthened ascending motion over 114°–122°E. Moreover, the stronger lifting over the coastal areas led to the increase in the vertically integrated moisture flux convergence (VIMFC) from 1000 to 300 hPa. Consequently, the different circulation and moisture flux reduced the rainfall over GKP and promoted the formation of clouds and the positive rainfall anomalies over southeastern coastal areas of China (**Figure 12a**). Also, in the southeast China, the surface cooling (**Figure 12b**) was induced by the increased amount of clouds and further a negative net cloud radiation forcing.

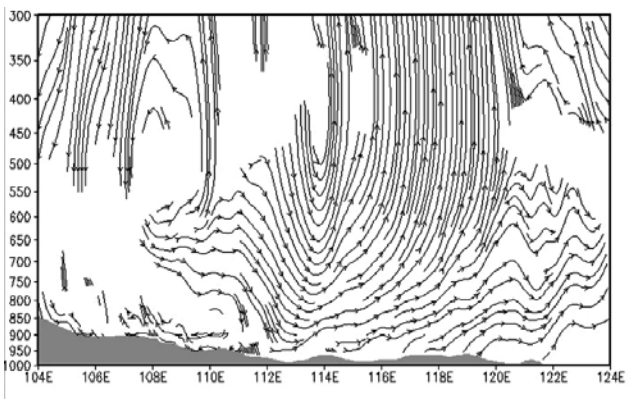

Figure 15. Zonal-height cross sections of ensemble mean differences in JJA zonal (ms^{-1}) and vertical (10–2 ms^{-1}) winds averaged over 24°–30°N. Gray shading indicates topography.

5. Conclusions

The growing-season NDVI increased significantly during the last 30 years in the Karst region of the southwest China. There were also differences in the increase rate of vegetation types. The distribution of NDVI presented obvious spatial patterns, specifically, lower values in the western part and higher values in the east. The correlation between NDVI and climatic factors implied the limiting role of temperature for the vegetation growth and distribution in the study

area, although the regression coefficients presented spatial heterogeneity. Additionally, the decreased NDVI was analyzed to detect the influencing mechanism. It was found that the increased cloud cover and rainfall led to the decrease in solar radiation and temperature, and further impeded photosynthesis.

We also observed that after the land cover change, there is need to consider its climatic effects through the impact of LCC on land surface water and energy budget. Karst rocky desertification (i.e., extensive exposure of basement rocks, serious soil erosion, drastic decrease in soil productivity and appearance of desert-like landscape) can modify the energy budget at land surface and then the regional climate. Specifically, after land degradation, the higher surface albedo and temperature caused the reduced net shortwave radiation and net longwave radiation. The sensible heat flux was increased by the higher temperature. Specifically, the substantial increase in sensible heat flux from ground offset the decrease in that from canopy. Due to higher stomatal resistance and lower LAI, the latent heat flux in KRD was reduced significantly. Less atmospheric heating from degraded land resulted in relative subsidence and less moisture flux convergence (MFC). The decrease in rainfall was probably attributed by both the reduced MFC and the reduced evaporation. A feedback loop was activated when precipitation was affected, for example, the altered soil moisture, vegetation growth, and phenology can further result in less diabatic heating rates, less moisture flux convergence, and lower rainfall. Moreover, the changed rainfall beyond the degraded areas was more significant. The modified energy and water balance due to land degradation weakened the southwest monsoon flow and affected the atmospheric circulation and moisture flux. In the southeastern coastal areas, the precipitation increased due to two reasons: (1) the weaker low-layer anticyclone causing the stronger vertical ascending motion, (2) the air mass diverging in the lower troposphere accompanying rising up over southeastern China.

Acknowledgements

We thank the National Basic Research Program of China (Grant No. 2015CB452702), the National Natural Science Foundation of China (Grant No. 41671098, 41301089), the National Science and Technology Support Program of China (Grant No. 2012BAC19B10, Grant No. 2013BAC04B02) for supporting this work.

Author details

Jiangbo Gao*, Wenjuan Hou, Kewei Jiao and Shaohong Wu

*Address all correspondence to: gaojiangbo@igsnrr.ac.cn

Key Laboratory of Land Surface Pattern and Simulation, Institute of Geographic Sciences and Natural Resources Research, Chinese Academy of Sciences, Beijing, China

References

[1] Parmesan C, Yohe G. A globally coherent fingerprint of climate change impacts across natural systems. Nature. 2003;421:37–42. DOI: 10.1038/nature01286.

[2] Piao SL, Wang XH, Ciais P, Zhu B, Wang T, Liu J. Changes in satellite-derived vegetation growth trend in temperate and boreal Eurasia from 1982 to 2006. Global Change Biology. 2011;17:3228–3239. DOI: 10.1111/j.1365-2486.2011.02419.x.

[3] Beck PSA, Atzberger C, Hogda KA. Improved monitoring of vegetation dynamics at very high latitudes, a new method using MODIS NDVI. Remote Sensing of Environment. 2006;100:321–336. DOI: 10.1016/j.rse.2005.10.021.

[4] Zhao M, Running SW. Drought-induced reduction in global terrestrial net primary production from 2000 through 2009. Science. 2010;329:940–943. DOI: 10.1126/science.1192666.

[5] Piao SL, Ciais P, Huang Y, Shen ZH, Peng SS, Li JS, et al. The impacts of climate change on water resources and agriculture in China. Nature. 2010;467:43–51. DOI: 10.1038/nature09364.

[6] Bounoua L, Defries R, Collatz GJ, Sellers PJ, Khan H. Effects of land cover conversion on surface climate. Climatic Change. 2002;52:29–64. DOI: 10.1023/A:1013051420309.

[7] Pielke RA, Avissar R, Raupach M, Dolman AJ, Xeng Y, Denning S. Interactions between the atmosphere and terrestrial ecosystems: Influence on weather and climate. Global Change. Biology. 1998;4:461–475. DOI: 10.1046/j.1365-2486.1998.t01-1-00176.x.

[8] Huang QH, Cai YL. Spatial pattern of Karst rock desertification in the middle of Guizhou province, southwestern China. Environmental Geology. 2006;52:1325–1330. DOI: 10.1007/s00254-006-0572-y.

[9] Yang QQ, Wang KL, Zhang CH, Yue YM, Tian RC, Fan FD. Spatiotemporal evolution of rocky desertification and its driving forces in Karst areas of northwestern Guangxi, China. Environmental Earth Sciences. 2001;64:383–393. DOI: 10.1007/s12665-010-0861-3.

[10] Xu YQ, Peng J, Shao XM. Assessment of soil erosion using RUSLE and GIS: a case study of the Maotiao River watershed, Guizhou Province, China. Environmental Geology. 2009;56:1643–1652. DOI: 10.1007/s00254-008-1261-9.

[11] Mann HB. Nonparametric tests against trend. Econometrica. 1945;13:245–259. DOI: 10.2307/1907187.

[12] Li Z, Huffman T, McConkey B, Townley-Smith L. Monitoring and modeling spatial and temporal patterns of grassland dynamics using time-series MODIS NDVI with climate and stocking data. Remote Sensing Environment. 2013;138:232–244. DOI: 10.1016/j.rse.2013.07.020.

[13] Gao YH, Xue Y, Peng W, Kang HS, Waliser D. Assessment of dynamic downscaling of the extreme rainfall over East Asia using a regional climate model. Advances in Atmospheric Sciences. 2011;28:1077–1098. DOI: 10.1007/s00376-010-0039-7.

[14] Kanamitsu M, Ebisuzaki W, Woollen J, Yang SK, Hnilo JJ, Fiorino M, Potter GL. NCEP-DOE AMIP-II Reanalysis (R-2). Bulletin of the American Meteorological Society. 2002;83:1631–1643. DOI: 10.1175/BAMS-83-11-1631.

[15] Ren H. A review on the studies of desertification process and restoration mechanism of Karst rocky ecosystem. Tropical Geography. 2005;25:195–200. DOI: 1001-5221(2005)03-0195-06.

Chapter 3

Risk Assessment of Land Degradation Using Satellite Imagery and Geospatial Modelling in Ukraine

Sergey A. Stankevich, Nikolay N. Kharytonov,
Tamara V. Dudar and Anna A. Kozlova

Additional information is available at the end of the chapter

http://dx.doi.org/10.5772/62403

Abstract

In this publication, the authors considered the effect of unprecedented human activity into land degradation and desertification processes in Ukraine. The land degradation mapping technique based on processing of a two-level model for multispectral satellite imagery of low and medium spatial resolution was described. This technique was used to investigate land degradation and desertification within relatively pristine and human-inspired mining and industrial landscapes located in the central, southern, and eastern parts of Ukraine. In each particular case, the authors offered thematic land degradation maps obtained as a result of multispectral images processing, allowed assessing the state and tendencies in land degradation processes within the study areas. Data obtained visually emphasize the level of anthropogenic stress, impact of long-term change of vegetation cover, and correlation of intensive development of mining, construction, agricultural and other human activities with high level of land degradation within investigated areas. The transition to adaptive farming systems implies the achievement of maximum compatibility between soil and plant, development of crop rotation, soil conservation tillage system. Conducted research on the creation of adaptive systems of crop production takes into account the environmental, landscape and geochemical peculiarities of the steppe zone of Ukraine, to get the production of environmentally safe agricultural products. They can be used in further studies of a differentiated approach to achieving a balanced potential of agricultural landscapes. Remote detecting of degradation and desertification processes intensification at early stages will be able to promote further measures for improving the territories conditions. The further research has to be directed on development of geoinformation technologies for landscape changes remote mapping.

Keywords: Anthropogenic landscape, Land degradation, Soil erosion, Satellite imagery, Geospatial modelling

1. Introduction

Land degradation is a relevant and important problem for Ukraine. The solution to this problem requires not only a detailed study of land degradation causes, but also involves identifying a risk of land degradation [1]. Unprecedented human activity destroys the landscape complexes globally. In this publication, the authors consider in brief the effect of such unpractical land use into land degradation and desertification processes in Ukraine on the examples of natural and human-inspired landscapes [2].

Ukraine is known for its fertile arable lands as a key natural resource. But throughout the twentieth century, Ukraine's lands were dramatically changed by anthropogenic stress. Virgin lands were ploughed and mires, swamps and wetlands drained, forests shrunk and steppe lands were severely mined. According to the UN Food and Agriculture Organization (FAO), data as much as 76% of the total land are severely degraded due to human activities [3]. This high figure results largely from a history of intensive agriculture and mining development. As land degradation is considered one of the major environmental problems, Ukraine joined the UN Convention to Combat Desertification (UNCCD) [4] in 2002. The Convention's annex on Regional Implementation for Central and Eastern Europe cites Ukraine as an example of serious land degradation [5].

The Law on land protection (2003, No. 962-IV) and the Law on state control of use and protection of land (2003, No. 963-IV) approved after joining UNCCD, include provisions to restrict improper use of land, but resources for ensuring their application are strictly limited.

From year to year, we observed the great growth of lands under mines, open pits and other industrial facilities that led to numerous lands subsidence, rocks slide, decrease areas of arable lands, etc. The arable areas had also greatly suffered from development of terricones, waste banks, pit refuse heaps as well as from building of an earth dams, bridges, roads, water reservoirs, etc. The enormous contaminants emitted into the environment from different industries have tangible effect on almost all the landscapes in the country.

Soil dehumification and consequently increased emissions of carbon dioxide (agent of the greenhouse effect) are significant causes of change in meteorological conditions. This enables another destructive mechanism of land degradation—desertification. In the spatial context, desertification can be considered as the phenomenon, which is to increase the area of depleted ecosystems. Desertification is a manifestation of the effects of biodiversity and biomass loss, and evaluation of the soil fertility impacts on primary productivity of ecosystems formed in the agrarian landscapes.

Large extent or inaccessibility of degraded areas, insufficient funding for soil and vegetation cover research, as well as unsatisfactory quality of relevant archival materials, makes multi-spectral satellite imagery a reliable information source for the assessment of potential land deterioration.

http://dx.doi.org/10.5772/62403

2. Natural and anthropogenic landscapes of Ukraine

As a result of long-term landscape changes, the level of territory transformation has deviated significantly in different parts of the country, the highest percentage of natural landscapes being observed in mountainous areas (**Figure 1**). However, mountainous landscapes occupy relatively insignificant parts of the territory (around 6%). According to **Figure 1**—the northern, northern-western, the mid reaches of the Dnieper River and the part of the territory under natural components makeup to 50%, and the forest–steppe and steppe geographical zones transformation exceed 90% of the total area. Natural components here are located on the restricted areas adjacent to rivers and to the Black sea coastal area.

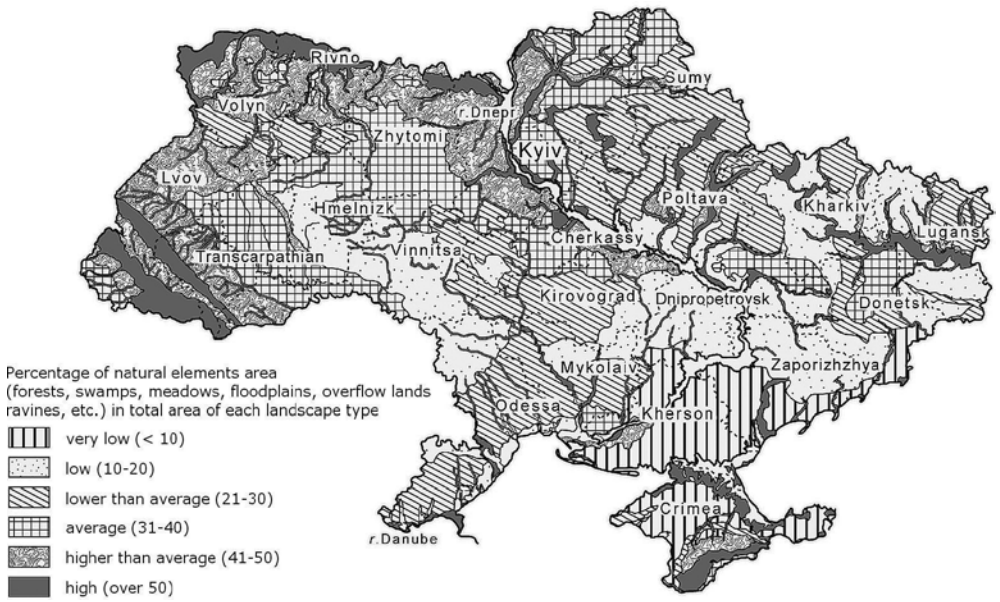

Figure 1. Anthropogenic landscapes of Ukraine.

Out-of-balance and unpractical natural resource management from the previous century have led to the environmental situation and the landscape architecture we see nowadays. It is too far from optimism. However, what is evident is that the level of land degradation is unequal (**Figure 1**). It is associated with human impacts of different intensities depending on territorial differentiation of natural conditions and resources, level of social and economic development and other factors peculiar to different areas of Ukraine.

In general, the percentage of tilled lands at the level of 60–80% (from the total area) is considered as unfavourable; 25–60%—conditionally favourable; and <25%—favourable. Optimal assessment of tillage is still met in the Ukrainian Polissya, mountainous areas of Carpathians and Crimea. Ukraine is characterized by highest percentage of tilled lands: As it mentioned above, just around 8% (5 million ha) of lands are in natural conditions. Agricultural develop-

ment of the land resources is 72.2%. And the steppe oblasts are characterized by the highest value of cultivated lands: Zaporizhia (88%), Kirovograd (86%), Dnepropetrovsk and Odessa oblasts (83% each), and Kherson (82%). A bit lower level is observed in the forest–steppe oblasts, and significantly lower level of cultivation (by 1.5–2 times) is within the Polissya territory. The percentage of cultivated lands in Ukraine is the highest in the world and the main contributors to that are the territories of forest–steppe and steppe zones [6]. For comparison: the percentage of tilled lands in the USA is 19%, France and Germany—33%, Italy—31% [7], that is these factors correspond to favourable and conditionally favourable characteristics. Such a high level of cultivated lands is unfavourable as from economic as well as from environmental points of view. It abruptly decreases a natural potential of the territory and makes it monotonous, and economy activity—highly specialized [8].

3. Soil erosion and other exogenous processes

As it was highlighted in the Land Code of Ukraine (art. 171), degraded lands are specifically those where erosion, landslides, karsts, floods, etc., are developed [9]. Ukraine's soil is prone to erosion, and over 30 million hectares (i.e. about half Ukraine's total territory) of land is strongly affected by erosion. Some agricultural practices, like planting of row crops (sugar beet, sunflower, etc.) in plantations, exacerbate the problem. Soil erosion is a significant problem which also decreases humus levels in soil.

Ukraine's relief and climate and its very high proportion of arable lands make erosion a widespread natural phenomenon. About a third of the arable lands are threatened by water and wind erosion. Poor land management practices, such as crop cultivation on steep slopes, excessive cutting of forests, shrubs and bushes, and overgrazing accelerate erosion. As a side effect, erosion is causing sedimentation in rivers, lakes and water reservoirs. As a result of erosion fertile soil is lost, plant nutrients are removed and there has been soil textural changes, deterioration of soil structure, declining land productive capacity, increased dissected fields, and increased streams and lakes pollution and pile ups on bottomlands, in stream channels, and in lakes and reservoirs. Over 500 million tons of soil is subjected to erosion processes annually leading to decrease of soil fertility. It is argued that with each dollar of added cost created by agricultural producers, one third is lost due to erosion [10]. The soil fertility decrease inevitably leads to increase in production cost. For the last 15 years, the intensity and frequency of droughts has significantly grown in the steppe zones of Ukraine. Droughts are observed to happen once in 3 years causing decrease of arable lands productivity. The climate change and expected extreme phenomena growth are supposed to exacerbate this tendency in the nearest future. Right in the steppe zone, the soil degradation processes are developed much harder than in the other parts of Ukraine. It is important to remember that a half of grain crops in the country are grown on the fertile chernozems in the steppe climate zone. In some south-east areas, the soils are degraded so heavily that additional donations are needed to restore their fertility.

The steppe zone occupies the southern part of Ukraine. It is spread from south-west to north-east up to 1100 km, and from north to south up to 500 km (**Figure 1**). Its total area is about 25

http://dx.doi.org/10.5772/62403

million hectares that makes up 40% of the whole territory of the country. The biggest steppe area is occupied under typical chernozems—10.4 million hectares. They are formed under grassland-fescue-feather vegetation in the northern part of the steppe zone. Because of the climate change, the humus layer thickness is gradually decreasing, and the typical chernozems are subdivided into medium-humic and low-humic chernozems of high (85–100 cm), medium (65–85 cm), and low (45–65 cm) thickness [11]. Agricultural activity promoted water and wind erosion spread. The wind erosion has covered more than 220,000 km^2 so far and spread even in those areas where it has never been noticed before. For some time past, the dust storms of 8–17 h duration happened three to five times per year [12, 13]. The wind speed reached up to 20 m/s. It is known that the southern chernozems structure damage can occur when the wind speed is of 5–6 m/s [14]. With an exception of soil erosion phenomena, the UNCCD Country Profile of 2006 consider other exogenous geological processes caused land degradation in Ukraine (**Table 1**, UNCCD Country Profile, 2006) [3].

Land degradation	**Land area**	
	Million ha	**Percent of total area**
Wind erosion	13.3	22.0
Water erosion	19.4	32.1
Combined erosion	2.1	3.4
Soil acidification	10.7	17.7
Soil salinization	1.7	2.8
Soil alkalization	2.2	3.7
Land slides	0. 2	0.3

Table 1. Land degradation drivers in Ukraine.

4. Dust storms in the southern part of Ukraine

The dust storm plume fixed in the central regions of the European part of the troposphere was observed on the space images dated 24 March, 2007 (**Figure 2**).

It turned out that that headwaters of this dust storm point out to the south of Ukraine. The wind currents of 30 m/s speed lifted up huge masses of the surface soils. The dust plume trajectory went through the territories of the Slovak Republic, the Czech Republic, and Germany. The solid particles concentration in that plume was between 200 and 1400 $\mu g/m^3$. The MODIS image analysis proved that the origin of dust plume was in the Kherson oblast, close to the Kakhovsky water reservoir. Huge masses of dust were lifted up in the air from the territory of 20,000 km^2 area under arable lands. The wind speed reached up to 25 m/s [15]. This unusually high wind speed together with the preceding of a 2-week drought and lack of vegetation caused that dust storm in March 2007. It has to be noticed that until quite recently, the Sahara desert was considered to be the main source of transboundary transfer of mineral

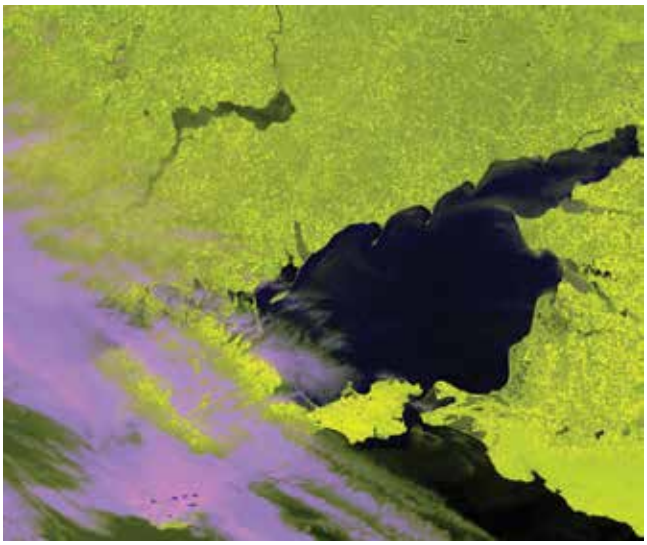

Figure 2. Dust storm in the region of the Kakhovske water reservoir, EOS/MODIS, 23.03.2007.

dust to Central Europe. Dust from the Sahara desert is transferred with windblast into the Central Europe several times per year. The solid particles concentration in the dust plume in the south of Germany is made up on the average 280 μg/m^3. According to the monitoring data from the "Borna" station in Germany, the concentration of solid particles from the Ukrainian dust reached 640 μg/m^3. As it is obvious, this value exceeded the African plume parameters by two times.

Up to 70 tons of soils per hectare and per hour is blown away during the dust storms. The storm of March, 2007 was not an extraordinary phenomenon for the south of Ukraine. It is known that in the early 1950s, the countermeasures were taken to prevent the wind erosion spread. The wind protective forest strips were planted on more than 440,000 hectares in all the natural zones of Ukraine [16].

Until recently, the soil dust natural particles were traditionally considered as harmless for the human health. But new research proved chronic bronchitis happened quite frequently in farmers [17] or increase of respiratory diseases in population residing in the territories of Karakalpak (Uzbekistan) [18], that is. in regions with the similar conditions described for the south of Ukraine.

5. Satellite imagery for the purpose of land degradation mapping

As it is obvious, land degradation phenomena is of high priority to be researched and different techniques are to be considered for that. The solution to this problem requires not only a detailed study of the land degradation causes, but also involves identifying the risk of degradation. Satellite imagery has its advantages and widely used for investigation of

http://dx.doi.org/10.5772/62403

landscape changes dynamics as a result of anthropogenic impact since it is able to cover areas at different scales. Processing of time series of geoinformation products allows reliable detecting and mapping of landscape changes at local, regional and even global level.

As it was mentioned above, large scale or inaccessibility of degraded areas, insufficient funding for research on soil and vegetation cover condition, as well as unsatisfactory quality of the relevant archival materials, make multispectral satellite imagery a reliable information basis for the assessment of potential land deterioration. At the same time, the main task of multispectral satellite imagery processing is the selection of land degradation indicators. In this study, vegetation change and soil erosion dynamics are defined as such indicators. To map them, besides medium spatial resolution multispectral satellite images, auxiliary geospatial data—digital terrain, soil maps and climatic parameters of the study area—are required.

The authors used the land degradation mapping technique to investigate land degradation within relatively pristine (Oleshki sands) and human-inspired mining and industrial areas (central part of Ukraine) [19]. In each particular case, the authors offered thematic land degradation maps obtained as a result of multispectral images processing, allowed assessing the state and tendencies in land degradation processes within the study areas. The research visually emphasizes the level of anthropogenic stress within investigated territories.

6. Land degradation geospatial model

The land degradation mapping technique was used on the basis of processing of a two-level model for multispectral satellite imagery of low and medium spatial resolution. First-level model applies several different thematic classifications of source multispectral images, for example vegetation change, soil erosion, etc. Second level gives data fusion of specific thematic classifications of the first level into final thematic map to improve accuracy and reliability owing for information support systems to provide land management.

Vegetation changes are usually detected on the multispectral satellite images by unified well-known methods [20]. It should be noted that a modified soil-adjusted vegetation index MSAVI F_v is more preferable over generic normalized vegetation index NDVI for vegetation mapping in terms of steppe soil erosion in the southern Ukraine. The MSAVI index can be calculated by special equation:

$$F_v = \rho_{inr} + \frac{1 - \sqrt{(2\rho_{nir} + 1)^2 - 8(\rho_{nir} - \rho_{red})}}{2} \quad (1)$$

where ρ_{nir} and ρ_{red} are land surface spectral reflectances in the near infrared and red spectral bands, respectively [21].

Water erosion depends on soil type and mineral composition, rainfall, slope steepness and vegetation density. The value of water erosion z_s (mm/month) can be calculated from the regression relationship of the form [22]

$$z_S = k_s Q^2 (\mathrm{tg}\alpha)^{1.67} \exp(-0.07V) \tag{2}$$

where k_s is a soil erosion factor, $k_s \cong 0.13$ (mm/month)$^{-1}$ for clay and sandy soils of the study area [23], Q is runoff (mm/month), α is a slope angle of the terrain, V is the vegetation cover fraction. Runoff is determined by the ratio of precipitation P (mm/month) and water retention in soil R (mm/month):

$$Q = \frac{(P - 0.2R)^2}{P + 0.8R} \tag{3}$$

where R depends on the table hydrological soil index C_s as [24]

$$R = 25.4\left(\frac{1000}{C_S} - 10\right) \tag{4}$$

The percentage of vegetation coverage V is generally considered to be proportional to scaled NDVI value square within the study area [25] and is easily calculated by multispectral imagery [26]:

$$V = \left(\frac{N_v - N_{v0}}{N_{v1} - N_{v0}}\right)^2 \tag{5}$$

where N_{v0} is NDVI threshold for open soil, N_{v1} is NDVI threshold for full coverage of vegetation,

$$N_v = \frac{\rho_{nir} - \rho_{red}}{\rho_{nir} - \rho_{red}} \tag{6}$$

Wind erosion is caused by the interaction of the structural soil particles from the ground-level air flow. A simplified model of wind erosion is given by [27]:

$$z_w \approx 0.059(w - u) d_S^{-3.67} \tag{7}$$

where z_w is the quantity of wind erosion (mm/month), w is the near-surface airflow velocity (m/s), u is critical air flow velocity (m/s),

$$u = 3.202 + 0.025 d_S \tag{8}$$

http://dx.doi.org/10.5772/62403

and d_s is soil structural particles equivalent size (mm). The near-surface airflow velocity at a steady dynamic wind velocity w_0 is determined mainly by vegetation resistance [28]:

$$w = w_0 \exp(-0.0139V) \tag{9}$$

The total soil erosion is a summation of (2) and (7) values.

To map land degradation of the study area calibrated multispectral images from medium resolution, Earth observation satellite systems can be used for the period of analysis. All multispectral satellite images must be undertaken with atmospheric correction and then converted to surface reflectance for each spectral band. The MSAVI F_v (1) index must be calculated, and its changes must be mapped. At the same time, the total erosion $z = z_s + z_w$ must be estimated and its changes must be mapped too. Required auxiliary parameters can be extracted directly from the input multispectral satellite imagery (fraction of vegetation cover), digital terrain elevations data (DTED—slopes), soil and climatic data [29, 30] (particle size distribution and hydrological parameters of soil, the average monthly rainfall, wind velocity profiles).

At the first stage of processing, time-series of satellite imagery-based classifications should be built. These classifications represent principally different land degradation indicators that are appeared in vegetation and soil erosion changes. At the second stage, the previously obtained partial first-level classifications should be fused into the resulting classification by data fusion methods [31]. In this study, Bayesian statistical inference can be applied as data fusion model [32]. Values obtained by fusing the partial classifications are subdivided conveniently into few classes. The first half of classes with negative values describes the negative changes of indicators which provide increasing land degradation risk.

The second half reflects the positive trends in land degradation indicators and shows a decrease in the risk of land quality deterioration. The special class must be reserved to map the territory where the evident changes did not occur during the period of analysis.

Thus, a hybrid two-level model for data fusion appears in land degradation risk mapping using remote sensing data and geospatial modelling: A few partial raster classifications are performed at the first level, and then, these classifications are fused into final map [33].

As relating to land degradation mapping, the geospatial model also has two levels. The model's first layer includes the spatial distribution of two main indicators of land degradation, namely trends in vegetation change and soil erosion. The model second layer provides the Bayesian fusion of the first-level data into the final map of land degradation. In detail, the geospatial model data flowchart is described in **Figure 3**.

At the model's first level, the data processing is performed in multiple concurrent threads to extract a temporal trends of land degradation indicators. For simplicity, **Figure 3** shows the multispectral imagery (*a, c*) and DTED (*b, d*) for the initial and final stages only. By the MSAVI (*e, g*), vegetation index maps the vegetation cover fractions (*h, j*) are estimated, and using additionally, the DTED and soil map (*f*) of territory the levels of soil erosion (*i, k*) are deter-

mined. At the model's second level, the partial classifications of trends in vegetation cover change (*l*) and soil erosion change (*m*) are fused into the land degradation final map (*n*) of study area.

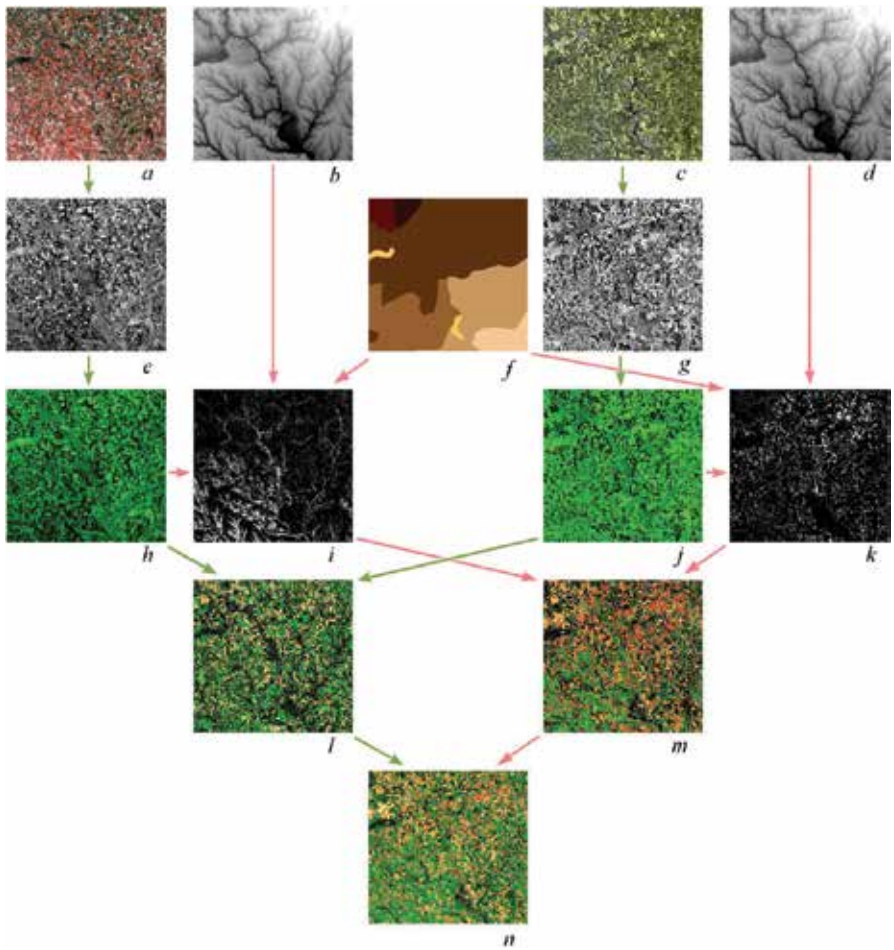

Figure 3. The land degradation mapping dataflow diagram.

7. Remote assessment of natural landscape degradation in the southern part of Ukraine

The research was carried out for parts of the Lower Dnieper Sands—Kozachelagerska and Oleshkovskaya arenas and Shelemensky sands located on the left bank of the Dnieper River in Tsyurupinsk and Golopristan districts of the Kherson oblast (**Figure 4**).

http://dx.doi.org/10.5772/62403

The Lower Dnieper Sands is a unique natural complex of forest–steppe. It is the greatest sandy area of Europe, restrained all around by largest artificial forest [34]. However, as a result of human activity and fires, changes in vegetation and forest cover and destruction of natural psammophyte communities are observed, which leads to increased erosion processes and may ultimately lead to a complete desertification of the area. The main factors of land degradation within the study area are water (about 78%) and wind (20%), erosions [35].

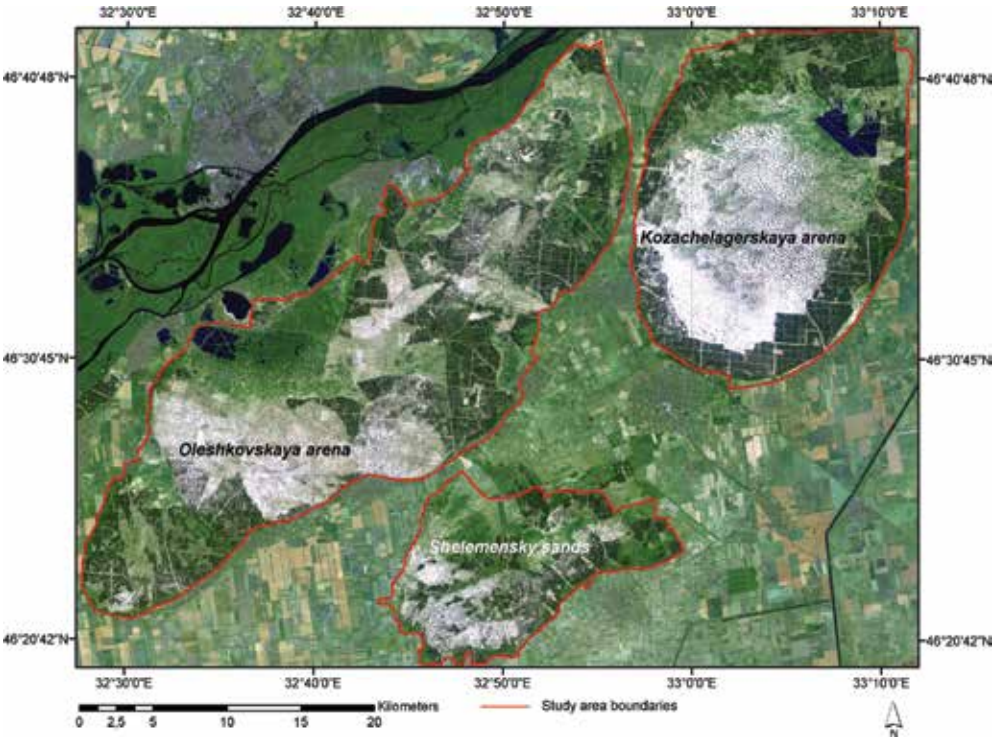

Figure 4. The research area located in Kherson oblast. The Landsat 5/TM scene from August 16, 2010 (RGB—321) shows three arenas of the Lower Dnieper Sands: Kozachelagerskaya, Oleshkovskaya and Shelemensky sands.

The resulting map of land degradation risk changes in the study area is shown in the **Figure 5**. Visual analysis of the map shows that, in general, the risk changes in land degradation are associated with changes in vegetation cover. During both periods under consideration, the degree of risk change was weak. A significant extension of the areas with increased land quality deterioration risk in the period from 1991 to 2010 is caused by the large-scale fires that took place in August 2007.

Thus, multispectral satellite imagery can be effectively used for studying land quality deterioration indicators as well as for change detecting the risk of degradation in vast areas during a certain period of time [36]. Furthermore, the use of satellite images allows not only cover a

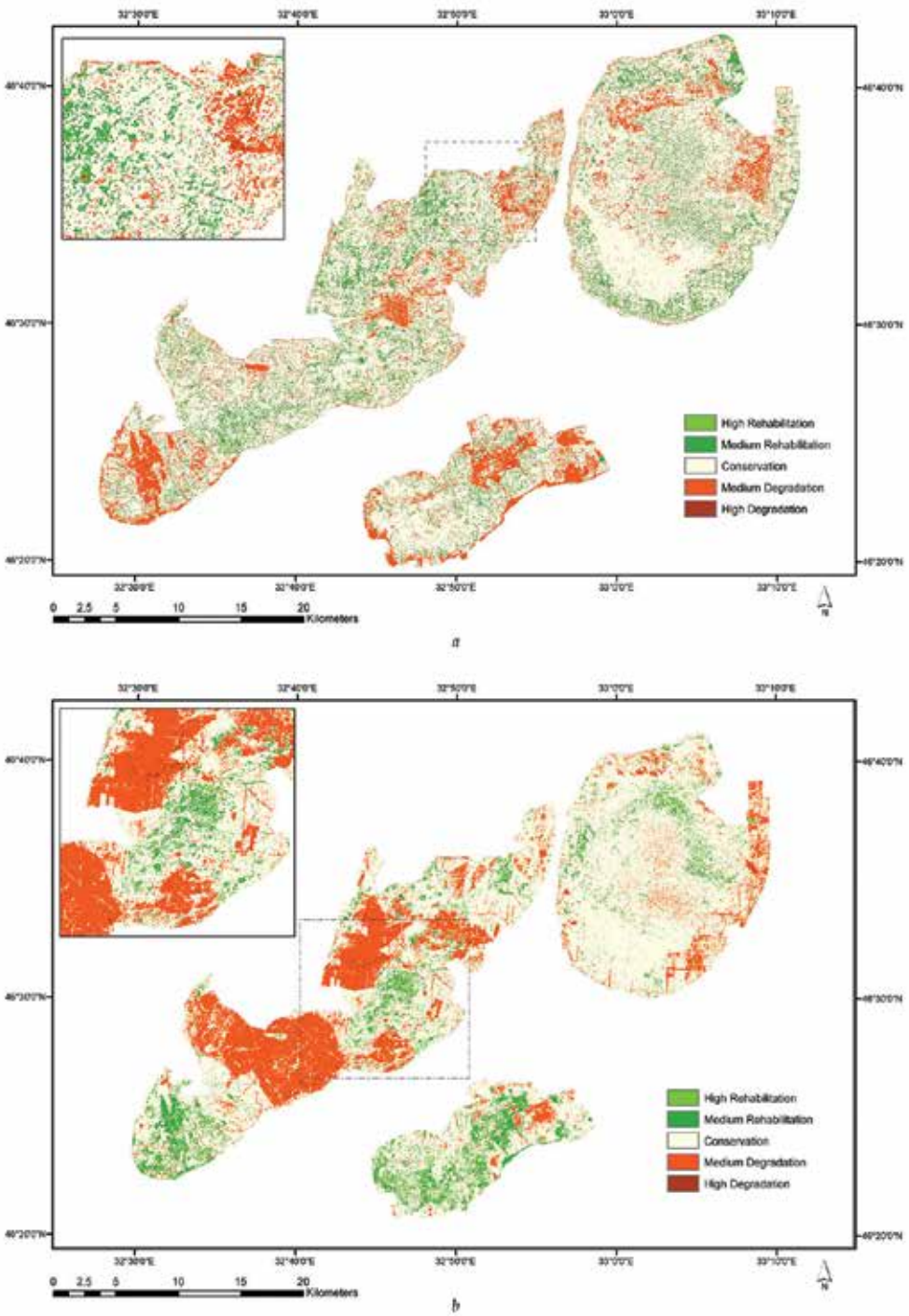

Figure 5. Land degradation risk within the study area for the periods: 1983–1991 (a) and 1991–2010 (b).

http://dx.doi.org/10.5772/62403

huge area of land affected by degradation and to establish reliable information from remote areas, but also significantly reduce the cost of the works on determination the land quality and its deterioration risks. In the future, the model proposed in this paper can be integrated in the geographic information system to support land management at the local and regional levels.

8. Arable land degradation in industrial area of south-eastern part of Ukraine

As it is known, the main sources of anthropogenic contamination are considered metallurgical and chemical enterprises, thermopower plants, and auto-transport. The arable lands within such industrialized areas are heavily degraded. As an example, let us consider the Dnepropetrovsk oblast located in the south-east of Ukraine, where anthropogenic stress of different origin is apparently available.

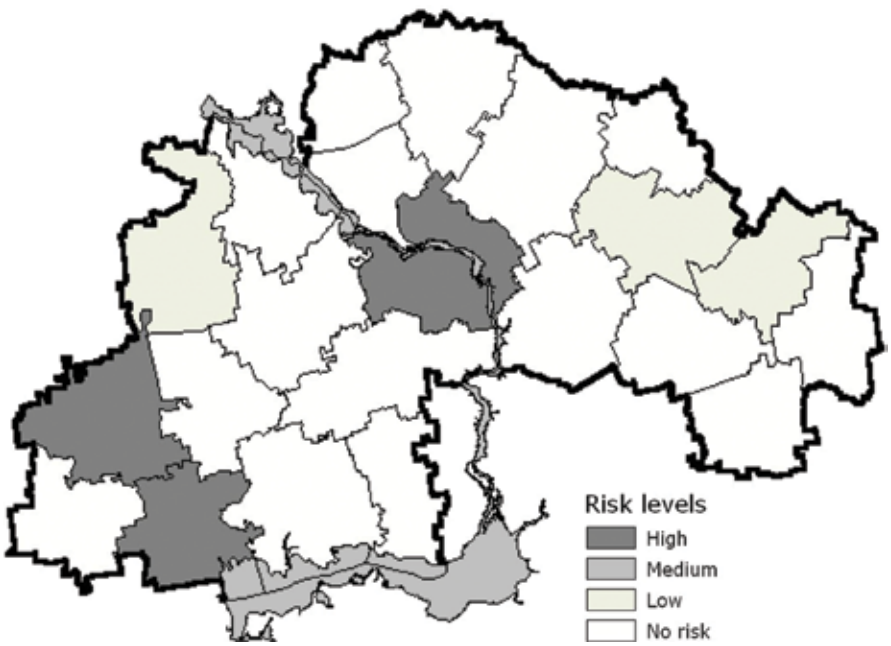

Figure 6. Integrated levels of anthropogenic impact on soil conditions within the Dnepropetrovsk oblast.

Agricultural chernozems here also suffer from erosion processes [37]. The humus accumulation regime is disturbed. As a result of ground ablation even of low level, from 0.5 to 2% of ordinary chernozem, humus content is lost. On the average for the oblast, the humus content used to be 5%, but this number is gradually decreasing to 3.7%. The average humus reserves in arable soil level are made up 120 tons/ha. Because of ablation, these reserves decrease up to 73–100 tons/ha.

Previous research [14, 37, 38] studied spread of water erosion and aerotechnogenic contamination on the territory of the Dnepropetrovsk oblast (**Figure 6**). Threaten condition for the small rivers ecosystems were emphasized. Surface layer washing out from the slopes led to water reservoirs silting-up, eutrophication, etc. [39]. The areas where agricultural works are worth carrying out are shown on the map. The soils here are the least subjected to water erosion and anthropogenic contamination, and so they are eligible for the safe crop growth.

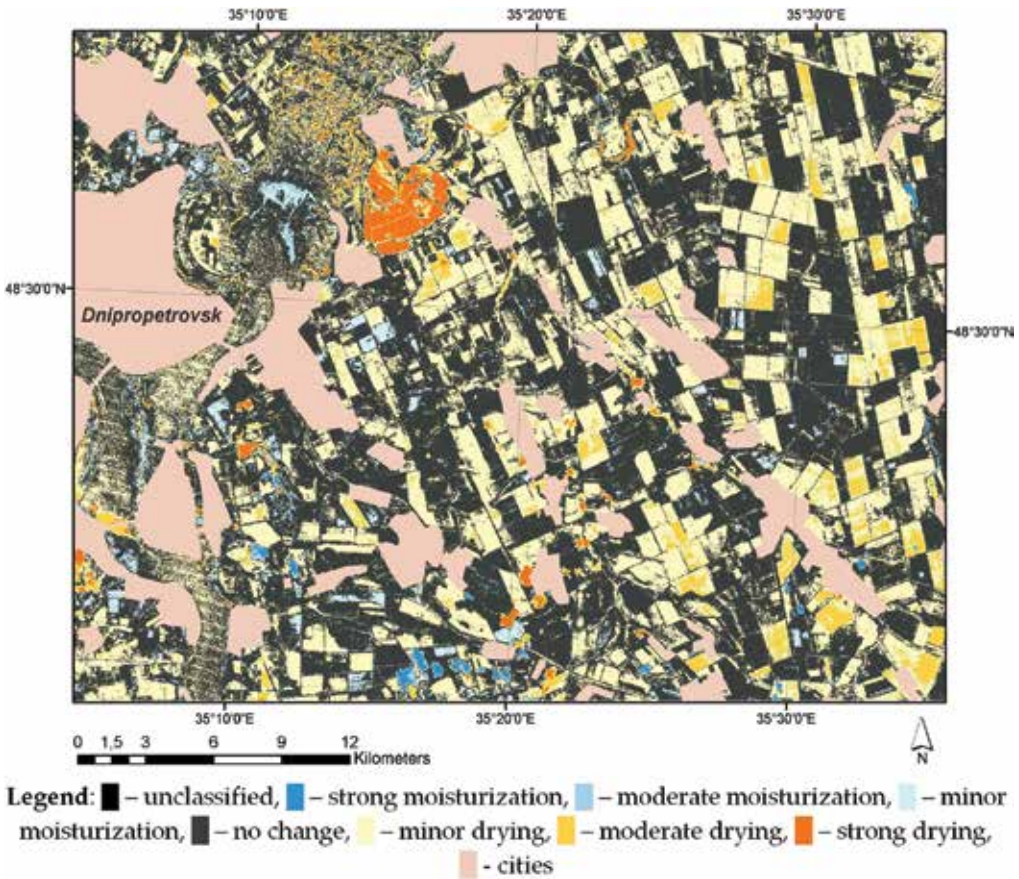

Figure 7. Soils moisture change within the left bank area of the Dnepropetrovsk oblast in 1988–2013.

Previous research [14, 37, 38] studied peculiarities of arable land degradation caused with several factors (arid climate, water and wind erosion, irrigation, salinization, old tillage systems application, acid rains, etc.). Additional environmental risks for the small rivers ecosystems were emphasized. In particular, surface layer washing out from the slopes led to water reservoirs silting-up, eutrophication, etc. [39]. Thus, all environmental risks of land degradation were taken in account to overlay them to select areas with four levels: high, medium, low and no-risk. High and medium levels of land degradation are the reason to

http://dx.doi.org/10.5772/62403

recommend a special phytoremediation and biomelioration measures. Low level of land degradation can be improved with low external input and sustainable agriculture.

Agricultural practices strongly depend on precipitation level. In the southern parts of the country, the amount of moisture in the soils remains one of the most important factors for the safe crop growth. To assess remotely the soil moisture, we used satellite imagery of Landsat-4,5/TM, Landsat-7/ETM+ and Landsat-8/OLI,TIRS with 30 m spatial resolution for the period 1998–2013. Registered at sensor radiance was recalculated into spectral reflectance of land surface taking into account the atmosphere influence—for visible, near, and short-wave infrared bands, and into the land surface temperature—for the thermal infrared bands [40]. Based on the ground measurements of the soil moisture on the test sites, the curvilinear regression relationship with remotely determined value $\ln(I_w/T+1)$ [41] was restored, where $I_w = \rho_{green}/(\rho_{green}+\rho_{swir})$—normalized water index, ρ_{green} and ρ_{swir}—land surface reflectance in green and short-wave infrared spectral bands, respectively, T—the land surface temperature. So, in this way, the soil moisture spatial distribution was mapped. Comparison of the remote sensing data and ground measurement results allowed us to study the soil moisture change within the left bank area of the Dnepropetrovsk oblast for the last 25 years (**Figure 7**).

Analysis of long-term change of soil moisture within the left bank of the Dnepropetrovsk oblast allowed us to elicit trends and to interpolate the results spatially. In particular, it was discovered that more than 50% of studied arable lands were in unfavourable conditions of different level drying.

9. Landscape degradation within mining area of central part of Ukraine

Mining is one of the most anthropogenic threats to the environment. The mineral deposits and operating mines are unevenly spread on the territory of the country. The Donetsk Basin in the south-east has large deposits of coal, while the east central area is rich in iron and uranium ores. Ukraine also has some of the world's largest manganese deposits, located in the southern Ukraine.

Mining industry stress promotes the creation of new elements in the landscape. These are refuse heaps of empty rocks, open pits, technogenic subsidence, disturbances created by technogenic accumulation—terricones, dumps, sludge depositories, etc. They are characterized by emergence of toxic rocks on the surface. Vegetation here is developed very slowly, and biocenosis is unstable. In case of the complete recultivation (deactivation of toxic rocks, formation of soil cover and remediation of phytocenosis), the secondary landscapes are formed.

The researched territory is called the Kirovograd uranium ore region and located in the central part of the Ukrainian Shield. It is subjected to a power pressure on the environment with consequent significant and often critical landscape transformations as a result of imperfect technologies and management. The mining development is accompanied by condemnation of considerable areas of fertile agricultural lands, predominantly chernozem. After temporal use,

the last ones are often transferred to a category of an anthropogenic desert. Next to each dumped fill of empty rocks, a risk zone is allotted (the first one is 200 m, the second one is 500 m) that leads to the significant loss of the land resources. Within such zones, the atmospheric air is polluted and the soils are salinized and waterlogged that makes impossible to use them in agriculture. Considerable areas are occupied with the solid wastes from reclamation industry, namely with ash dumps, storage tales, sludge pits. They have a significant amount of toxic elements that contaminate the atmospheric air, soils, surface and underground waters of neighbouring and remote landscape complexes.

Figure 8. Study area source multispectral satellite image (Landsat-5/TM, 23.08.2010, 30 m resolution pseudo-natural colour composite, Kirovograd oblast, Ukraine) (*a*); high-resolution images of researched mines: Smolinska mine (*b*), Novokostyantynivska mine (*c*) and Ingulska mine (*d*).

The Ukrainian uranium deposits are characterized by a low content of uranium. Nevertheless, developed infrastructure of their mining and uranium concentrate production along with big sizes of uranium deposits, high thickness of uranium-containing rocks, relatively low water content in mining tunnels, relatively simple measure of radiation protection (because of low content of uranium in ores)—all these facts provide competitive capacity for the uranium concentrate on the market and thus stipulates the development of uranium mining [42].

http://dx.doi.org/10.5772/62403

To investigate vegetation cover and soil erosion processes as the most reliable indicators of land degradation, we followed the same technique as it is described above at Section 6. We used Landsat-5/TM multispectral images for the period 1992–2010 from Landsat data store (http://landsatlook.usgs.gov) through the Earth Explorer geoportal. DTED SRTM (http://srtm.csi.cgiar.org) as of 1991 and ASTER GDEM (http://gdem.ersdac.jspacesystems.or.jp) as of 2010, soil map of the Kirovograd region, and climate characteristics by World Climate portal (http://www.climate-charts.com/Countries/Ukraine.html) were additionally involved into calculations. Source images that were used for further processing are shown in the **Figure 8**.

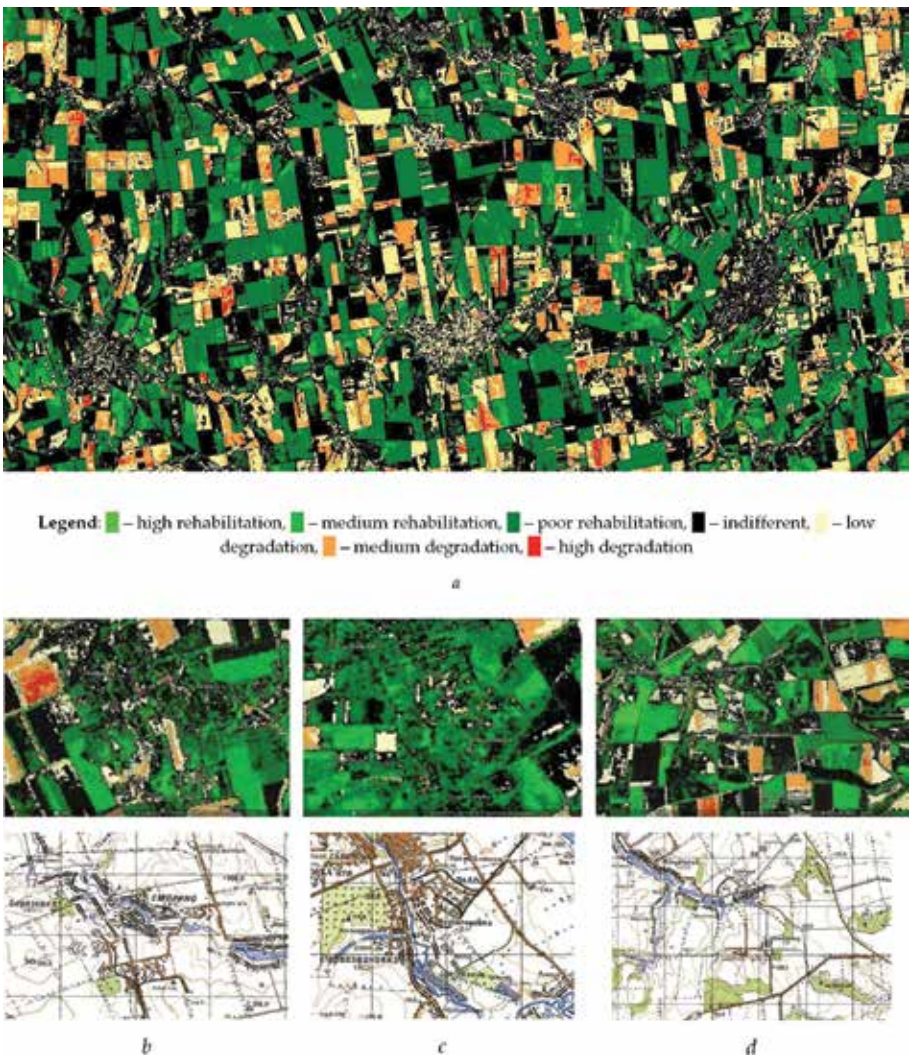

Figure 9. Mining area land degradation for the period from 1992 to 2010 (a); land degradation map within the Smolinska mine vicinity and the topographic base (b); c—land degradation map within the Ingulska mine vicinity and the topographic base (c), d—land degradation map within the Novokostyantynivska mine and the topographic base.

As a result of multispectral imagery processing, the land degradation map was obtained where seven classes of land degradation are depicted (**Figure 9a**) [43]. The areas of high degradation can be noticed within the territory of mine's infrastructure. But on the other hand, high level of anthropogenic transformation (the same yellow-orange colour) is also observed along the highway infrastructure and agricultural lands (overburden with unprecedented usage of fertile chernozem).

Negative and positive changes within the study area can be described for the period researched. The main part of the territory (around 35%) remains indifferent. These are urban areas of the Smolino town, woods and meadows around [44]. The same as we mentioned above for the Kirovograd ore region, high-degradation sites are observed in more detail on the arable lands perhaps due to crop rotation and poor management, along the small rivers and irrigated channels perhaps due to water erosion. The area around the mine itself is highly degraded which is understandable especially if to look at huge refuse heaps located nearby (**Figure 10**).

Figure 10. Refuse heaps of the Smolinska mine: directly next to the heap (a) and at a 200 m distance of from the heap (b).

The land degradation mapping technique on the basis of processing of a two-level model for multispectral satellite imagery can be used to investigate land degradation within human-inspired areas elsewhere, for example within energy facilities [45]. Let us consider the last example of the South-Ukrainian power-generation territory. This area where several energy facilities are located is considered as the one of high priority for further development of energy sector in Ukraine. Even though the environmental impact in this respect is expected to grow, the scientific research on impact assessment are being constantly held for the last time, their importance and new techniques development are always being brought to the agenda.

The aim of this study is preliminary assessment of land resource degradation within a radius of approximately 30 km around the South-Ukrainian Nuclear Power Plant (NPP) using multispectral satellite imagery and further development of geoinformation technologies for remote mapping of landscape changes.

http://dx.doi.org/10.5772/62403

In terms of physical and geographical location the researched area belongs to the Novo-Ukrainsk region of the steppe zone. The basic soil-forming rocks here are loess that determines formation of chernozem soils of different level salinity and humus content. Fertile chernozem soils were formed on Quaternary loess and loess-like loams within watershed divides and their slopes. Specific soil type called solonchak was formed within close location of high mineralized underground waters. Altogether around 60 different soil subtypes are found within the researched area. That is why auxiliary geospatial data were needed for remote land degradation research—digital terrain elevations, soil maps, climatic characteristics of study area, etc.

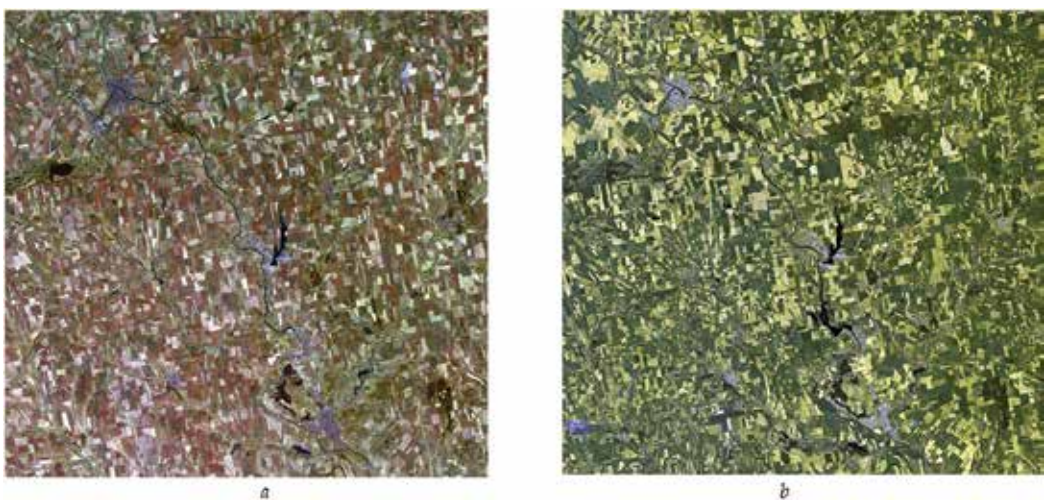

Figure 11. Study area source multispectral satellite images Landsat-5/TM, 24.08.1993 (a) and Landsat-8/OLI, 30.07.2013 (b); both ones are 30 m resolution pseudo-natural colour composite, Yuzhnoukrainsk, Ukraine.

In this case following the same technique, we used Landsat/TM and Landsat/OLI multispectral images of 1993 and 2013 correspondingly, obtained from the USGS Landsat Global Archive.

Thematic landscape changes maps obtained as a result of multispectral images processing (**Figure 11**), allowed assessing the state and trends in land degradation processes within the territory researched (**Figure 12**). The thematic map reflects the areas of low, medium and high degradation level. More than 40% of the territory within a radius of approximately 30 km from the NPP is subjected to anthropogenic impact of medium and high level [46]. These are mainly agricultural lands highly transformed due to crop rotation and poor management technique. The data demonstrate correlation between long-term industrial and agricultural impact and land degradation.

In all cases study, the research visually emphasizes the level of anthropogenic stress within the mining and energy facilities location and within arable lands around those facilities.

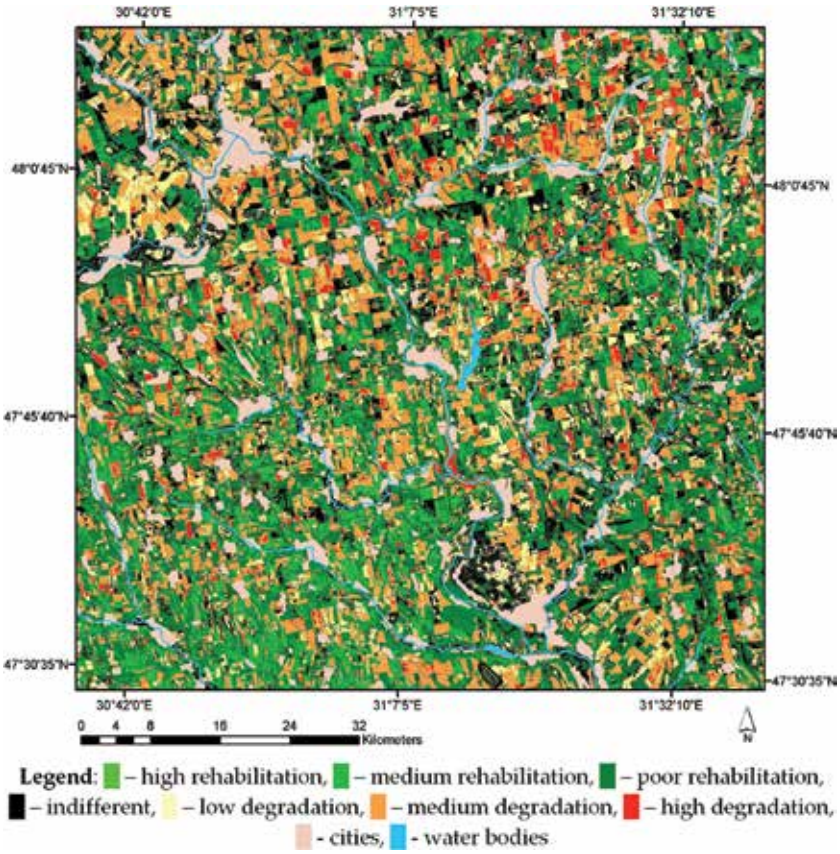

Figure 12. Land degradation map of the South-Ukrainian power-generation territory for the period from 1993 to 2013.

10. Conclusions

Remote methods introducing new dimensions into the study and understanding of long-term land degradation and desertification processes is of high priority for Ukraine because of their low cost, reliability and ability to cover large areas. Thematic landscape changes maps obtained as a result of multispectral images processing, allowed assessing the state and tendencies in land degradation and decertification processes occurred within landscape complexes undergone different level of anthropogenic stress.

Data obtained visually emphasize the level of anthropogenic stress, impact of long-term change of vegetation cover and correlation of intensive development of mining, construction, agricultural and other human activities with high level of land degradation within investigated areas. Especially, it is obvious within the territories of mining activities of the Kirovograd region.

http://dx.doi.org/10.5772/62403

The transition to adaptive farming systems implies the achievement of maximum compatibility between soil and plant, development of crop rotation, soil conservation tillage system. Conducted research on the creation of adaptive systems of crop production takes into account the environmental, landscape, and geochemical peculiarities of the steppe zone of Ukraine, to get the production of environmentally safe agricultural products. They can be used in further studies of a differentiated approach to achieving a balanced potential of agricultural landscapes.

Remote detecting of degradation and desertification processes intensification at early stages will be able to promote further measures for improving the territories conditions. The further research has to be directed on development of geoinformation technologies for landscape changes remote mapping.

Author details

Sergey A. Stankevich[1*], Nikolay N. Kharytonov[2], Tamara V. Dudar[3] and Anna A. Kozlova[1]

*Address all correspondence to: st@casre.kiev.ua

1 Scientific Centre for Aerospace Research of the Earth, National Academy of Sciences of Ukraine, Kiev, Ukraine

2 Dnepropetrovsk State Agrarian and Economic University, Dnepropetrovsk, Ukraine

3 Institute of Environmental Security, National Aviation University, Kiev, Ukraine

References

[1] Kharlamova G. Environmental security and its economical aspect. In: Vitale K, editor. Environmental and Food Safety and Security for South-East Europe and Ukraine. Dordrecht: Springer; 2012. pp. 73–80.

[2] Rudenko L, Maruniak E, Lisovsky S, Golubtsov O, Chekhniy V, Farion Y. The landscape plans system as a tool for sustainable development in Ukraine. In: Luc M, Somorowska U, Szmańda JB, editors. Landscape Analysis and Planning: Geographical Perspectives. Cham: Springer; 2015. pp. 217–244.

[3] United Nations. Environmental performance reviews series: Ukraine. Second review. Chapter 10. 2007; 24: pp. 131–142. Available from: https://www.unece.org/fileadmin/DAM/env/epr/epr_studies/Ukraine%20II.pdf

[4] United Nations Convention to Combat Desertification in Those Countries Experiencing Serious Drought and/or Desertification, Particularly in Africa [Internet]. 12.09.1994

[Updated: 30 January 2016]. Available from: http://www.unccd.int/Lists/ SiteDocumentLibrary/Publications/UNCCD_Convention_Eng.pdf

[5] UNCCD Annex V. Regional Implementation Annex for Central and Eastern Europe [Internet]. 25.11.2002 [Updated: 30 January 2016]. Available from: http://www.unccd.int/en/about-the-convention/Pages/Text-Annex-V.aspx

[6] Shvidenko A, Lakyda P, Schepaschenko D, Vasylyshyn R, Marchuk Y. Global change and landscape structure in Ukraine: Ecological and socio-economic implications. In: Geophysical Research Abstracts, Vol. 15.-EGU2013-10627; 7–12 April 2013; Vienna. Available from: http://meetingorganizer.copernicus.org/EGU2013/EGU2013-10627.pdf

[7] Davydenko VA, Bilyavsky GO, Arseniyk SY. Landscape ecology. Kiev: Libra; 2007. 280 p.

[8] Dudar TV. Landscape ecology. Kyiv: Publishing House of National Aviation University; 2014. 244 p.

[9] Verkhovna Rada of Ukraine. Land Code of Ukraine [Internet]. 25 October 2001 [Updated: 29 December 2015]. Available from: http://zakon2.rada.gov.ua/laws/card/2768-14

[10] Bernoux MMY., Fileccia T, Guadagni M, Hovhera V. Ukraine: Soil fertility to strengthen climate resilience: preliminary assessment of the potential benefits of conservation agriculture. Rome: World Bank Group; 2014. 96 p.

[11] Kharytonov M, Bagorka M, Gibson P. Erosion effects in the central steppe chernozem soils of Ukraine. Agricultura. 2004; 3(1):12–18.

[12] Dolgylevich M, Shvebs G, Zykov I. Scientific background for erosion forecasting and warning system. Moscow: Kolos; 1992. 197 p.

[13] Chornyi S, Chorna T. Dust storms on 23–24 March 2007: causes and effects. In: Regional problems of Ukraine: geographical analysis and search for solutions. Kherson: Vshemyrskyi; 2007. pp. 323–333.

[14] Chornyi S, Pysmennyi O. Wind resistance of soils in Ukrainian steppe. Bulletin of Kharkov National Agrarian University. 2002; 2: 147–150.

[15] Birmili W, Schepanski K, Ansmann A, Spindler G, Tegen I, Wehner B, Nowak A, Reimer E, Mattis I, Müller K, Brüggemann E, Gnauk T, Herrmann H, Wiedensohler A, Althausen D, Schladitz A, Tuch T, Löschau G. A case of extreme particulate matter concentrations over Central Europe caused by dust emitted over the southern Ukraine. Atmospheric Chemistry and Physics. 2008; 8(4):997–1016.

[16] Dolgylevich M. Dust storms and agroforestry. Moscow: Kolos; 1978. 159 p.

[17] Schenker M. Exposures and health effects from inorganic agricultural dusts. Environmental Health Perspectives. 2000; 108(4):661–664.

[18] Wiggs GFS, O'Hara SL, Wegerdt J, van Der Meer J, Small I, Hubbard R. The dynamics and characteristics of aeolian dust in dryland Central Asia: possible impacts on human exposure and respiratory health in the Aral Sea basin. The Geographical Journal. 2003; 69(2):142–157.

[19] Popov MA, Stankevich SA, Kozlova AA. Remote risk assessment of land degradation using satellite images and geospatial modeling. Reports of the National Academy of Sciences of Ukraine. 2012; 6: 100–104.

[20] Lu D, Mausel P, Brondízio E, Moran E. Change detection techniques. International Journal of Remote Sensing. 2004; 25(12):2365–2401.

[21] Zhongming W, Leesa BG., Feng J, Wanning L, Haijing S. Stratified vegetation cover index: A new way to assess vegetation impact on soil erosion. Catena. 2010; 83(1):87–93.

[22] Hairsine PB, Rose CW. Modeling water erosion due to overland flow using physical principles. Water Resources Research. 1992; 28(1):237–250.

[23] Khotynenko M O. Stability to deflation of agrolandscape surfaces in the Southern Ukrainian Steppe. Bulletin of Agricultural Science. 2007; 7: 78–80.

[24] United States Department of Agriculture. National Engineering Handbook Hydrology: Chapter 9. Hydrologic Soil-Cover Complexes [Internet]. July 2004 [Updated: July 2004]. Available from: http://www.nrcs.usda.gov/wps/portal/nrcs/detailfull/national/water/?cid=stelprdb [Accessed: January 2016]

[25] Carlson TN, Ripley DA. On the relation between NDVI, fractional vegetation cover, and leaf area index. Remote Sensing of Environment. 1997; 62(3):241–252.

[26] Kaspersen PS, Fensholt R, Drews M. Using Landsat vegetation indices to estimate impervious surface fractions for European cities. Remote Sensing. 2015; 7(6):8224–8249.

[27] Dolgilevich MJ. Extent and Severity of Wind Erosion in the Ukraine [Internet]. 28 January 1999 [Updated: 28 January, 1999]. Available from: https://infosys.ars.usda.gov/WindErosion/symposium/abstracts/dolgilev.htm [Accessed: 20 January, 2016]

[28] Stepanenko SN, Voloshin VG. Wind speed profiles in a permeable roughness layer. Ukrainian Hydrometeorological Journal. 2010; 6: 24–34.

[29] Hoffmann M, Zhovtonog O, Popovich V, Bolkina O, Mikhaylenko S. Use of GIS and GIS-based models for river basin management tasks and water management within rural areas. In: 23rd European Regional Conference "Progress in managing water for food and rural development"; 18–21 May 2009; Lviv, Ukraine. Lviv: Ivan Franko National University; 2009.

[30] Chorny SG, Khotinenko ON. Evaluation of Soil resistance to deflation due to modern climate change. Agricultural Chemistry and Pedology. 2009; 70: 69–76.

[31] Solberg AHS. Data fusion for remote-sensing applications. In: Chen CH, editor. Image Processing for Remote Sensing. Boca Raton: CRC Press; 2008. pp. 249–271.

[32] Zeng Y, Zhang J, van Genderen JL. Comparison and analysis of remote sensing data fusion techniques at feature and decision levels. In: Kerle N, Skidmore A, editors. ISPRS Symposium on Remote Sensing: from Pixels to Processes; May 8–11, 2006; Enschede, The Netherlands. Available from: http://www.isprs.org/proceedings/XXXVI/part7/PDF/014.pdf

[33] Stankevich SA, Kozlova AA, Vasko AV, Gerda MI. Hybrid model for data fusion in remote sensing research of the Earth. In: Abstracts of 11th Ukrainian Conference on Space Research; August 29–September 2, 2011; Yevpatoria, Ukraine. Yevpatoria: Space Research Institute; 2011. p. 74

[34] Kotenko TI, Umanets OJ, Selyunin ZV. Natural complex of Kozachelagerska arena in Lower Dnieper sands and problems of its conservation. Wildness Protection in Ukraine. 1999; 5(1):61–72.

[35] Svetlitchny AA. Soil erosion induced degradation of agrolandscapes in Ukraine: Modeling, computation and prediction in conditions of the climate changes. In: Groisman PY, Ivanov SV, editors. Regional Aspects of Climate-Terrestrial-Hydrologic Interactions in Non-boreal Eastern Europe. Odessa: Springer; 2009. pp. 191–199.

[36] Stankevich SA, Kozlova AO. Evaluation and mapping biodiversity of the North Black Sea region of Ukraine based on multispectral satellite imagery and GIS technology. Space Science and Technology. 2007; 13(2):18–24.

[37] Bagorka M, Mytsyk O, Pashova V, Kharytonov M. Features of soil formation processes in disturbed and unproductive sloping lands in Ukrainian steppes. Proceedings of Poltava State Agrarian Academy. 2005; 4(23):159–167.

[38] Stankevich S, Titarenko O, Kharitonov N, Khlopova V. Mapping air pollution of Pridneprovsky industrial region by nitrogen and sulphur dioxides using satellite data. Reports of the National Academy of Sciences of Ukraine. 2013; 3: 106–111.

[39] Kharytonov M, Anisimova L. Environmental assessment of surface water quality of the Dnieper River Basin. Ecology and Environmental Sciences. 2013; 17: 75–86.

[40] Roy DP, Wulder MA, Loveland TR, Woodcock CE, Allen RG, Anderson MC, . Landsat-8: Science and product vision for terrestrial global change research. Remote Sensing of Environment. 2014; 145(4):154–172.

[41] Sakhatskyi OI, Stankevich SA. To possibilities for land cover moisture assessment using multispectral satellite images of the optical range: Case study for Ukraine. Reports of the National Academy of Sciences of Ukraine. 2007; 11: 122–128.

[42] Nekludov IM. State and problems of nuclear energy in Ukraine. Problems of Atomic Science and Technology. 2007; 2: 3–9.

http://dx.doi.org/10.5772/62403

[43] Dudar TV, Stankevich SA, Tymoshenko YO, Bugera VA. Remote mapping of anthropogenic-induced landscape changes in uranium mining areas. Technogenic and Ecological Safety and Civil Protection. 2014; 6: 82–88.

[44] Dudar TV, Vedmedenko IV, Stankevich SA. Analysis of anthropogenic landscape changes in the Smolinskoy mine of Kirovograd region using satellite imagery. Environmental Safety and Management. 2014; 15: 40–4.

[45] Stankevich SA, Vasko AV, Gubkina VV. Two-level model for land degradation mapping on multispectral satellite imagery. In: Proceedings of the 8th International Conference on Digital Technologies (DT'2011); November 10–11 2011; Žilina, Slovak Republic. Žilina: University of Žilina; 2011. pp. 289–293.

[46] Stankevich SA, Lysychenko GV, Dudar TV. Remote assessment of chernozem soils degradation in the vicinity of nuclear industry facilities: South-Ukrainian power-generation area case study. In: Proceedings of the 3rd International Conference "Chemical and Radiation Safety: Problems and Solutions"; May, 19–22, 2015; Kyiv, Ukraine. Kyiv: Institute of Environmental Geochemistry NAS of Ukraine; 2015. pp. 44–45.

Section 2

Soil Quality and Land Degradation

Chapter 4

The Impact of Land Degradation on the Quality of Soils in a South African Communal Rangeland

Phesheya Dlamini and Vincent Chaplot

Additional information is available at the end of the chapter

http://dx.doi.org/10.5772/63128

Abstract

Grassland productivity of communal rangelands is limited by land degradation, which leads to nutrient depletion, soil fertility decline and overall soil quality. However, little is known as to what the soil quality threshold is for different degradation intensities. To address this, we selected a 0.05 m surface soil layer of a communal rangeland site in Drakensburg, South Africa, exhibiting a degradation gradient varying from heavily degraded (0–5%, grass aerial cover), moderately degraded (25–50%) and non-degraded (75–100%) grasslands, to evaluate the effects of land degradation on soil aggregate stability, compaction, bulk density and texture. Results indicate that land degradation decreased soil aggregate stability by 47%, increased soil compaction by 42% and increased soil bulk density by 12%, and these were accompanied by a pattern of lower sand and almost two times greater clay content in heavily degraded grassland compared with non-degraded grassland. Ultimately, this decline in the soil quality of the communal rangeland has serious implications for the ecosystem services and functions it provides, such as storing water, carbon sequestration and nutrient cycling. We recommend the protection and improvement of grass vegetation because of its dense sward characteristics, which intercept raindrop energy, slow surface runoff and increase the structural stability of the soil to minimize and prevent degradation in rangelands.

Keywords: land degradation, rangeland, soil quality, grass cover, smallholder

1. Introduction

Rangelands, including grasslands, scrublands and tundra, cover approximately 50% of the world's land surface [1]. The Land Degradation Assessment in Drylands (LADA) estimates that 16% of rangelands are currently undergoing degradation, with 20–25%

of the total land area being degraded, ultimately affecting the livelihoods of about 1.5 billion people worldwide [2]. Notably, this soil degradation is occurring in addition to historic degradation.

The degradation of rangelands is a consequence of several key activities, including overgrazing, livestock trampling and soil erosion [3, 4]. The widespread occurrence of soil degradation is also due to the mismanagement of marginal lands (semiarid, steep, shallow soils) in harsh and highly variable climates [5, 6]. With increasing population densities and the associated pressures on land, soil degradation is intensifying [7, 8].

Land degradation adversely depletes soil nutrients, which in turn directly affects their fertility, productivity and overall soil quality [9]. According to Vanlauwe et al. [8], soil fertility decline is directly linked to low productivity and food insecurity and is at the heart of rural poverty. Because soils are one of the largest stores of carbon that are in direct exchange with the atmosphere, soil degradation also negatively affects society through climate change feedbacks [10].

Because soil fertility depletion is one of the major threats to the sustainability of rangelands, precise determination of changes in soil quality is important in understanding the role of soils in the global cycle [11, 12]. A better understanding of the mechanisms of land degradation is crucial, not only to limit its consequences but also for mitigation and sustainable soil management [13]. While environmental degradation is expanding globally at an alarming rate, there is a major gap in our knowledge on the extent, severity and intensity of land degradation [14].

For many smallholder farmers in Sub-Saharan Africa (SSA), communal rangelands are grazed by livestock, which provide rural people with meat and dairy products and a source of income. However, one of the greatest challenges is that the rangelands are in a state of degradation due to an increase in human activities on marginal lands, misuse and mismanagement (overgrazing) and the associated problems of soil erosion [7, 9, 15, 16]. Soil fertility depletion and soil quality decline are major threats to the sustainability of these communal rangelands, partly because fertilizer inputs are not available or affordable in sufficient quantities [12].

Little is known on the impact of different intensities of land degradation on soil quality, with the most pertinent key issue being the threshold at which the effect of degradation will lead to a decline in soil quality. The main objective of this study was to evaluate the impact of a decrease in grass aerial cover as a consequence of land degradation on the quality of soil in a communal rangeland in the uplands of the Drakensburg region, KwaZulu-Natal Province, South Africa, that is managed by smallholder farmers. Grass cover was used as an indicator of land degradation, and quantification of such a land degradation indicator was done to help identify areas under threat and provide a basis for developing effective land management and rehabilitation options to improve the quality of communal rangeland soils [17, 18].

http://dx.doi.org/10.5772/63128

2. Materials and methods

2.1. Study site description

The study was carried out at the Potshini catchment, which is 10 km north of the Bergville District in the KwaZulu-Natal Province of South Africa (longitude: 29° 21′; latitude: –28° 48′). The site has a mean annual precipitation of 684 mm, the majority of which falls during the summer months (October and March), a mean annual potential evaporation of 1600 mm and a mean annual temperature of 13°C [19]. The altitude ranges from 1080 to 1455 m.a.s.l. The site is on a dark brown sandy loam soil (15% clay) derived from sandstone, mudstone and intruding dolerite boulders and classified as Acrisol [20], with the dominant clay mineral being kaolinite. The soil is moderately deep and well-drained and has an undulating slope of 6–8%. It is acidic (pH 3.78–3.86), with an effective cation exchange capacity (ECEC) ranging between 1.86 and 5.86 $cmol_c\ kg^{-1}$ and an acid saturation ranging between 48 and 80%. The vegetation in the area is classified as Moist Highland Sourveld [21], and the dominant vegetation species include *Hyparrhenia hirta* and *Sporobolus africanus*.

2.2. Soil sampling and preparation

A degraded communal rangeland site with homogeneous soil type and grazed extensively by livestock, a common and widespread land use practice in SSA [22], in the uplands of the Drakensburg region of South Africa (**Figure 1**) was selected because it exhibited a degradation

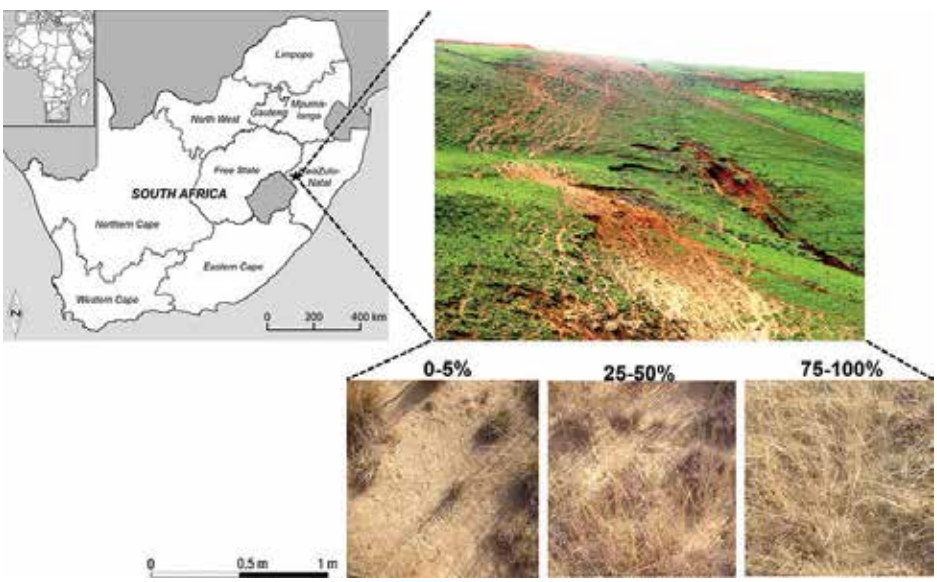

Figure 1. Location of the study area in the Drakensburg uplands of South Africa. Shown are images of soil surface coverage by vegetation for the different land degradation intensities or grass aerial cover from 0 to 5% (heavily degraded), 25 to 50% (moderately degraded) and 75 to 100% (non-degraded).

gradient varying from heavily degraded grassland with visible bare soils in the north to non-degraded grassland in the south. Such a state of degradation is a common feature of many communal rangelands in this part of South Africa.

Three categories of grass aerial cover were identified from surface soils across a degradation gradient of the communal rangeland site. A direct assessment was conducted based on vegetation cover [23], specifically grass aerial cover, which is the area of the ground covered by the vertical projection of the aerial portion of plants [24], to determine whether the land was degraded or not. Aerial cover was assessed by placing a 1 m×1 m plot frame at fixed intervals along each corresponding aerial cover category, while aerial cover of the plants in the plot was recorded as an estimate of the percentage of the total area [25]. The following grass aerial cover categories were established: 75–100% (Cov_{100}), corresponding to non-degraded grassland; 25–50% (Cov_{50}), corresponding to moderately degraded grassland; and 0–5% (Cov_5), corresponding to heavily degraded grassland. At each grass cover category, three sampling points were randomly selected, resulting in nine equidistant sampling locations along the degradation gradient. Four replicate soil samples 1 m apart at each sampling point were collected in a radial basis sampling strategy from a 0.05 m surface layer, giving a total of 12 samples per grass cover category and 36 soil samples along the degradation gradient. The surface layer was intensively sampled because the effects of land degradation on the quality of soil have been shown to be more pronounced in this soil layer [9, 26, 27]. In addition to these samples, triplicate core samples were also collected for bulk density using a 0.075 m diameter metallic cylindrical core (height=0.05 m) following a similar sampling strategy. Soil samples for bulk density were taken directly from the field to the laboratory and immediately oven-dried at 105°C to determine the oven-dry weight using the gravimetric method [28].

Once in the laboratory, field moist samples for soil aggregate stability were passed through an 8 mm sieve by gently breaking the soil along planes of weakness, air-dried and stored at room temperature before soil analyses. The remaining air-dried soils were ground to pass through a 2 mm sieve for further soil physical and chemical analyses.

2.3. Penetration resistance

In the field, penetration resistance (PR) was evaluated by randomly selecting 15 positions in each grass aerial cover category, and PR readings were taken in the topsoil surface layer. The PR of the soil, which is a proxy for soil compaction, was determined using a handheld cone penetrometer [29]. Notably, PR measurements were taken before the soil surface was disturbed for soil sample collection.

2.4. Determination of chemical and physical properties

Particle size distribution was determined by the sieve and pipette method [30]. Soil pH was determined in a 1:2.5 solution ratio in both deionized water and 1 M KCl suspension using a Calimatic M766 pH meter. The exchangeable cations Ca and Mg were determined by extraction in 1 M KCl, while P, K, Zn, Mn and Cu were determined by extraction in an Ambic 2 extract containing 0.25 M NH_4HCO_3 [31], with detection by inductively coupled plasma optical

http://dx.doi.org/10.5772/63128

emission spectrometry (ICP-OES) using an Optima 7300DV spectrometer (Perkin Elmer, Inc., Shelton, CT). Effective cation exchange capacity (ECEC) was calculated as the sum of extractable cations, with base saturation calculated as the proportion (%) of the ECEC accounted for by exchangeable bases (Ca, Mg, K and Na).

2.5. Determination of soil aggregate stability

After field sampling, moist soil samples were taken to the laboratory and air-dried at room temperature. During this period, large soil aggregates were periodically broken down by hand along lines of weakness to obtain maximum millimeter-sized aggregates. Soil samples were then sieved to isolate 3–5 mm aggregates for aggregate stability testing. Soil aggregate stability was determined on the 3–5 mm aggregates following the ISO standard method (ISO/DIS 10930:2012) outlined by Le Bissonnais [32]. The aggregates were subjected to rapid wetting by immersion into water, slow wetting by capillarity and mechanical disaggregation by shaking after wetting with ethanol, which correspond to different aggregate breakdown mechanisms, *viz*. slaking, differential clay swelling and mechanical breakdown, respectively. For the rapid wetting test, 10 g of 3–5 mm aggregates was submerged in 50 ml of distilled water in a beaker for 10 minutes, resulting in slaking of the soil. For the slow wetting test, 10 g of 3–5 mm aggregates was spread on top of a foam soaked in water. Thereafter, aggregates were allowed to wet through capillarity for 60 minutes. For the mechanical disaggregation test, 10 g of 3–5 mm aggregates was first immersed in a beaker with ethanol and then transferred to a beaker with distilled water to rest for 30 minutes. The aggregates were then transferred to an Erlenmeyer flask using distilled water and gently shaken up and down by hand 10 times. The weights of the aggregates collected on each sieve size (2, 1, 0.5, 0.2, 0.1 and 0.05 mm) were measured and expressed as the percentage of the initial dry mass sample. The mean weight diameter (MWD) for each disaggregation mechanism was calculated using the following equation:

$$\mathrm{MWD} = \frac{\sum (x_i w_i)}{100}, \tag{1}$$

where x is the mean inter-sieve size and w_i is the percentage of fragments retained by the sieve i. The greater the MWD, the more resistant the soil aggregates are to the aggregate breakdown mechanisms.

2.6. Statistical analysis

Results are presented as standard error (SE) of the means for each grass cover along the degradation gradient and, where specified, subjected to one-way analysis of variance using GenStat (VSN International, Hemel Hempstead, UK). Differences between means were tested using Duncan's multiple range test at $P<0.05$.

3. Results and discussion

In this study, land degradation reduced rangeland soil quality through a linear decrease in grass cover. Consequently, soil aggregate stability in the topsoil layer decreased from an average of 1.35 mm in non-degraded grassland to 0.71 mm in heavily degraded grassland, corresponding to a decline of 47% (**Figure 2**). The decline in the protective grass cover induced by degradation led to soil structural alteration, disruption of soil aggregates, increasing susceptibility of degraded soil to soil crusting and compaction. The less structural stability of the degraded soil may in turn increase soil erodibility — the inherent susceptibility of soil to detachment and transport by rainsplash and runoff [32].

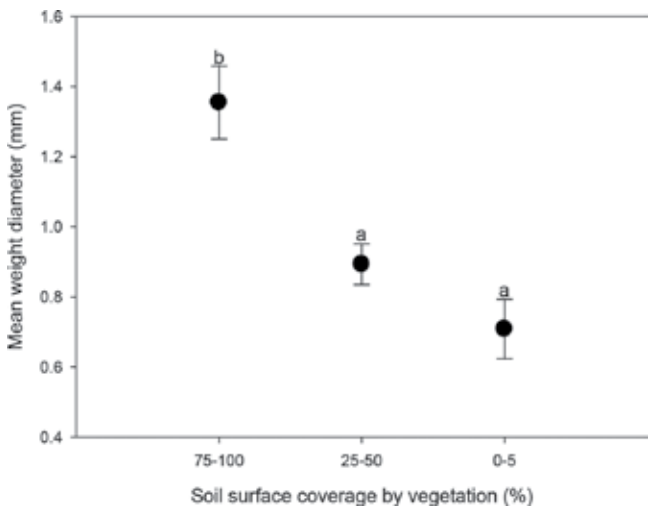

Figure 2. Relationship between soil aggregate stability and soil surface coverage by vegetation. Data are presented as mean±SE (n=12) per soil surface coverage by vegetation, and bars with different letters are significantly different at the P<0.05 level.

Penetrometer resistance, an important mechanical property used as an indicator of soil compaction [33], increased with decreasing grass cover from an average of 11.3 kg cm^{-2} in non-degraded grassland to 19.5 kg cm^{-2} in heavily degraded grassland, corresponding to an increase of 42% (**Figure 3A**). In agreement with our study, Snyman and du Preez [26] found that rangeland degradation decreased soil compaction by 65% from 18.3 kg cm^{-2} in non-degraded fine sandy loam soil to 6.4 kg cm^{-2} in heavily degraded fine sandy loam soil in a semiarid region in Bloemfontein, South Africa. One of the profound effects of soil compaction is the reduction in pore space and macroporosity, which is associated with increased bulk density [34, 35]. Such was the case in the present study, as soil bulk density increased by 12% from an average of 1.43 g cm^{-3} in non-degraded grassland to 1.61 g cm^{-3} in heavily degraded grassland, indicating increasing compaction (**Figure 3B**). Similarly, Hiltbrunner et al. [36] observed a 20% increase in soil bulk density on degraded grassland in a Swiss subalpine grassland, and this led to changes in biomass production.

http://dx.doi.org/10.5772/63128

Some studies have shown that soil compaction decreases the infiltration capacity of the soil [35, 37]. At our study site, Podwojewski et al. [38] found using rainfall simulation on runoff plots that land degradation decreased the soil infiltration rate by 72% from 21.6 mm h^{-1} in non-degraded grassland to 6 mm h^{-1} in heavily degraded grassland. While in South West England, the authors [38] found that the infiltration capacity was reduced by 80% and surface runoff volumes were increased by nearly 12 times on heavily degraded grassland compared with non-degraded grassland. The decrease in the infiltration capacity of soils with increasing degradation intensity may be explained by several reasons. First, a decline in protective grass cover and associated dense sward characteristics by land degradation leads to reduced intercepted raindrops and water movement through the soil. Second, a decline in the protective cover offered by grass decreases surface roughness, leading to decreased detention storage [38]. Although not investigated here, some studies have shown that soil compaction and the reduction in pore space also decrease the hydraulic conductivity of soil [34, 39].

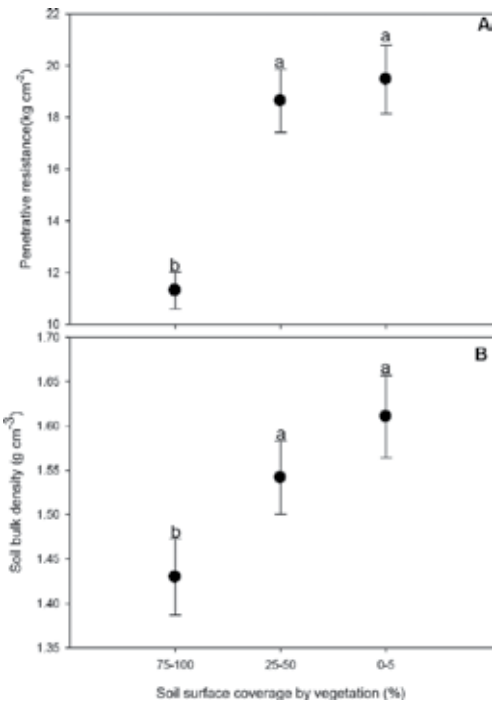

Figure 3. Mean±SE values of (A) penetrative resistance, a proxy for soil compaction (n=15), and (B) soil bulk density (n=12) per soil surface coverage by vegetation, and bars with different letters are significantly different at the P<0.05 level.

In this study, a pattern of lower sand (49%) was observed in heavily degraded grassland, compared with 72% in moderately degraded and 73% in non-degraded grassland. The depletion in sand was so marked that the mean clay content was almost two times (34%) greater in heavily degraded grassland compared with 14% in non-degraded grassland, while the distribution of silt content was similar along the degradation gradient (**Figure 4**). Indeed,

intensification of degradation can induce shifts in the distribution of texture, as indicated in the study by Dong et al. [27] in the Qinghai-Tibetan Plateau in China, which found that grassland degradation led to a shift in soil texture from loamy toward sandy loamy soils. This phenomenon was corroborated by Fullen et al. [40], whose study compared the textures of grassland and degraded sandy soils from Shropshire, UK, and concluded that degradation changed mean soil texture from a very slightly stony loamy sand to a slightly stony sandy loam. The authors also found that the degraded soil was particularly deficient in sand, especially medium and coarse sands, and the depletion in sand was so marked that the degraded bare soil had significantly greater mean percentage clay content than non-degraded grassland soil. A recent meta-analysis by Dlamini et al. [41] concluded that grassland degradation has a significantly negative effect on coarser textured soils than fine textured soils due to the lack of physical protection of organic matter and weak aggregation in sandy soils.

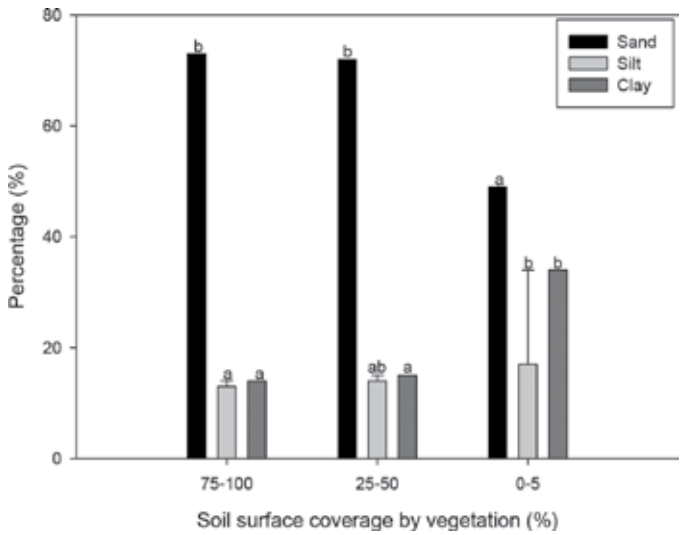

Figure 4. Relationship between sand, silt, clay and soil surface coverage by vegetation. Data are presented as mean±SE (n=12) per soil surface coverage by vegetation, and bars with different letters are significantly different at the P<0.05 level.

Land degradation results in the reduction of vegetation cover, which is unfavourable to soil protection. Degraded soils generated through the loss of vegetation cover are exposed to raindrop impact, which may lead to crust formation and a reduction in the infiltration capacity of the soil [42]. Such effects may lead to bare soil being more susceptible to surface runoff generation as drainage becomes impeded. These changes to soil hydrology have implications for runoff from degraded land, potentially modifying not only the quantity but also the quality of runoff, in terms of sediment and nutrient loads transported over and through the soil [37]. Vegetation cover by intercepting raindrops and enhancing infiltration protects the soil surface from the erosional effects of rainsplash and surface runoff, and this in turn helps preserve the water quality in surface waters of rangelands.

http://dx.doi.org/10.5772/63128

4. Conclusion

The reduction in grass cover induced by degradation in the communal rangeland resulted in a decrease in soil aggregate stability. The reduced soil structure or aggregation was concomitant with an increase in soil compaction and bulk density as well as a shift in soil texture associated with decreasing sand content and increasing clay content in the soil surface layers. Soil structure and texture are soil quality parameters crucial to the provision of ecosystem services and desirable for functioning of rangelands. Land degradation by adversely altering the quality of these soil properties negatively affects the services they provide, such as storing water, carbon and nutrients, which affect grassland productivity when lost. For many smallholder farmers, the grass vegetation of communal rangelands is essential to livestock production by providing forage for grazing animals, meat, dairy products and income to the people. As such, quantitative data on the effects of degradation on the quality of rangeland soils and the processes involved are crucial for developing effective land management and rehabilitation options, with the goal of improving rangeland productivity. Soil quality in degraded rangelands can be enhanced by adopting focused initiatives, such as the UN Convention to Combat Desertification. Improvement of rangelands can involve various grassland management options — from fertilization, soil tillage, livestock exclusion, burning and appropriate grazing regimes, which can lead to more sustainable rangelands. More work of this nature needs to be carried out on different soil types under diverse rangeland environments.

Acknowledgements

This work was funded by the Water Research Commission (Project No. K5 2266). We thank Dr. A. Manson and Charmaine Mchunu from the Soil Fertility and Analytical Services (Cedara) of the Department of Agriculture and Environmental Affairs (DAEA) for their help with laboratory analysis, as well as the Potshini community for granting us access to their communal rangeland.

Author details

Phesheya Dlamini[1*] and Vincent Chaplot[2]

*Address all correspondence to: dlaminiPE@ufs.ac.za

1 Department of Soil, Crop and Climate Sciences, University of the Free State, Bloemfontein, South Africa

2 IRD-LOCEAN c/o School of Agricultural, Earth & Environmental Sciences, Centre for Water Resources Research, University of KwaZulu-Natal, Scottsville, South Africa

References

[1] Kiage LM. Perspectives on the assumed causes of land degradation in the rangelands of Sub-Saharan Africa. Progress in Physical Geography. 2013;37:664–684.

[2] Bai ZG, Dent DL, Olsson L, Schaepman ME. Assessment of Land Degradation and Improvement. 1. Identification by Remote Sensing. Report 2008/01. ISRIC — World Soil Information, Wageningen; 2008.

[3] Daily GC. Restoring value to the world's degraded lands. Science. 1995;269:350–354.

[4] UNEP. Global Environmental Outlook GEO4: Environment for Development. United Nations Environmental Programme, Nairobi, Kenya; 2007.

[5] FAO. Review of evidence on drylands pastoral systems and climate change. In: Neely C, Bunning S, Wilkes A, editors. Land Tenure and Management Unit (NRLA). Land and Water Discussion Paper 8; 2009. p. 50.

[6] Lal R. Soil management in the developing countries. Soil Science. 2000;165:57–72.

[7] Dlamini P, Orchard C, Jewitt G, Lorentz S, Titshall L, Chaplot V. Controlling factors of sheet erosion under degraded grasslands in the sloping lands of KwaZulu-Natal, South Africa. Agricultural Water Management. 2011;98:1711–1718.

[8] Vanlauwe B, Six J, Sanginga N, Adesina AA. Soil fertility decline at the base of rural poverty in Sub-Saharan Africa. Nature Plants. 2015;1:1.

[9] Dlamini P, Chivenge P, Manson A, Chaplot V. Land degradation impact on soil organic carbon and nitrogen stocks. Geoderma. 2014;235:372–381.

[10] Wall DH, Six J. Give soils their due. Science. 2015;347:695.

[11] Schrumpf M, Schulze ED, Kaiser K, Schumacher, J. How accurately can soil organic carbon stocks and stock changes be quantified by soil inventories? Biogeosciences Discussions. 2011;8:723–769.

[12] Allen DE, Pringle MJ, Bray S, Hall TJ, O'Reagen PO, Phelps D, Cobon DH, Bloesch PM, Dalal RC. What determines soil carbon stocks in the grazing lands of north-eastern Australia? Soil Research. 2013;51:695–706.

[13] Kiage LM. Land degradation. In: Warf B, editor. Encyclopedia of Geography, Volume 4. SAGE, London; 2010. pp. 1679–1684.

[14] Andersson E, Broggaard S, Olsson L. The political ecology of land degradation. Annual Review and Resources. 2011;36:295–319.

[15] Suttie JM, Reynolds SG, Batello C. Grasslands of the World. Food and Agricultural Organization of the United Nations, Rome, Italy; 2005.

[16] Mchunu C, Chaplot V. Land degradation impact on soil carbon losses through water erosion and CO_2 emissions. Geoderma. 2012;79:177–178.

[17] Waswa B, Vlek PLG, Tamene LD, Okoth P, Mbakaya D, Zingore S. Evaluating indicators of land degradation in smallholder farming systems of western Kenya. Geoderma. 2013;195–196:192–200.

[18] Chaplot V, Dlamini P, Chivenge P. Potential of grassland rehabilitation through high density-short duration grazing to sequester atmospheric carbon. Geoderma. 2016;271:10–17.

[19] Schulze RE. South African Atlas of Agrohydrology and Climatology, TT82/96. Water Research Commission, Pretoria, RSA; 1997.

[20] World Reference Base for Soil Resources: A Framework for International Classification, Correlation and Communication. Intern. World Soil Resources Report No. 103. FAO, Rome; 2006.

[21] Camp KGT, Hardy MB. Veld condition assessment. Veld in KwaZulu-Natal. KwaZulu-Natal Department of Agriculture, RSA; 1999.

[22] Yayneshet T, Treydte AC. A meta-analysis of the effects of communal livestock grazing on vegetation and soils in Sub-Saharan Africa. Journal of Arid Environments. 2015;116:18–24.

[23] NRC. Rangeland Health: New Methods to Classify, Inventory, and Monitor Rangelands. National Academy Press, Washington, DC; 1994.

[24] USDA. Sampling Vegetation Attributes. Interagency Technical Reference, BLM/RS/ST-96/002+1730; 1996.

[25] Daubenmire R. A canopy-coverage method of vegetational analysis. Northwest Science. 1959;33:43–64.

[26] Snyman HA, du Preez CC. Rangeland degradation in a semi-arid South Africa — II. Influence on soil quality. Journal of Arid Environments. 2005;60:483–507.

[27] Dong SK, Wen L, Yi YY, Wang XX, Zhu L, Li XY. Soil-quality effects of land degradation and restoration on the Qinghai-Tibetan Plateau. Soil Science Society of America Journal. 2012;76:2256–2264.

[28] Blake GR, Hartge KH. Bulk density. In: Klute, A. editor. Methods of Soil Analysis. Part 1. Physical and Mineralogical Methods. Agronomy Monograph No. 9, Book Series, 2nd ed. Soil Science Society of America, Madison, WI; 1986. pp. 363–375.

[29] Herrick AM, Jones TL. A dynamic cone penetrometer for measuring soil penetrative resistance. Soil Science Society of America Journal. 2002;66:1320–1324.

[30] Gee GW, Bauder JW. Particle size analysis. In: Klute A, editor. Methods of Soil Analysis. Part 1. Agronomy No. 9. American Society of Agronomy, Inc., Madison, WI; 1986.

[31] Manson AD, Roberts VG. Analytical Methods Used by the Soil Fertility and Analytical Services Section. KZN Agri-Report No. N/A2001/04. KwaZulu-Natal Department of Agriculture and Environmental Affairs, Pietermaritzburg, South Africa; 2000.

[32] Le Bissonnais Y. Aggregate stability and assessment of soil crustability and erodibility: I. Theory and methodology. European Journal of Soil Science. 1996;47:425–437.

[33] Vanags C, Minasny B, McBratney AB. The Dynamic Penetrometer for Assessment of Soil Mechanical Resistance. SuperSoil 2004: 3rd Australian New Zealand Soils Conference, 5–9 December 2004. Published on CD-ROM; University of Sydney, Australia; 2006.

[34] Willatt ST, Pullar DM. Changes in soil physical properties under grazed pasture. Australian Journal of Soil Research. 1983;22:343–348.

[35] Mulholland B, Fullen MA. Cattle trampling and soil compaction on loamy sands. Soil Use Management. 1991;7:189–193.

[36] Hiltbrunner D, Schulze S, Hagedorn F, Schmidt MWI, Zimmermann S. Cattle trampling alters soil properties and changes microbial communities in a Swiss sub-alpine pasture. Geoderma. 2012;170:369–377.

[37] Heathwaite AL, Burt TP, Trudgill ST. Land-use controls on sediment production in a lowland catchment, south-west England. In: Boardman J, Foster IDL, Dearing JA, editors. Soil Erosion on Agricultural Land. John Wiley and Sons, Ltd.; Chichester, UK. 1990. pp. 70–86.

[38] Podwojewski P, Janeau JL, Grellier S, Valentin C, Lorentz S, Chaplot V. Influence of grass soil cover on water runoff and soil detachment under rainfall simulation in a sub-humid South African degraded rangeland. Earth Surface Processes and Landforms. 2011;36:911–922.

[39] Greenwood KL, Macleod DA, Hutchinson KJ. Long-term stocking rate effects on soil physical properties. Australian Journal of Experimental Agriculture. 1997;37:413–419.

[40] Fullen MA, Zhi WB, Brandsma RT. A comparison of the texture of grassland and eroded sandy soils from Shropshire, UK. Soil & Tillage Research. 1998;46:301–305.

[41] Dlamini P, Chivenge P, Chaplot V. Overgrazing decreases soil organic carbon stocks the most under dry climates and low soil pH. Agriculture, Ecosystems and Environment. 2016;221:258–269.

[42] Assouline S, Thompson SE, Chen L, Svoray T, Sela S, Katol GG. The dual role of soil crusts in desertification. Journal of Geophysical Research. Biogeosciences. 2015;20:2108–2119.

Chapter 5

Land Degradation in the Çelikli Basin, Turkey

İrfan Oğuz, Ertuğrul Karaş, Sabit Erşahin and Tekin Susam

Additional information is available at the end of the chapter

http://dx.doi.org/10.5772/64624

Abstract

The relationship between soil degradation and wheat yield was analyzed in the Çelikli basin, Turkey. Geographic information system (GIS) and factor analysis techniques were used for evaluations. Wheat yield has changed between 600 and 3780 kg ha^{-1}. Soil penetration resistance (PR) was below 2 MPa in 34.92% of the topsoils and was over 2 MPa in the entire of subsoils. The soil loss changed from 0 to 152.8 ton ha^{-1} $year^{-1}$. Soils in the study area were generally low in plant-available water (PAW) content. Compared to P, K content was sufficient in top and subsoils in most of the study area. The results showed that B and Zn contents were low, and Cu, Mn, Fe, and Cd contents were adequate. Boron content was less than 0.5 mg kg^{-1} in 85.5% of the cultivated and 82.9% of the grassland, and Zn was less than 0.5 mg kg^{-1} in 99.7% of the study area. Low organic matter, low water-holding capacity, high penetration resistance, and deficiency of some macro- and micronutrients were the most important limiting factors of wheat yield. Crop rotation and P, B, and Zn application can help restore soil productivity in cultivated areas of the study area.

Keywords: land degradation, wheat yield, organic matter, water-holding capacity, penetration resistance, crusting index

1. Introduction

Land degradation comprises human-induced processes that affect land resources and environmental sustainability. Land degradation is recognized as one of the most serious ecological and economical problems globally. Soil erosion, soil compaction, deterioration in soil structure, nutrient depletion, acidification, and salinization have been defined as major soil degradation processes [1]. The human activities such as fires, floods, soil loss (SL), and

yield reduction may affect land degradation directly or indirectly. In the twenty-first century, land degradation is considered an important factor affecting food security. The world's agricultural land that is seriously degraded is estimated to have reached up to 40% [2].

Land degradation in Turkey has been mainly in the form of soil erosion, agricultural mismanagement, deforestation, and overgrazing, and is a result of human activities for the last century. The most prominent result of soil degradation in Turkey has been soil erosion, which develops due to the region's climate, topography, soil, and land-use problems. In Turkey, 59% of rangelands, 54% of forest lands, and 71% of agricultural lands are under active erosion threat [3]. Furthermore, an area of 4.2 million ha has lost its productivity partly or completely due to salinity problems [4]. Topographic and climate conditions have made it necessary to combat soil erosion. In Turkey, 24.1 million livestock graze on pastures, but the pastures can no longer provide sufficient roughage for the livestock to feed, and the existing land cover on pasture areas are used intensively. Overgrazing, especially noticeable in Turkey's Mediterranean, Aegean, Southeastern, and Central Anatolia regions, damages vegetation, increases runoff, and promotes erosion. The surface coverage of pasture areas ranges from 15 and 30%. Severe water and wind erosion are visible in those areas. To avoid soil erosion, surface coverage should be increased in the pasture areas where misuse is taking place—an area of 21.7 million ha. The amount of grazing animals and their grazing time must be brought under control [5]. Land use has changed in significant ways over the last 100 years in Turkey due to agricultural expansion. For example, while pasture areas made up about 56.8% (44.2 million ha) of land use in 1940, today they are only 18.6% (14.6 million ha). Most of changes to land use occurred on pasture land that was converted to agricultural purposes [3].

The main objective of this study is to evaluate soil degradation regarding wheat yield (WY) as affected by deteriorated soil properties in the Çelikli basin, located in North Central Anatolia of Turkey.

2. Materials and methods

2.1. The study area

This study was conducted in the Çelikli basin, located in Tokat province, which is known as the transitional belt of Turkey. This area is situated between Central Anatolia and Black Sea regions (latitude 40°06′31″N, longitude 36°21′40″E). The types of soil in the basin are classified as Entisols, Mollisols, and Alfisols according to Soil Survey Staff [6] and are moderately well to well drained with a slope of 2–12% in the majority of the area. The basin is 1041.2 ha and has an average elevation of 1300 m above sea level. Although native land use of the basin was for pasture and forest, over the last five decades, most of the pasture and forest areas were converted to agriculture. The main crop in the cultivated areas is wheat, which is grown under rainfed conditions. Although 14.07% of the basin is available for agriculture, the dry farming area occupies 67.88% of the basin. The main vegetation type in uncultivated areas is degraded pasture with *Graminea*, *Fabaceae*, and *Labiatae* as the dominant species, occupying 24.86% of the basin. The coverage rate in the degraded pasture areas is about 50%. Other features in the area

http://dx.doi.org/10.5772/64624

are shrubs, bare rock, and water surfaces, which make up 5.45, 0.82, and 0.98%, respectively, shown in **Figure 1**. The study area has semiarid climate. The average annual temperature is 8.1°C, and the mean annual precipitation is 535.9 mm, 84.7% of which falls between October and May. The amount of evaporation from Class A pan between March and October is about 900 mm, which is greater than almost two times of the yearly precipitation [7].

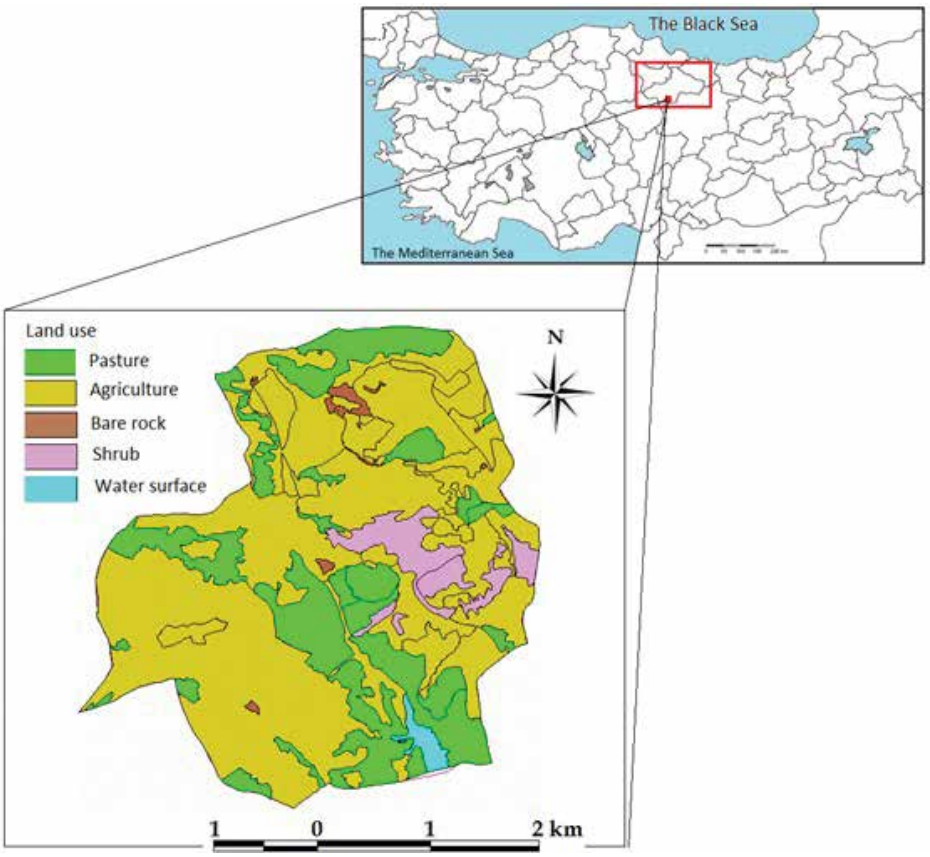

Figure 1. The location and land-use map of the Çelikli basin.

2.2. Soil sampling and laboratory analysis

A total of 142 georeferenced soil samples were taken from topsoil (0–0.3 m) and subsoil (0.3–0.6 m) (**Figure 2**). Organic matter [8], soil pH [9], lime ($CaCO_3$) [10], electrical conductivity (EC) [11], cation exchange capacity (CEC) [12], textural distribution [13], saturated hydraulic conductivity (HC) (Ks) [14], and volumetric water content [15] were analyzed. Erodibility was calculated by a soil erodibility nomograph [16].

Fractions that were greater than 2 mm in diameter were separated and reported as coarse material (CM) [12]. Saturated hydraulic conductivity (Ks) was measured on undisturbed

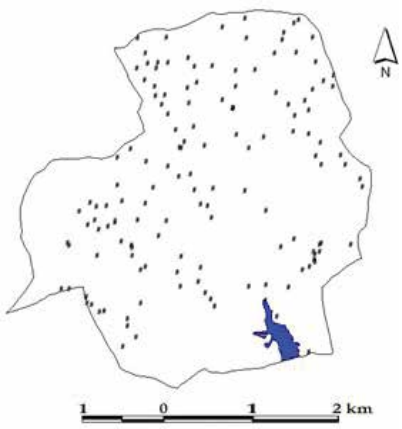

Figure 2. Locations of soil sampling points in the basin.

cores [14]. Soil penetration resistance (PR) was measured with a cone penetrometer at depths of 0–10 and 30–40 cm [17], and the soil-crusting index (CI) was calculated by Eq. (1) using soil organic matter (SOM), clay, and, silt contents [1]:

$$CI = \frac{100SOM(\%)}{Clay\% + Silt\%} \tag{1}$$

Wheat yield was measured at sampling sites. Field capacity ($\theta_{0.33\text{MPa}}$) and wilting points ($\theta_{1.50\text{MPa}}$) were determined with a pressure plate [14], and plant-available water content (PAWC) was calculated by Eq. (2):

$$PAW = \left(\theta_{0.33MPa}\right) - \left(\theta_{1.50MPa}\right) \tag{2}$$

Slope, %	Permeability classes					
	Rapid-very rapid	Moderate rapid	Moderate	Moderate slow	Slow	Very slow
Concave	N[a]	N	N	N	N	N
<1	N	N	N	L	M	H
1–5	N	VL	L	M	H	VH
5–10	VL	L	M	H	VH	VH
10–20	VL	L	M	H	VH	VH
>20	L	M	H	VH	VH	VH

N[a], negligible; VL, very low; L, low; M, medium; H, high; VH, very high.

Table 1. Indices determined for surface runoff classes in the study area.

http://dx.doi.org/10.5772/64624

Surface runoff was calculated using slope steepness and permeability of the soils (**Table 1**) [18]. Soil loss was calculated by the Universal Soil Loss Equation (USLE) [19] as

$$A = RKLSCP \tag{3}$$

where A is the soil loss (Mg ha^{-1}), R is the rainfall factor (MJ mm ha^{-1} h^{-1} yr^{-1}), K is the soil erodibility factor (t ha h ha^{-1} MJ^{-1} mm^{-1}), LS is the topography factor, C is the crop management factor, and P is the management practice factor.

2.3. Data analysis

Descriptive statistics of mean, standard deviation (SD), coefficient of variation (CV), kurtosis, skewness, maximum, and minimum were calculated for the variables of particle-size components, coarse material, wheat yield, soil loss, available water content (AWC), runoff, crusting index, penetration resistance, saturated hydraulic conductivity (Ks), soil organic matter, electrical conductivity, pH, cation exchange capacity, available K, available P, and available micronutrients (Fe, Cu, Mn, Cd, Zn, and B).

Factor analysis was conducted separately on topsoil and subsoil using Statistical Package for the Social Sciences (SPSS; Chicago, IL) to summarize correlations among variables [20]. First, correlation matrices, eigen values, and eigen vectors were calculated. Second, main factors were determined by the maximum likelihood method [21] and scree analysis [20]. Factors with a loading of >0.5 were retained. Finally, principal components were determined [22]. Relations among the variables were explained using the factor loadings. The principal components derived from the prepared correlation matrices were subjected to an orthogonal rotation of axes (varimax rotation) when multiple loadings occurred. Nine factors (Factor 1: "erodibility factor"; Factor 2: "soil fertility factor"; Factor 3: "soil chemistry factor"; Factor 4: "soil-crusting factor"; Factor 5: "soil erosion factor"; Factor 6: "soil conductivity factor"; Factor 7: "plant-available water content factor"; Factor 8: "macroelement factor"; Factor 9: "crop yield factor") for topsoil and seven factors (Factor 1: "microelements factor"; Factor 2: "soil physics factor"; Factor 3: "soil fertility factor"; Factor 4: "soil chemistry factor"; Factor 5: "yield factor"; Factor 6: "soil potassium factor"; and Factor 7: "soil cadmium factor") for subsoil were retained. The loading (or eigenvectors) of a variable in a factor is similar to the correlation between the variable and the factor.

2.4. Data processing with geographical ınformation system

Spatial relations between soil properties (EC, pH, SOM, P, K, B, Zn, Cu, Fe, Mn, Cd, CEC, Sand, Clay, Silt, K factor, CI, PAWC, PR) and wheat yield were investigated by GIS. Soil, digital elevation, land use, productivity, soil compaction, plant-available water content, surface runoff, and soil loss maps were prepared using ArcView 3.1 GIS Software [23]. The basin soil, elevation, and land-use maps with a 1:25,000 scale were digitized in vector format and then transformed to raster format to prepare GIS applications [24].

3. Results and discussion

3.1. Wheat yield

Wheat is the main crop in the study area, covering 68% of the study area. Although only 14% of the basin is suitable for cultivation, most of the pasture areas have been converted to agriculture for the last 60 years. The agricultural areas in the basin are mostly shallow, varying between 20 and 50 cm. The mean plant-available water content for the cultivated areas is about 100 mm. Therefore, water stored in soils often fails to meet crop water requirement. In the dryland farming areas receiving less than 400 mm annual precipitation such as the Çelikli basin in Turkey, a winter wheat-fallow system is used to reduce the risk of uneconomical yield [24]. Wheat yield was measured at 115 sites with three repetitions in the basin (**Table 2** and **Figure 3**). While the wheat yields ranged from 600 to 3780 kg ha^{-1}, only 4.78% of the cultivated areas had yield greater than 2500 kg ha^{-1} as shown in **Table 3**.

	Yield (kg ha^{-1})
Sample number	115
Maximum	3780
Minimum	600
Average	1794
Standard deviation	744
Coefficient of variation	0.41

Table 2. Statistical results of the wheat yield.

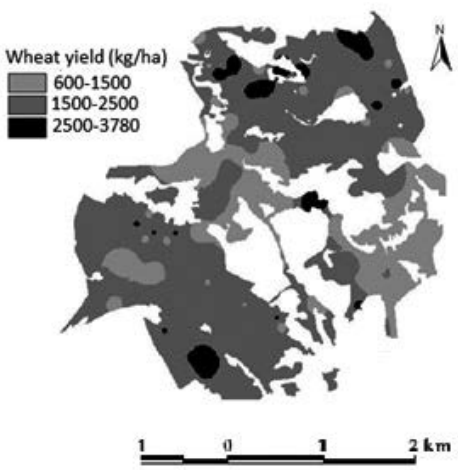

Figure 3. The wheat yield distribution in the basin.

http://dx.doi.org/10.5772/64624

Wheat yield (kg ha^{-1})	600–1500	1500–2500	2500–3780
Area, km^2	1.715	5.016	0.338
Area, %	24.26	70.96	4.78

Table 3. Areal distribution of the wheat yield in the basin.

3.2. Evaluation of soil degradation in the basin

3.2.1. Soil penetration resistance

The penetration resistance values and their statistical results for the basin are given in **Tables 4** and **5** and **Figure 4a** and **b**. While 34.92% of the topsoils in the basin had under 2.0 MPa, the penetration resistance of all subsoils had penetration resistance values over 2.0 MPa. High PR values were attributed to soil texture (fine) and low water content of the soils. Penetration resistance is sensitive to soil water content. In addition, in subsoils, high penetration resistance could be attributed to the existence of a dense plow layer, which is mainly the case in cultivated fine-textured soils subjected to conventional tillage. The mean penetration resistance values of the surface and subsoils were 1.671 and 2.579 MPa, respectively, which are below 3.0 MPa above which growth of many crops is inhibited [25]. The penetration resistance was measured in 0–20 cm only due to that soil depth was too shallow in grasslands. In general, the coefficient of variation and standard deviation for penetration resistance in topsoil were greater than in the subsoil due to soil tillage effect.

	The penetration resistance, kPA				**Tendency to crust, CI**		**Plant available water content, PAWC**		
	Topsoil		**Subsoil**						
	<2000	**>2000**	**<2000**	**>2000**	**0–5**	**5–10**	**27–50**	**50–100**	**100–160**
Area, km^2	6.776	3.636	0.081	10.331	9.940	0.472	0.445	4.686	5.281
Area, %	65.08	34.92	0.78	99.22	95.47	4.53	4.27	45.01	50.72

Table 4. Areal distribution of the penetration resistance, crusting index, and plant-available water content of the basin soils.

	Penetration resistance		**Crusting index**
	Topsoil	**Subsoil**	
Sample numbers	142	115	142
Maximum	3882.38	3522.00	9.41
Minimum	170.78	1590.03	0.78
Mean	1671.22	2579.63	3.21
Standard deviation	1080.86	332.04	1.75
Coefficient of variation	0.65	0.13	0.55

Table 5. Statistical results for penetration resistance and tendency to crust of the basin soils.

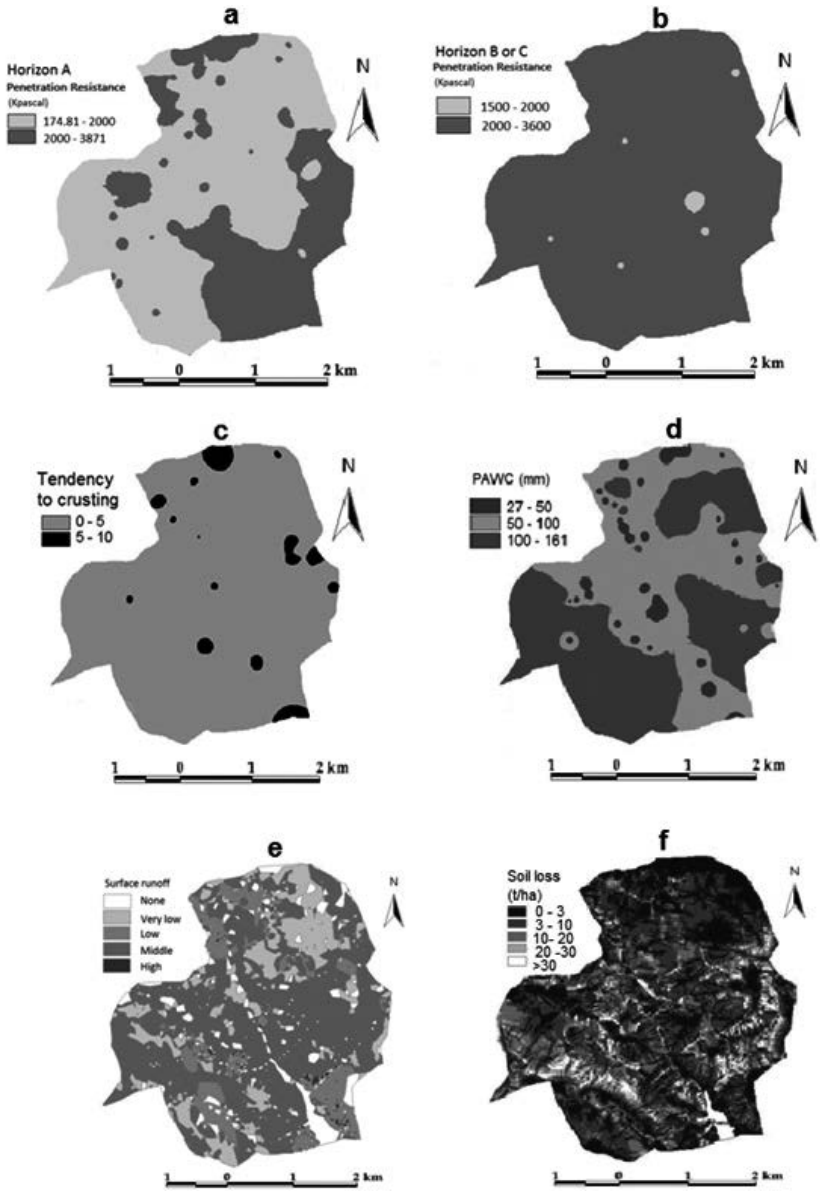

Figure 4. The penetration resistance (a and b), crusting index (c), plant available water content (d), surface runoff (e) and soil loss (f) maps of the basin.

The penetration resistance affecting crop yield is not a constant value and varies according to other soil properties. Indeed, it was reported that there was no penetration problem under 2000 KPa, but crop yields were affected over 2.00 MPa [26]. However, some researchers claim that the crop yield is affected by PR of >3.00 MPa [27–29]. Soil penetration resistance is a valuable indicator of the soil physical quality. A value of 2 MPa has been widely used as a

critical limit to determine PR in both no-tillage and conventional systems [25, 26]. PR varies spatially as well as temporarily and is related to clay type, clay content, and soil water content. It is used to evaluate soil quality and to identify layers with increased compaction [30].

Soil compaction is a deterioration process that weakens the plant growth, reducing the soil porosity, slowing the infiltration rate, and restricting the root growth. The most effective factors on soil compaction are accepted as vehicular traffic and wetting-drying circles. Soil compaction impacts pore-size distribution and reduces total soil volume, increases surface runoff and soil erosion in sloping areas, causing ponding in level areas [31].

Results from recent studies showed that plant growth could continue in soil with PR values as high as 3.5 MPa in no-tillage conditions due to the presence of continuous and biological pores, which allowed plant-root development in areas with low PR [32]. The PR and soil moisture showed a spatial relationship where lower values of PR concentrated on smaller values of soil moisture [33]. In another study, PR values varied with the density of the soil, regardless of moisture and penetration rate. The relationship between PR and moisture was not always linear, once it is influenced by soil-bulk density [34]. While PR was indicated as a good indicator of physical soil-crust formation in scalped soils over time, it was not of any effect on biological soil-crust development, erosion behavior of the soils [35]. PR in shallow ploughing in autumn at 10–25 cm was significantly higher than deep ploughing at 45–50 cm in a research [36]. The root length of soybean was obtained as the most susceptible to soil compaction, and the change in soil PR was poorly related with the change in the degree of compactness [37]. The mechanized cultivation system presents greater soil PR values to penetration down to 0.15 m depths and less humidity, when compared to the manual cultivation system [38].

3.2.2. Soil crusting

Crusting index is recognized as one of the major forms of soil degradation. In this study, CI was calculated using soil organic matter, clay, and silt contents. Soils with high CI values tend to have a higher tendency to form crust [39]. Soil organic matter content ranged from 0.41 to 4.33% for topsoil and from 0.14 to 2.32% in subsoil. Approximately 95% of the soils in the basin had low CI values (CI of <5), which indicates low tendency to form crust. The CIs of the basin soil results are shown in **Tables 4** and **5** and **Figure 4c**.

3.2.3. Surface runoff and soil loss

Surface runoff was low in 83.51% of the basin soils and moderate to high in 16.49%. In spite of low runoff, a considerable siltation was observed in Çelikli pond, which was attributed to high-intensity rainfall causing high water erosion.

The mean predicted annual soil loss was 7.66 tons ha^{-1} for Çelikli basin. Total soil loss for basin is approximately 8028.42 tons per year with 86.91% of the loss occurring from agricultural areas (73.56% of total land area). Pasture and shrublands contribution to soil loss was 9.51 and 3.58%, respectively. When soil loss was considered in terms of soil depth in the basin, the mean soil loss tolerance values [40] were around 4.5 tons ha^{-1}, which may be accepted as the threshold

level of the basin. In the basin, the agricultural areas are mainly converted from forest and pasture. According to USDA land capability classification, most of the agricultural land-use areas fall under classes VI and VII [24]. In these areas, conventional tillage should not be used. Due to limitations of slope and depth, these areas are mostly suitable for rangeland, pasture, wildlife habitat, or forestland. Although only 14% of the basin is suitable for cultivation, currently 68% of the entire basin is used for agriculture. Surface runoff and soil erosion maps of the study area (**Figure 4e** and **f**) reveal that the area has high potential for erosion, suggesting that measures should be taken to lessen soil erosion in the area.

Globally, soil erosion is responsible for 84% of soil degradation, 56% of water erosion, and 28% of wind erosion [41]. Soil erosion removes the nutrient-rich topsoils. It was pointed out that soil loss by erosion is a widespread global problem and has adverse effects on natural ecosystems such as agriculture, forests, and rangelands [42, 43]. Its effect is accepted as one of the prime environmental problems, impacting water availability, energy, and biodiversity. It causes several environmental damages such as nutrient loss, sedimentation, pollution, and flooding thus impacting productivity and sustainability of the soils [44].

3.2.4. Plant-available water content

Soil in the study area is generally low in PAWC (**Table 4**). Approximately 50% of the soil had PAWC values of <100 mm, and the PAWC values in the area varied (**Figure 4d**). This implies that the stored water in the soil cannot meet the plant water requirement during the summer months (from June to August) as per calculated daily evapotranspiration for reference crop of 6.4–6.8 mm in Tokat province [45].

Plant-available water content is generally considered as one of the most critical properties of soils, especially in the dry farming regions [46]. In semiarid regions, precipitation is generally scarce in summer, and evapotranspiration needs are not met due to low and improper distribution of the precipitation. Plant-available water content is a limiting factor for the rooting depth [47–49]. The amount of rainwater stored in the soil depends on water-holding capacity of soil in effective rooting depth. The remaining water moves beyond the plant-root zone. Thus, the amount of water held by the soil may be critical in dryland areas.

3.2.5. Other soil properties

Physical and chemical soil properties of the topsoil and subsoil with 142 and 115 sampling points, respectively, showed a moderate to high variability. Coarse material exhibited greatest variation in topsoils and P content in subsoils. The soil properties were inconsistent in the coefficient of variation by depth. Values of CV for soil properties of EC, pH, K, Zn, Fe, Mn, and CEC were relatively uniform by depth and this could be attributed to the similarity in the distribution of clay in topsoil and subsoil as these variables are mainly controlled by soil clay content and types of clay.

Variable	Mean	SD	Min	Max	CV	Skewness	Kurtosis
#EC, mmhos cm^{-1}	0.63	0.14	0.32	0.92	22.73	0.06	0.57
pH	7.41	0.47	6.37	8.63	6.28	0.30	0.67
#SOM, %	1.61	0.65	0.41	4.33	82.19	1.25	2.50
P, mg kg^{-1}	6.65	5.47	0.92	35.20	51.34	2.40	8.91
K, mg kg^{-1}	220.71	113.32	34.04	1008.58	40.46	3.37	17.72
B, mg kg^{-1}	0.20	0.44	0.01	4.67	20.67	8.25	75.82
Zn, mg kg^{-1}	0.20	0.15	0.05	1.82	30.32	8.33	83.99
Cu, mg kg^{-1}	1.86	0.89	0.41	5.03	16.86	0.90	0.56
Fe, mg kg^{-1}	9.69	4.52	2.20	24.02	40.08	0.48	0.34
Mn, mg kg^{-1}	162.00	1805.00	3.00	21524.00	57.09	11.79	137.00
Cd, mg kg^{-1}	0.04	0.02	0.00	0.10	215.93	0.37	0.60
#CEC, cmol kg^{-1}	34.98	9.67	17.63	67.04	27.64	0.66	0.45
Sand, %	46.55	9.62	28.27	74.84	76.53	0.57	0.41
Clay, %	30.01	9.10	4.08	47.88	47.72	0.13	0.36
Silt, %	23.45	3.95	12.91	33.20	46.61	0.14	0.02
#CM, %	19.66	11.22	4.14	67.92	1114.20	1.11	1.80
#HC, cm h^{-1}	22.17	8.89	4.13	47.79	54.91	0.36	0.22
K Factor, t ha h ha^{-1} MJ^{-1} mm^{-1}	0.11	0.06	0.00	0.30	52.46	0.50	0.27
#CI, dimensionless	3.18	1.67	0.78	9.41	52.55	1.74	3.04
#PAWC, mm	100.38	45.79	27.40	161.40	45.62	0.40	1.39
Soil loss, Mg ha^{-1}	6.15	7.99	0.00	62.97	129.90	3.16	16.84
#PR, KPa	1671.20	1080.90	170.80	3882.40	6.47	0.11	1.44
WY, Mg ha^{-1}	1.79	0.72	0.60	3.79	4.04	0.63	0.15

#SD, standard deviation; CV, coefficient of variation; EC, electrical conductivity; SOM, soil organic matter; CEC, cation exchange capacity; CM, coarse material; HC, hydraulic conductivity; CI, crusting index; PAWC, plant-available water content; PR, penetration resistance.

Table 6. Descriptive statistics of some soil properties in topsoil (0–0.3 m) of study area (n = 142).

The soil textural components, coarse material, soil organic matter, and Cd were highly variable in topsoil, and P, B, hydraulic conductivity (Ks), and some micronutrients (e.g., boron) were highly varied in subsoil. On the other hand, wheat yield showed low variation with a relatively normal distribution as indicated by moderate skewness and low kurtosis values (**Table 6**). This was attributed to fertilizer applications for a long time. In contrast to subsoil, where most of the variables were slight to moderately skewed, the majority of the variables were highly skewed in topsoil, which may be attributed to the existence of many irregular slopes with erosion and/or depression localities. Extreme values are likely to occur at these localities. Soil

loss, SOM content, and concentrations of P, K, B, Zn, Mn, CM, and crusting index were noticeable among these variables. All these variables are known to control yield in wheat [22]. However, wheat yield interestingly showed low variation with a relatively normal distribution as indicated by moderate skewness and low kurtosis values. In contrast to subsoil, where most of the soil variables were slight to moderately skewed, the majority of the variables were highly skewed in topsoil. The variables Mn, P, K, B, Zn, and soil loss exhibited a considerably constant distribution in topsoil, as suggested by kurtosis values (**Table 6**). Therefore, this low variation in wheat yield may be attributed to the application of fertilizers in the study area.

The P level was low (<10 mg kg^{-1}) in 94% of the study area and was medium to high (>10 mg kg^{-1}) in only 6% of the study area. By contrast, the K content was adequate in both soil depths in most of the study area. Combined with highly variable and skewed distribution of SOM, the low P content of the majority of soil indicated that P and N fertilizers application should be site specific.

Microelement contents of the study soils were classified based on procedures [50]. Calculations showed that B and Zn contents were low due to parent material and that Cu, Mn, Fe, and Cd contents were adequate. Boron content was lower than 0.5 mg kg^{-1} in 85.5% of the cultivated areas and 82.9% of the grassland areas, and Zn was lower than 0.5 mg kg^{-1} in 99.7% of the entire study area. Both B and Zn are essential microelements in wheat production. This indicates that the use of B and Zn additive fertilizers is necessary. Also, the highly variable and skewed distribution of these elements should be considered in fertilizer application [22].

3.3. Factor analysis

The evaluation of soil degradation is difficult because of the diversity and complexity of soil-degrading processes. Interrelations between the variables frequently obscure the evaluation of each soil-degrading process' contribution. Factor analysis is frequently used to reduce the number of variables in a dataset, and so we used factor analysis to identify the key variables of soil degradation in the study area.

All the studied soil properties namely EC, pH, P, K, SOM, CEC, B, Zn, Cu, Fe, Mn, Cd, sand, clay, silt, coarse material, hydraulic conductivity, soil erodibility (K) factor, crusting index, runoff, PAWC, soil loss, penetration resistance, and wheat yield were subjected to factor analysis (see **Table 7**).

Topsoil: The 24 variables were considered for the factor analysis of topsoils and grouped in nine factors accounting for 71.2% of the total variance (**Table 8**).

The variables clay, sand, and erodibility were loaded in Factor 1 and this factor was named as "erodibility factor". The "erodibility factor" accounted for 14.7% of the total variation. We found a negative correlation between clay content and soil erodibility. This was attributed to the effect of clay on soil aggregate strength, which decreases soil erodibility. Likewise, when we compared soil loss in clayey and sandy clay soils, clay soil was more resistant to erosion because of its stronger aggregates.

Variable	Mean	SD	Min	Max	CV	Skewness	Kurtosis
#EC, mmhos cm^{-1}	0.62	0.14	0.30	0.94	22.22	0.01	0.43
pH	7.55	0.42	6.37	8.30	5.50	0.61	0.39
#SOM, %	1.12	0.45	0.14	2.32	40.68	0.06	0.37
P, mg kg^{-1}	2.79	3.33	0.40	22.40	119.33	3.22	12.68
K, mg kg^{-1}	171.71	69.43	33.75	461.92	40.43	0.93	2.10
B, mg kg^{-1}	0.19	0.22	0.00	1.48	112.34	3.21	13.06
Zn, mg kg^{-1}	0.12	0.04	0.03	0.32	37.40	1.04	2.76
Cu, mg kg^{-1}	1.73	0.82	0.17	3.83	47.53	0.57	0.45
Fe, mg kg^{-1}	8.70	3.85	2.57	20.50	44.28	0.60	0.02
Mn, mg kg^{-1}	11.05	6.43	3.01	35.90	58.18	1.16	1.31
Cd, mg kg^{-1}	0.04	0.02	0.00	0.12	57.17	0.03	0.05
#CEC, cmol kg^{-1}	36.36	9.38	19.19	66.86	25.81	0.42	0.02
Sand, %	45.17	9.01	26.72	76.39	19.94	0.50	0.63
Clay, %	32.82	8.56	10.73	53.39	26.08	0.10	0.48
Silt, %	22.01	3.50	12.88	30.19	15.88	0.31	0.12
#CM, %	18.45	10.34	2.18	49.84	56.05	0.81	0.06
#HC, cm h^{-1}	45.17	9.01	26.72	76.39	19.94	0.50	0.63
#PR, KPa	2579.60	332.00	1590.00	3522.00	12.87	0.40	0.64

#SD, standard deviation; CV, coefficient of variation; EC, electrical conductivity; SOM, soil organic matter; CEC, cation exchange capacity; CM, coarse material; HC, hydraulic conductivity; PR, penetration resistance.

Table 7. Descriptive statistics of some soil properties in subsoil (0.3–0.6 cm) of study area (n = 115).

The K factor of 10 measurements of surface soil in the Hornos area in Spain was calculated and compared with three aspects of aggregate stability [51]. A significant correlation was found between the K factor and the percentage of particles <100 μm, which is accepted as a measure of the vulnerability of soil to erosion by overland flow.

The variables Fe, Cu, and pH were loaded in Factor 2, which were named as "soil fertility" factor. The soil fertility factor described 10.74% of the total variation and had a positive correlation with the two micronutrients (Cu and Fe). However, there was a negative relationship between soil pH and these nutrients. A research result [52] showed that the increased clay and iron (Fe) contents resulted in decreased soya bean emergence and soil strength. The eroded soils had lower infiltration rates and higher clay dispersion.

Properties Cu, EC, and CEC were loaded in Factor 3, and it was named as "soil chemistry factor". The soil chemistry factor described 9.89% of the total variation. Positive correlation occurred between Cu and CEC and between Cu and EC. Factor 4 was named as "soil-crusting factor" that included SOM and CI and described 8.37% of the total variation.

Variables	Factor 1	Factor 2	Factor 3	Factor 4	Factor 5	Factor 6	Factor 7	Factor 8	Factor 9
Clay, %	0.95	−0.02	0.14	−0.06	−0.02	−0.09	0.10	0.01	−0.01
K Factor, t ha h ha^{-1} MJ^{-1} mm^{-1}	−0.88	0.15	0.12	0.00	0.03	−0.15	0.14	−0.15	0.04
Sand, %	−0.76	−0.08	−0.35	−0.06	0.08	0.24	−0.33	−0.02	0.03
Silt, %	−0.48	0.19	0.40	0.24	−0.11	−0.29	0.44	0.01	−0.04
Fe, mg kg^{-1}	0.11	−0.84	0.10	0.16	−0.15	−0.17	−0.09	−0.11	−0.11
pH	−0.06	0.81	0.09	−0.09	0.05	0.13	−0.21	−0.15	−0.08
Cu, mg kg^{-1}	−0.00	−0.59	0.52	−0.06	−0.20	−0.12	−0.25	0.08	−0.13
#CEC, cmol kg^{-1}	−0.05	−0.14	0.87	0.00	0.05	0.07	−0.04	−0.03	−0.00
#EC, mmhos cm^{-1}	0.40	0.43	0.64	0.23	−0.06	−0.03	−0.08	0.03	0.05
#SOM, %	0.13	−0.06	0.10	0.93	−0.03	−0.01	0.13	0.16	0.00
#CI, dimensionless	−0.19	−0.10	−0.04	0.92	−0.01	0.10	−0.02	0.14	0.01
Soil loss, Mg ha^{-1}	0.01	0.04	−0.05	−0.05	0.88	0.13	0.01	0.12	−0.08
Runoff, dimensionless	−0.09	0.18	0.07	0.02	0.78	−0.16	−0.17	−0.19	0.17
#HC, cm h^{-1}	0.06	0.21	0.21	−0.04	−0.04	0.71	−0.05	−0.10	0.06
#CM, %	−0.19	0.14	−0.23	0.09	0.05	0.68	0.00	0.04	−0.13
B, mg kg^{-1}	0.28	−0.15	0.05	0.15	−0.01	0.36	0.13	−0.10	0.31
#PAWC, mm	0.19	−0.11	−0.15	0.14	−0.11	0.00	0.77	−0.03	−0.02
Mn, mg kg^{-1}	0.12	−0.03	−0.14	0.24	−0.00	−0.06	−0.39	−0.17	−0.32
P, mg kg^{-1}	0.01	−0.14	0.06	0.14	0.08	0.06	0.02	0.83	−0.02
K, mg kg^{-1}	0.06	0.44	0.08	0.28	−0.17	−0.23	−0.21	0.58	0.07
Zn, mg kg^{-1}	0.25	0.01	−0.11	0.05	−0.08	−0.14	0.14	0.35	−0.10
#PR, kPa	0.07	−0.04	−0.13	0.07	−0.01	−0.18	0.09	−0.06	0.74
WY, Mg ha^{-1}	0.18	−0.22	−0.10	0.04	−0.04	−0.23	0.26	0.06	−0.61
Cd, mg kg^{-1}	−0.10	0.03	0.41	−0.21	0.25	0.07	0.26	0.17	0.42
Variance, %	14.57	10.74	9.89	8.37	6.46	6.31	5.73	4.63	4.46
Cumulative variance	14.57	25.31	35.20	43.57	50.03	56.34	62.07	66.70	71.16

#CEC, cation exchange capacity; EC, electrical conductivity; SOM, soil organic matter; CI, crusting index; CM, coarse material; HC, hydraulic conductivity; PAWC, plant-available water content; PR, penetration resistance; WY, wheat yield.

Table 8. Factor analysis for topsoil in study area.

Factor 5, "soil erosion factor", which includes soil loss and runoff, described 6.46% of the total variation. As expected, there was a positive correlation between soil loss and runoff. Factor analysis was applied to predict erosion in an area intensively cultivated with sugarcane near the city of Piracicaba, São Paulo [53]. The researchers revealed that soil erosion was influenced by slope length and steepness (LS) factor (topographic) more than by the K factor (soil erodibility).

Factor 6 was named as "soil conductivity factor", which included the hydraulic conductivity and coarse material content and described 6.31% of the total variation (**Table 8**). We found a strong positive loading for CM (0.68) and HC (0.71). In a study [54], land-use effects on soil compaction considering the saturated hydraulic conductivity (Ks) in a field continuously growing corn and a hayfield both having clay soil in Canada were evaluated. The Ks-values for hayfield-growing soils were approximately 10 or 100 times greater than for the corn-growing soils of which degradation level for upper B horizons had changed from slight to severe. While there was no difference for B horizons in terms of Ks, their results showed that the corn yield was reduced by about 50% due to severe compaction and low Ks. The Ks-values for the 30–50-cm depth can be a reliable indicator for assessing soil structure degradation.

Factor 7, the plant-available water content or "PAWC factor" described 5.7% of the total variation (**Table 8**). The PAWC is considered the most critical indicator for land degradation, especially for dryland farming regions [46]. In dryland regions, spring and summer months are generally dry, and plant water needs are not met due to low and improper distribution of precipitation. The PAWC is a limiting factor for root depth [47–49]. Precipitation water is stored in the soil, depending on soil depth and water-holding capacity. In cases of infiltration rate lower than rainfall intensity, a portion of rainwater may be lost via surface runoff or ponded on the surface. The amount infiltrating into soil may be stored depending on soil depth or lost via deep percolation or underground lateral flow in sloping layered soils. As a result, the amount of water stored in the soil may be critical in areas where water is the principal growth-limiting factor [47, 48]. Spatial variability of topsoil (0–30 cm) and subsoil (30–60 cm) in the Kazova Plain was investigated by factor analysis [55]. Six of 10 variables for both top and subsoils were loaded in four factors accounting for 94.80 and 92.80% of total variance, respectively. The results showed that the plant-available water content and available phosphorus content (P) were the most important soil properties for soil management and soil fertility studies in the study area.

Macroelements K and P were loaded in Factor 8. Factor 8 was named as "macroelement factor". The loadings showed a high correlation between these two variables. The imbalance of macronutrients (e.g., N, P, K, Ca, Mg, and S) and microelements (e.g., Zn, Cu, Mo, B, and Se) may cause a yield decline in degraded soils. Factor analysis has been used to identify the most sensitive indicators of some soil characteristics for evaluating soil tillage in Vertisol and Entisols in the Bafra province of Turkey [56]. The soil physicochemical properties of Vertisols were grouped in three groups and of Entisols were grouped in two groups. Available water content, field capacity, soil organic matter, wilting point, and $CaCO_3$ were in the first group; bulk density, sand, and carbon were in the second group; and penetration resistance was in the third group for Vertisols. Soil organic matter, available water content, wilting point, field capacity,

soil organic matter, sand, and bulk density were in the first group and $CaCO_3$, silt, and penetration resistance were in the second group for Entisols.

Variables	Factor 1	Factor 2	Factor 3	Factor 4	Factor 5	Factor 6	Factor 7
Mn, mg kg^{-1}	0.86	0.05	0.11	−0.11	0.07	0.04	−0.19
pH	−0.82	0.03	−020	−0.01	−0.22	−0.15	0.00
Fe, mg kg^{-1}	0.82	0.17	−0.03	0.32	−0.09	−0.16	−0.08
Clay, %	0.07	0.93	−0.05	0.09	−0.03	0.00	−0.02
Sand, %	−0.08	−0.93	0.09	0.05	−0.19	−0.12	−0.08
#EC, mmhos cm^{-1}	−0.44	0.57	0.04	0.49	0.25	−0.19	−0.10
#HC, cm h^{-1}	−0.24	−0.55	0.54	0.04	0.19	−0.15	−0.07
Zn, mg kg^{-1}	0.34	−0.11	0.75	0.05	0.17	0.20	0.17
P, mg kg^{-1}	0.06	−0.02	0.73	−0.21	−0.29	0.10	0.04
#CM, %	0.14	−0.32	0.45	−0.25	−0.02	−0.33	−0.26
#CEC, cmol kg^{-1}	−0.00	0.02	−0.15	0.86	0.03	−0.05	0.10
Cu, mg kg^{-1}	0.44	0.07	0.00	0.71	−0.37	0.15	0.06
WY, Mg ha^{-1}	0.07	−0.02	− 0.07	−0.03	0.72	−0.09	0.12
Silt, %	0.05	0.19	−0.10	−0.31	0.54	0.29	0.25
#SOM, %	0.07	0.17	0.42	0.10	0.53	0.08	−0.22
K, mg kg^{-1}	−0.05	0.24	0.17	−0.10	−0.12	0.82	−0.06
B, mg kg^{-1}	−0.23	0.31	0.00	−0.18	−0.37	−0.62	0.18
Cd, mg kg^{-1}	−0.04	0.02	0.04	−0.01	0.05	0.08	0.87
#PR, KPa	0.15	−0.02	−0.01	−0.13	−0.07	0.28	−0.58
Variance, %	16.95	16.27	10.96	8.29	7.19	6.88	6.68
Cumulative variance	16.95	33.22	44.18	52.47	59.66	66.54	73.22

#EC, electrical conductivity; HC, hydraulic conductivity; CM, coarse material; CEC, cation exchange capacity; WY, wheat yield; SOM, soil organic matter; PR, penetration resistance.

Table 9. Factor analysis for subsoil in study area.

Finally, wheat yield and penetration resistance were loaded in Factor 9 and it was named as "crop yield factor". The crop yield factor described 4.46% of the total variation. Loadings showed a high negative correlation ($R^2 = -0.735$) between these two variables in the study area. Similar results were found elsewhere, PR reduced wheat and soybean yields [57]. Others [58]

http://dx.doi.org/10.5772/64624

showed that PR had a highly adverse effect on wheat spike number. Results of another study [59] showed that PR was a limiting factor of soybean yield due to its adverse effect on field capacity.

In subsoil, 19 variables were grouped in seven factors that accounted for 73.2% of total variance, as shown in **Table 9**. Available Mn content, pH, and available Fe content were loaded in Factor 1, which described 16.9% of the total variation in the studied variables. Factor 1 was named as "microelement factor". The loadings showed a positive relationship among Mn, Cu, and Fe contents and a negative correlation between pH and each of these variables. The variables of clay, sand, EC, and HC were loaded in Factor 2, which described 16.2% of the total variance. Factor 2 was named as "soil physics factor". Hydraulic conductivity had a negative loading, whereas EC and clay had positive loadings in Factor 2, suggesting that contrary to sand, both clay content and EC had a negative effect on HC. Factor 3 described 10.9% of the total variance. The variables Zn and available P were loaded in this factor. Hydraulic conductivity was also loaded in this factor. Factor 4, named "soil chemistry", included CEC, Cu, and EC and described 8.3% of the total variance. Wheat yield, silt, and SOM were loaded in Factor 5, which described 7.2% of the total variance. Factor 5 was named as "yield factor". Available K and B were loaded in Factor 6, and Cd and PR were loaded in Factor 7. Factor 6, describing 6.9% of variance, was named as "soil potassium factor", and Factor 7, describing 6.7% of total variance, was named as "soil cadmium factor".

4. Conclusion

Factor analysis revealed that PR in topsoil had a profound adverse effect on wheat yield, whereas silt and SOM content in subsoil had a positive effect. A moderate positive correlation occurred between PAWC and wheat yield. Therefore, insufficient water-holding capacity, low SOM content, and high PR are the major variables affecting wheat yield in the catchment. These variables can be controlled by management practices such as residue management, crop rotation, and use of organic materials in crop production. Soil loss is one of the major contributors to soil degradation. Our results showed that 89% of the study area is under the influence of surface runoff to some degree. Conservation tillage (CT) can be adapted to decrease the potential of surface runoff in the study area. However, CT should be applied carefully to the areas with high PR, since it can also increase PR.

In combination with crop rotation and variable fertilizer application, these practices can help restore soil productivity in cultivated areas, which cover 95.4 ha of the study area. Forage crops should be used in crop rotation to increase SOM content and decrease PR in the study area. It is likely that increasing SOM and decreasing PR will decrease surface crusting, which would increase water-holding capacity by increased water infiltration into soil and decreases the potential for soil loss through surface runoff. The localities covered by grass and shrubs should be managed properly to avoid further deterioration. This may be accomplished by the application of rotational grazing, which reduces animal trafficking, in turn decreasing PR in grasslands.

Author details

İrfan Oğuz[1], Ertuğrul Karaş[2*], Sabit Erşahin[3] and Tekin Susam[4]

*Address all correspondence to: ekaras@ogu.edu.tr

1 Department of Soil Science and Plant Nutrition, Faculty of Agriculture, University of Gaziosmanpaşa, Tokat, Turkey

2 Department of Biosystem Engineering, Faculty of Agriculture, University of Osmangazi, Eskişehir, Turkey

3 Department of Forest Engineering, School of Forestry, Çankiri Karatekin University, Çankiri, Turkey

4 Department of Geomatics Engineering, Faculty of Engineering and Natural Sciences, University of Gaziosmanpaşa, Tokat, Turkey

References

[1] Lal R, Blum NH, Valentine C, Stewart BA (1997) Methods for assessment of soil degradation. New York: CRC Press.

[2] Eswaran H, Lal R, Reich PF (2001) Land degradation: An overview. In Responses to land degradation. Proceedings of the 2nd international conference on land degradation and desertification. New Delhi, India: Oxford Press. Retrieved 2012-02-05.

[3] Kalaç M (1998) The usage and conservation of Turkey agricultural soil. Tarım ve Mühendislik. 57: 38–43 (in Turkish).

[4] Anonymous (2014) Sustainable use of agricultural land. Study report, p. 79, Ankara (in Turkish).

[5] Koç A, Gökkuş A, Serin Y (1994) Situation of pastures in Turkey, Ecology Journal, October- November-December, No: 13, p 36–41 (in Turkish).

[6] Soil Survey Staff (2010). Keys to Soil Taxonomy, 11th ed. Lincoln, NE: USDA, National Resources Conservation Service, National Soil Survey Center.

[7] Oğuz İ (1997) K, R, C and P factors of USLE equation in alluvial soil group at Tokat province. Research Report, 102, 69–79, Ankara (in Turkish).

[8] Nelson DW, Sommers LE (1982) Total carbon, organic carbon, and organic matter. In Methods of soil analysis, part 2, 2nd ed., ed. A. L. Page, pp. 539–579. Madison, Wisc.: ASA and SSSA.

http://dx.doi.org/10.5772/64624

[9] McLean EO (1982) Soil pH and lime requirement. In Methods of soil analysis, part 2, 2nd ed., ed. A. L. Page, pp. 199–224. Madison, Wisc.: ASA and SSSA.

[10] Nelson RE (1982) Carbonate and gypsum. In Methods of soil analysis, part 2, 2nd ed., ed. A. L. Page, pp. 181–197. Madison, Wisc.: ASA and SSSA.

[11] Richards LA (1954) Diagnosis and improvement saline and alkali soils (USDA Agricultural Handbook No. 60). Washington, D.C.: U.S. Government Printing Office.

[12] Rhoades JD (1982) Cation exchange capacity. In Methods of soil analysis, part 2, 2nd ed., ed. A. L. Page, pp. 149–157. Madison, Wisc.: ASA and SSSA.

[13] Gee GW, Bauder JW (1986) Particle size analysis. In Methods of soil analysis, part 1, 2nd ed., ed. A. Klute, pp. 383–411. Madison, Wisc.: ASA.

[14] Black CA (1965) Methods of soil analysis, part 2: Chemical and microbiological properties. Madison, Wisc.: ASA.

[15] Klute A (1986) Water retention: Laboratory methods. In Methods of soil analysis, part 1, ed. A. Klute, pp. 635–662. Madison, Wisc.: ASA and SSSA.

[16] Wischmeier WH, Johnson CB, Cross BV (1971) A soil erodibility monograph for farmland and construction sites. Journal of Soil and Water Conservation. 26:189–193.

[17] Bradford GM (1986) Penetrability. In Methods of soil analysis, part 1, 2nd ed., ed. A. Klute, pp. 463–478. Madison, Wis.: ASA.

[18] NRCS (1998) National Soils Handbook. Washington, D.C.: U.S. Government Printing Office.

[19] Wischmeier WH, Smith DD (1978) Predicting rainfall erosion losses (Agricultural Handbook No. 537). Washington, D.C.: U.S. Government Printing Office.

[20] Kleinbaum DG, Kupper LL, Muller KE, Nahim A (1988) Applied Regression Analysis and Other Multivariate Methods. Belmont, CA: Duxbury Press.

[21] Norusis MJ (1986) Advanced statistics SPSS/PC for the IBM PC/TX/AT. Chicago, III.: SPSS.

[22] Oğuz İ, Susam T, Erşahin S, Karaş E (2012) Evaluation of soil degradation ımpact on wheat yield by geographical ınformation system. Communications in Soil Science and Plant Analysis. 43(14): 1867–1882.

[23] ESRI (2003) GIS standards and interoperability. ArcNews, ESRI. 25Spring (1), 2003, 1.

[24] Oğuz İ, Karaş E, Susam T, Tetik A, Noyan ÖF, Akar Ö (2006) Watershed planning for sustainable agricultural management by determining soil degradation in Tokat-Artova Çelikli basin, Ministry of Agricultural and Rural Affairs, General Directorate of Agricultural Researches, TAGEM–BB-TOPRAKSU-2006/19, Publication No: 230, Technical publication No: 45, 116 p. Tokat (in Turkish).

[25] Moraes MT, Debiasi H, Carlesso R, Franchini JC, Silva VR (2014) Critical limits of soil penetration resistance in a rhodic Eutrudox. Revista Brasileira de Ciência do Solo. 38: 288–298.

[26] Taylor HM, Robertson GM, Parker JJ (1966) Soil strength-root penetration relations for medium and coarse textured soil materials. Soil Science. 102: 18–22.

[27] Gerard CJ, Sexton P, Shaw G (1982) Physical factors influencing Soil strength and root growth. Argonomy Journal. 74: 875–879.

[28] Vepreskas MJ, Miner GS (1986) Effects of subsoiling and mechanical impedance on tobacco root growth in coarse-textured soils. Soil Science Society of America Journal. 50: 423–427.

[29] Vepraskas MJ, Wagger MG (1989) Cone index values diagnostic of where subsoiling can increase corn root growth. Soil Science Society of America Journal. 53: 1499–1505.

[30] Franchini JC, Costa JM, Debiasi H, Torres E (2011) Importance of crop rotation for sustainable agricultural production in Parana, Londrina, Embrapa Soja, 2011. 52p. (Embrapa Soja. Documentos, 327).(in Portuguese).

[31] Brady NC, Weil RR (2002) The Nature and Properties of Soils, 13th ed. Upper Saddle River, N.J.: Prentice Hall.

[32] Tormena CA, Araújo MA, Fidalski J, Costa JM (2007) Temporal variation of the least limiting water range of an oxisol under no-tillage systems. R. Bras. Ci. Solo, 31:211–219. (in Portuguese)

[33] Campos MCC, Aquino RE de, Oliveira IA de, Bergamim AC (2013) Spatial variability of soil resistance to penetration and soil moisture in the area cultivated with sugar cane in the region of Humaitá, Amazonas, Brazil. Revista Brasileira de Ciências Agrárias. 8(2): 305–310 (Recife: Universidade Federal Rural de Pernambuco, 2013).

[34] Valadão Junior DD, Biachini A, Valadão FCA, Rosa RP (2014) Penetration resistance according to penetration rate, cone base size and different soil conditions. Bragantia. 73(2): 171–177 (Campinas: Instituto Agronômico do Estado de São Paulo, 2014).

[35] Chamizoa S, Rodríguez-Caballeroa E, Cantóna Y, Asensioa C, Domingob F (2015) Penetration resistance of biological soil crusts and its dynamics after crust removal: relationships with runoff and soil detachment. Catena. 126: 164–172.

[36] Steponavičiene V, Boguzas V, Mikučioniene R, Sinkevičiene A, Feiza V (2015) Influence of tillage systems and straw incorporation on soil shear strength and penetration resistance, Conference paper. Zinatniski praktiska konference Lidzsvarota Lauksaimnieciba, Jelgava, Latvia 19–20 Februari 2015, ISBN:9789984481760.

[37] Oliveira PD de, Sato MK, Lima HV de, Rodrigues S, Silva AP da (2016). Critical limits of the degree of compactness and soil penetration resistance for the soybean

crop in N Brazil. Journal of Plant Nutrition and Soil Science. 179(1): 78, 10p (Feb 2016).

[38] Palma MAZ, Volpato CES, Silva FC da, Souza P de, Silva JA (2014). Soil penetration resistance in coffee plantations cultivated with mechanized and manual systems. Coffee Science. 8(3): 364–370 (Lavras: Coffee Science, Universidade Federal de Lavras, 2013).

[39] Lal R (1988) Soil erosion research methods. Iowa, USA: Soil and Water Conservation Society.

[40] McCormack DE, Young KK, Kimberlin LW (1982) Current criteria for determining soil loss tolerance. In Determinants of soil loss tolerance, ed. D. M. Kral, pp. 95–111. American Society of Agronomy Special Publication 45. Madison, Wisconsin.

[41] Oldeman LR, Hakkeling RTA, Sombroek WG (1990) World map of the status of human-induced soil degradation. Wageningen, The Netherlands: International Soil Reference and Information Centre.

[42] Pimentel D (2006) Soil erosion: a food and environmental threat. Environment, Development and Sustainability. 8: 119–137. DOI:10.1007/s10668-005-1262-8.

[43] Lal R, Stewart BA (1990) Soil degradation. New York: Springer-Verlag.

[44] Morgan RPC (2005) Soil Erosion and Conservation, 3rd ed. 350 Main Street, Malden, MA 02148-5020, USA: Blackwell Science Ltd.

[45] Balçın M, Kodal S, Karaata M, Güleç H (2004) Suitable equation of crop water consumption for Transactional region of Black Sea., Journal of Agricultural Research, 10 (4), p. 435–443. (in Turkish).

[46] Brady NC (1990) The Nature and Properties of Soils, 10th ed. McMillan: New York, 639p.

[47] Godwin DC, Jones CA, Ritchie JT, Vlek PLG, Youngdahl LG (1984) The water and nitrogen components of the CERES models. International Symposium on Minimum Data Sets for Agrotechnology Transfer. Patancheru, India.

[48] Ratliff LF, Ritchie JT, Cassel DK (1983) A survey of field-measured limits of soil water availability and related to laboratory-measured properties. Soil Science Society of America Journal. 47: 770–775.

[49] Gardner BF, Blad BL, Watts DG (1981) Plant and air temperatures in differentially irrigated corn. Agricultural Meteorology. 25: 207–217.

[50] Viets FG, Lindsay WL (1973) Testing soils for zinc, copper, manganese, and iron. In Soil testing and plant analysis, ed. L. M. Wals and J. D. Beaton, pp. 153–172. Madison, Wisc.: SSSA.

[51] Meester T, Jungerius PD (1978) The relationship between the soil erodibility factor K (Universal soil loss equation), aggregate stability and micromorphological properties

of soils in the Hornos area, S. Spain. Earth Surface Processes. 3(4): 379–391, DOI: 10.1002/esp.3290030406.

[52] Miller CF, Watson EB, Harrison TM (1988) Perspectives on the source, segregation and transport of granitoid magmas. Transactions of the Royal Society of Edinburgh: Earth Sciences. 79: 135–156.

[53] Weill MAM, Sparovek G (2008) Erosion study in the Ceveiro Watershed (Piracicaba, SP): I – estimation of soil loss rates and sensitivity factor analysis of the USLE model. Revista Brasileira de Ciencia do Solo. 32(2): 801–814. ISSN 1806-9657. http://dx.doi.org/10.1590/S0100-06832008000200034.

[54] Wang C, McKeague JA, Switzer-Howse KD (1985) Saturated hydraulic conductivity as an indicator of structural degradation in clayey soils of Ottawa area, Canada. Soil and Tillage Research. 5(1): 19–31, DOI:10.1016/S0167-1987(85)80014-3.

[55] Erşahin S, Karaman R (2000) Use of factor analysis in the assessment of soil variability for site specific management and soil fertility studies. Tarım Bilimleri Dergisi. 6(2): 76–81.

[56] Sağlam M, Dengiz O, Sarıoğlu FE, Saygın F, Elgin C, Atasoy Ç (2012) Determination of some soil physico-chemical characteristics using factor analysis for soil tillage in Vertisol and Entisol, INMATEH – Agricultural Engineering. 38(3): 65–72.

[57] Busscher WJ, Frederick JR, Bauer PJ (2000) Timing effects of deep tillage on penetration resistance and wheat and soybean yield. Soil Science Society of America Journal. 64: 999–1003.

[58] Zhang XY, Cruse RM, Sui YY, Jhao Z (2006) Soil compaction induced by small tractor traffic in northeastern China. Soil Science Society of America Journal. 70(2): 613–619.

[59] Beutler AN, Centurion IJF, daSilva AP (2005). Soil resistance to penetration and least limiting water range for soybean yield in a haplustox from Brazil. Brazilian Archives of Biology and Technology 48(6), Curitiba Nov. 2005. http://dx.doi.org/10.1590/S1516-89132005000800002.

Edited by Abiud Kaswamila

Land degradation which is caused by multiple forces-extreme weather conditions and anthropogenic activities that pollute or degrade the quality of soils and land utility-negatively affects food production, livelihoods, and the provision of other ecosystem goods and services. Land degradation can also lead to climate change and affect human health. The problem is more pronounced in least developing countries due to overdependence of natural resources for survival. Sustainable ways to reduce land degradation and desertification demand research and advocacy of sustainable land management practices. This book is organized into two sections. The first section covers three major aspects, viz., an understanding of patterns of land degradation and desertification for developing mitigation strategies, land-atmosphere interaction from response of land cover to climate change effects of Karst rocky desertification, and the effect of unprecedented human activity into land degradation and desertification processes using natural and human-induced landscape research. The last section dwells on the relationship between soil degradation and crop production and an examination on how land degradation impacts the quality of soil in communal rangelands.

Environmentalists, land-use planners, ecologists, pedologists, researchers, and graduate students will find this book to be an essential resource.

ISBN 978-953-51-5084-8

Photo by MariuszPrusaczyk / CanStock

IntechOpen